Pergamon

Prog. Quant. Electr. 1996, Vol. 20, No. 4 pp. 271–358
Published by Elsevier Science Ltd
Printed in Great Britain

SSDI: 0079-6727(95)00007-0

0079-6727/96 $32.00

UPCONVERSION LASER PROCESSES

RICHARD SCHEPS

Naval Command, Control and Ocean Surveillance Center, RDT&E Division (NRaD), Code 754, San Diego CA 92152, U.S.A.

Abstract—Pump processes that produce upconversion laser emission in trivalent rare earth ion-doped gain media are described, and the performance of upconversion lasers pumped by these processes is reviewed. Sequential two-photon absorption upconversion, cooperative energy transfer upconversion and photon avalanche upconversion are discussed in relation to the production of visible laser emission. Using Er:YALO as an example, the specific energy flow pathways for each of these pump processes are described in detail. Experimental results are presented for laser emission in Er:YALO pumped by sequential two-photon absorption, cooperative energy transfer and photon avalanche upconversion. The spectral and temporal dependence of upconversion emission is reviewed and experimental evidence for photon avalanche upconversion in Er:YALO is presented. The laser oscillation conditions including gain and loss are related to upconversion lasers using a three-level ion kinetics model. Rate equations are presented that illustrate the impact of various competing pump processes on the upconversion laser output. Upconversion laser emission under Q-switched operation is discussed and equations for optimum output coupling are presented. The design considerations for efficient upconversion laser resonators and pump optics are addressed. Upconversion laser results obtained over the past three decades are reviewed. The laser performance obtained for crystals doped with trivalent Pr, Nd, Er and Tm ions is discussed. Sensitized upconversion using Yb ion co-doping is described and results obtained for Yb–Er and Yb–Ho upconversion lasers are summarized. Upconversion fiber laser development is also reviewed and details are presented for room temperature upconversion laser emission using ZBLAN fibers doped with trivalent Pr, Nd, Ho, Er and Tm ions. The effect of upconversion processes on the efficiency and operation of conventional lasers is discussed. Upconversion pumping involving the upper laser level is shown to increase the laser threshold power and lower the optical conversion efficiency. Upconversion pumping involving the lower laser level of a self-terminating transition lowers the terminal level lifetime. The conditions are described under which upconversion pumping can enable cw laser operation on a self-terminating transition. Published by Elsevier Science Ltd

CONTENTS

Dedication—This review is dedicated to the memory of my friend and brother Sheldon Scheps.

1. INTRODUCTION

Upconversion lasers are among the most efficient sources of coherent visible and near-ultraviolet radiation. Laser emission has been demonstrated in both the continuous (cw) and pulsed modes and these types of lasers can provide practical solutions for applications as diverse as medical diagnosis and treatment, underwater surveillance and full color (RGB) all-solid state displays. Upconversion generally refers to energy transfer processes that are initiated by photon absorption. Upconversion produces population in an excited state whose energy exceeds that of the pump photon. Optical emission from the excited state occurs at a wavelength shorter than that of the optical pump field, accounting for one of the more powerful features of this pump mechanism. Conversion of infrared radiation to the visible has generated much of the current interest in upconversion, as advances in both solid state lasers and semiconductor laser diodes have resulted in highly efficient sources of infrared emission. While upconversion materials can be used for visible detection of infrared radiation or for displays of infrared images, the most compelling application lies in laser emission. First demonstrated in 1971, upconversion laser emission offers a simple and efficient alternative to non-linear optical techniques for converting infrared laser output to the visible and near ultraviolet.

Upconversion requires the absorption of two or more photons but, unlike multi-photon absorption, the photons can be absorbed sequentially rather than simultaneously. A condition for efficient upconversion pumping is that the absorbing center has a metastable state that is intermediate in energy between the ground state and the emitting state. The intermediate state acts as an energy reservoir. A sequential two-photon absorption upconversion pump process is illustrated in Fig. 1 for a simple three-level system. In this example, absorption of pump photon "a" populates metastable level 2. A second pump photon "b" then promotes the ion from metastable level 2 to emitting level 3, producing fluorescence on the $3 \rightarrow 1$ optical transition. The transient population in metastable level 2 depends on a number of factors, but under appropriate conditions this population is high enough to produce substantial excited state absorption on the $2 \rightarrow 3$ transition.

The requirements for efficient upconversion make the rare earth ion-doped solid state crystals ideal for this application. Rare earth ions are unique in that transitions within the $4f^n$ core are substantially screened from outside influences and sharp spectroscopic lines having high peak cross sections result when these ions are doped into crystalline lattices. As a consequence, much of the solid state laser research since the 1960s has concentrated on transitions between the $4f^n$ states of the trivalent rare earth ions. The energy transfer processes involved in upconversion rely upon the very small interactions between rare earth ions and the crystal field-split (Stark) level structure of the rare earth ions provides many intermediate levels. Pr^{3+}, Nd^{3+}, Ho^{3+}, Er^{3+} and Tm^{3+} ions are particularly well-suited for upconversion

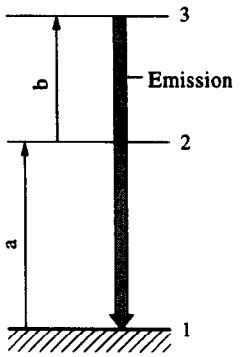

Fig. 1. Sequential two-photon absorption upconversion in a three-level ion. Letters "a" and "b" refer to photon wavelengths corresponding to the $1 \rightarrow 2$ and $2 \rightarrow 3$ transitions, respectively. The thick arrow labeled "emission" represents radiative decay from level 3. Level 1 is the ground state, level 2 is metastable, and emission from level 3 produces visible radiation.

laser emission, as these ions are characterized by numerous intermediate metastable levels. The metastable state energies are well-matched to the emission wavelengths of several efficient pump laser sources. Many can be populated by absorption from tunable near infrared-emitting lasers such as Ti:sapphire and AlGaAs semiconductor laser diodes. In addition, the trivalent rare earth ions have several long-lived upper excited states that give rise to strong visible emission.

While upconversion pumping can take place on a single center as shown in Fig. 1, upconversion energy transfer involving two distinct ions can also occur. For example, each of two neighboring ions can absorb a pump photon of the same energy, thereby populating the metastable level. This process has the advantage of requiring only one pump wavelength and is illustrated in Fig. 2 for a three-level ion. In this case two photons "a" are absorbed by identical ions A and B, promoting both to metastable state 2. A cooperative energy transfer process similar to Auger recombination can then occur, promoting ion B to emitting level 3 while ion A relaxes back to ground state 1. Relatively large doping densities and intense, narrow band optical excitation are required for efficient upconversion pumping by cooperative energy transfer. These conditions can be readily satisfied in a number of materials and this upconversion energy transfer process is quite common. Similar to the sequential

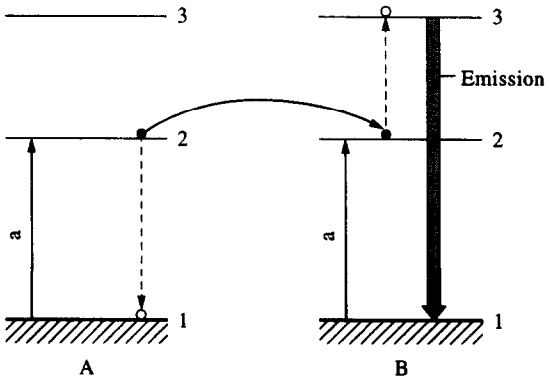

Fig. 2. Cooperative energy transfer upconversion between two three-level ions labeled "A" and "B", respectively. The solid circles represent population in level 2 prior to the energy transfer interaction, while the open circles represent population in levels 1 and 3 subsequent to energy transfer. The dashed arrows indicate the intra-ion energy flow path, while the curved arrow illustrates the direction of energy flow between the two ions. The heavy line labeled "emission" shows the visible radiative transition produced by the cooperative energy transfer interaction.

two-photon absorption upconversion process described above, simultaneous absorption of photons by ions A and B is not required for cooperative energy transfer. The long lifetime of metastable level 2 allows the excitation of the two neighboring ions to occur sequentially within a given time frame. As excitation energy in a crystal lattice migrates or diffuses, this type of upconversion can be observed even under weak excitation conditions.

Most solid state lasers produce fundamental radiation in the infrared. Nd:YAG is one of the most common trivalent rare earth ion-doped solid state lasers. The crystalline host YAG ($Y_3Al_5O_{12}$) is a garnet and the laser can operate at either 1.06 μm or 1.3 μm. Another common solid state laser is Ti:sapphire, a commercially available trivalent transition ion-doped tunable laser with a peak emission wavelength at 780 nm. To convert the fundamental infrared emission to the visible, non-linear optical techniques such as harmonic generation or optical parametric oscillation (OPO) are generally employed. There are several stringent conditions relating to the infrared beam quality, beam divergence, polarization orientation, crystal temperature and crystal axis alignment that must be satisfied when using non-linear methods. Poor conversion efficiency will result if these conditions are not met. In addition, non-linear techniques are most appropriate for Q-switched, pulsed infrared lasers. Because of the strong dependence of the efficiency on the fundamental power, non-linear conversion of cw radiation must be performed within a laser resonator cavity or in an external cavity. The intracavity technique often brings about unwanted amplitude instability unless the laser is operated in single longitudinal mode, while the external cavity requires not only a single frequency input beam but an intricate feedback mechanism to ensure that the external cavity is continuously in resonance with the single frequency input radiation.

In contrast, upconversion laser emission is an effective means of converting infrared radiation to the visible without many of the constraints associated with non-linear optical techniques. Infrared beam requirements for upconversion are similar to those for other longitudinal laser pumping techniques. Common examples of longitudinally pumped lasers include argon ion–pumped dye or Ti:sapphire lasers. Good transverse mode quality (TEM_{00}) is important to achieve a high optical excitation density within the upconversion crystal but alignment of the infrared beam polarization is only important when the absorption of the pump flux is strongly polarization-dependent. As many upconversion lasers operate at cryogenic temperatures, the absorption bandwidths are narrow and should be matched by the pump laser output bandwidth. These conditions are easily satisfied with the efficient, tunable infrared solid state laser sources that are commercially available, making upconversion a strong alternative to non-linear optical conversion.

Rare earth ions produce upconversion over a wide range of wavelengths in the visible and one is not restricted to a given harmonic of the fundamental wavelength. For example, second harmonic generation produces 400 nm output from a nominally 800 nm laser diode. Longer visible wavelengths can be accessed by changing the wavelength of the laser diode, but the longest wavelength emitted by AlGaAs diodes is approximately 850 nm. By contrast, upconversion in trivalent Er produces 550 nm emission when pumped at 800 nm. When pumping a Pr-doped fiber, 800 nm emission from a laser diode produces tunable upconversion laser emission in the blue, green, orange and red.

This paper will present a review of upconversion laser processes. In Section 2 an overview of upconversion energy transfer and pumping will be described. The three observed types of upconversion will be discussed qualitatively. Section 3 contains the bulk of the review work. After a brief review of the relationship between the laser oscillation fundamentals and upconversion laser emission, the conditions for efficient laser resonator design and complementary pump optics are discussed. The section then presents recent experimental results obtained with upconversion in Er:YALO. Er:YALO is of unique interest for this review in that the three types of upconversion pump mechanism are observed when pumping in the 800 nm absorption band. Some of the more interesting facets of upconversion laser

emission can be illustrated using this crystal as an example. The section then concludes by summarizing other upconversion laser results, including room temperature fiber upconversion. A table of upconversion lasers and wavelengths is also provided. The final technical section describes two additional aspects of upconversion. The first discusses upconversion as a loss mechanism. When attempting to produce conventional infrared emission in rare earth doped materials, the energy transfer processes associated with upconversion deplete the upper laser level and reduce the operating efficiency. The second effect is complementary to the first, in that upconversion can also remove population from the metastable terminal level of a conventional infrared laser. This enhances infrared laser emission and it has been suggested that this process allows cw operation of a laser where the terminal level lifetime is longer than that of the upper laser level.

2. UPCONVERSION PROCESSES

2.1. *Introduction*

Generally, three types of upconversion pump processes have been observed to produce upconversion lasers. All pump processes are characterized by photon absorption and subsequent energy transfer. In the case of sequential two-photon absorption, energy transfer takes the form of multiphonon relaxation between levels of a single ion. Photon absorption is followed by relaxation in which the ion releases part of the absorbed energy to the crystal lattice. More often, upconversion energy transfer takes place between two neighboring ions. In cooperative upconversion, two ions in excited states interact as a donor–acceptor ion pair. The two ions may occupy identical states but this is not a requirement. As a result of the cooperative energy exchange process the acceptor ion is promoted to a higher excited state while the donor ion relaxes to the ground state. Photon avalanche upconversion is the third and perhaps the most complicated upconversion pump process, involving energy transfer between an excited ion and a ground state ion. This process is similar to quenching and results in both ions populating a level intermediate in energy to the excited state originally occupied by the donor ion.

Each process will be described using basic three-level ions, leaving the details of actual upconversion pumping of rare earth ions to Section 3. It is important to bear in mind that even the most straightforward examples of upconversion are often highly complex, involving numerous competing energy transfer processes. As a result, our understanding of these pump processes in a specific rare earth ion doped system is often incomplete. Fortunately, this has not prevented the continued development of efficient upconversion pumped visible lasers.

Descriptions of the various upconversion processes will be presented below in a qualitative manner. For more information on the rich diversity of upconversion pump processes, the reader is referred to two excellent reviews of energy transfer-induced fluorescence that appear in the literature. A paper by Auzel[1] provides numerous examples of upconversion mechanisms and describes much of the pioneering work performed by that author. A review by Wright[2] presents a mathematical description of ion pair interactions and describes the kinetics of energy transfer. The focus of Wright's review is Yb^{3+}-sensitized upconversion in co-doped crystals but many of the conclusions are applicable to singly doped upconversion systems as well.

2.2. *Sequential two-photon absorption upconversion*

Sequential two-photon absorption, also called sequential two-step absorption, is the most intuitive upconversion process. It is also one of the best-known types of upconversion, having been discussed by Bloembergen as the basis for an infrared quantum counter.[3] The upper state is populated by the sequential absorption of two photons. The first photon populates

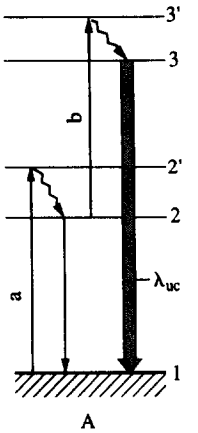

Fig. 3. Sequential two-photon absorption upconversion in a modified three-level ion. Population in level 2′ and 3′ decays rapidly to level 2 and level 3, respectively. Wavy arrows indicate non-radiative decay. The arrow labeled "λ_{uc}" shows the radiative transition resulting from this upconversion pumping mechanism. Ionic levels 1, 2 and 3 represent the same states as indicated in Fig. 1.

a long-lived state intermediate in energy between the ground state and the upper fluorescing state. A second photon promotes this ion from the intermediate state to the upper emitting level.

Sequential two-photon absorption is illustrated in Fig. 3. The ion energy levels are similar to the three-level system illustrated in Fig. 1 but with levels 2′ and 3′ included. These additional levels make the illustrated system more representative of the actual level structure typical of a rare earth ion involved in upconversion. Pumping is initiated by the absorption of photon "a" resonant with the wavelength of the $1 \rightarrow 2'$ transition. Relaxation to level 2 is rapid and generally occurs through multiphonon non-radiative decay. Level 2 is metastable and can, in turn, decay radiatively to the ground state. Multiphonon non-radiative decay of the metastable state is also possible but the non-radiative transition probability is low since the energy gap between the metastable state and the next lower level (the ground state in the case of the ion shown in Fig. 3) is typically large compared to the phonon energy. In Fig. 3 decay of metastable level 2 is considered to be entirely radiative and lifetimes of this level in the trivalent rare earth ions range between 1 and 10 ms.

If a second photon "b" arrives at the excited ion site before the metastable state decays to the ground state it can induce the transition to level 3′. Subsequent relaxation from level 3′ populates level 3. Typically, level 3 has a lifetime of $\sim 100\ \mu$s, appropriate for good energy storage, and a high cross section for emission to level 1. The $3 \rightarrow 1$ transition produces the observed upconversion-pumped visible emission, as the transition wavelength (λ_{uc}) is shorter than that of either photon "a" or "b". Decay from level 3 in this simplified representation occurs through fluorescence to level 1. The time frame for the arrival of photon "b" at the site of an ion in metastable level 2 is determined by the metastable state lifetime τ_2. The intensity of the pump field of "b" photons should therefore be as high as possible to produce efficient upconversion. To see this, the pump rate coefficient for the $2 \rightarrow 3$ transition, W_{23} can be written as

$$W_{23} = \left[\frac{\sigma_{23} I_b}{h\nu_b}\right] \tag{1}$$

where σ_{23} is the absorption cross section for the $2 \rightarrow 3'$ transition, I_b is the "b" photon pump intensity, $h\nu_b$ is the "b" pump photon energy and the relaxation transition $3' \rightarrow 3$ is assumed to be rapid. The population in level 3, n_3, is determined by the rate equation

$$\frac{dn_3}{dt} = W_{23}n_2 - W_{31}n_3 \tag{2}$$

where W_{31} is the upconversion fluorescence transition rate coefficient given by

$$W_{31} = \frac{1}{\tau_3}, \tag{3}$$

τ_3 is the (fluorescence) lifetime of level 3 and n_2 is the number density of ions in the metastable state. In the steady state $dn_3/dt = 0$ and

$$W_{31}n_3 = W_{23}n_2 \tag{4}$$

Equation (4) shows the direct relationship between the $3 \rightarrow 1$ fluorescence intensity and both the "b" pump photon intensity and the steady state population in the metastable state. From the rate equation for the population in the metastable level we can obtain the explicit dependence of the fluorescence intensity ($W_{31}n_3$) on the lifetime of the metastable level 2:

$$\frac{dn_2}{dt} = W_{12}n_1 - W_{23}n_2 - \frac{n_2}{\tau_2} \tag{5}$$

where n_1 is the population in the ground state. The pump rate coefficient W_{12} is given by

$$W_{12} = \frac{\sigma_{12}I_a}{h\nu_a} \tag{6}$$

where σ_{12} is the absorption cross section for the $1 \rightarrow 2'$ transition, I_a is the intensity of pump photons "a", $h\nu_a$ is the "a" photon energy and the relaxation rate for the $2' \rightarrow 2$ transition is assumed rapid. The steady state solution to Eqn (5) is

$$W_{12}n_1 = W_{23}n_2 + \frac{n_2}{\tau_2} \tag{7}$$

For fixed pump intensities I_a and I_b, the metastable state population varies directly with the metastable state lifetime unless $W_{23} \gg 1/\tau_2$. If this inequality holds, implying a long metastable lifetime relative to the $2 \rightarrow 3$ pump transition rate, then the fluorescence intensity is linearly proportional to I_a and I_b but independent of τ_2 since $W_{12}n_1 = W_{23}n_2 = W_{31}n_3$. Otherwise, from Eqns (4) and (7) the fluorescence intensity increases as τ_2 increases.

In the most general case, the wavelength of photon "a" is different than that of photon "b". This creates several problems in terms of pumping. One is the requirement for two different tunable pump lasers. If the pump sources are two dye lasers, for example, the excitation source for the pump lasers must be considered. This would generally be an ion laser for cw pumping or a doubled Nd:YAG laser for pulsed pumping. In either case, the excitation laser would have to have its output divided between the two dye lasers, reducing the overall drive power to each dye. Alternatively two excitation lasers could be used, driving up the costs of the pump system. If pulsed pumping is used, the pulses from each of the lasers must be synchronized as well in order to reach the crystal at approximately the same time. This is not particularly complicated, however, given the long lifetimes of the states involved in upconversion.

A more demanding problem in using two pump lasers arises from alignment and beam quality issues. For effective cw upconversion the pump beams are generally focused to a spot of 50 μm or less in diameter. The two pump beams must overlap within the focused beam diameter along the entire propagation path through the crystal. If a single lens is used, it should be corrected for chromatic aberration and the possibility of wavelength dispersion

within the crystal suggests that the pump beams be oriented for normal incidence. The most straightforward alignment arises from polarization beam combination, in which a polarizing beam splitter cube is used in reverse to combine two different beams with orthogonal polarization. In order to be effective, however, the pump sources must be linearly polarized and the crystal should not exhibit a strong polarization dependence of the absorption coefficient. If polarization-combination is not appropriate, then other, less efficient techniques can be used such as a dichroic beamsplitter or angular multiplexing. Finally, if the two pump lasers are not mode matched the focused spot size of each beam will not be identical, leading to further loss of pump efficiency.

2.3. *Cooperative energy transfer upconversion*

The presence of a metastable state, important for sequential two-photon absorption, is also a requirement for cooperative energy transfer upconversion. As a consequence many ions that demonstrate efficient sequential two-photon absorption upconversion pumping also exhibit cooperative energy transfer. In some ions the cooperative process is substantially more efficient than sequential two-photon absorption upconversion. It has been found in such cases that when cooperative upconversion occurs by pumping the $1 \rightarrow 2$ transition, the addition of pump flux to stimulate the $2 \rightarrow 3$ transition has little effect on the upconversion fluorescence intensity. Upconversion by cooperative energy transfer has the important advantage of requiring a single pump wavelength, obviating the problems relating to beam alignment and pump efficiency that are associated with sequential two-photon absorption using two different pump lasers.

Much of the early research on upconversion during the 1960s was performed on co-doped crystals, particularly fluorides. One of the ions, typically Yb^{3+}, is the "sensitizer". The sensitizer serves the function of energy donor, absorbing infrared radiation and cooperatively transferring energy by one or more steps to the co-dopant ion. Yb^{3+} has only one excited state and cooperative upconversion is initiated by absorption of radiation at approximately 1 μm. The lifetime of the excited state in Yb^{3+} is about 1 ms. The co-dopant, usually Er^{3+}, Ho^{3+} or Tm^{3+}, is the energy acceptor. Successive cooperative donor–acceptor interactions produce visible emission from the excited state of the acceptor ion.

In singly doped crystals cooperative upconversion is somewhat different, since the intermediate metastable state can be populated indirectly by absorption and subsequent non-radiative relaxation. Figure 4 illustrates energy transfer in a schematic ion pair. As in Fig. 3, the three-level ion is shown with levels 2′ and 3′ included to be more representative of the actual level structure of ions undergoing cooperative upconversion. Pumping is

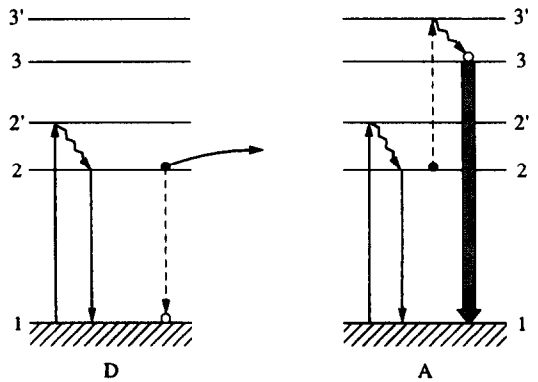

Fig. 4. Cooperative energy transfer upconversion for two modified three-level ions. Ions are labeled "D" and "A" for donor and acceptor, respectively.

initiated by the absorption of a photon by each of the ions labeled "A" and "D" (for acceptor and donor, respectively). The photon wavelength corresponds to the $1 \rightarrow 2'$ transition and rapid relaxation from level $2'$ populates level 2. As in sequential two-photon absorption, level 2 is metastable. Population in level 2 may decay by radiation to the ground state as shown by the solid arrows in Fig. 4, or may be removed by cooperative upconversion. In the latter case the donor ion transfers its energy to the acceptor ion. This process is indicated in the figure with dashed lines and results in ion A being promoted to level $3'$. Rapid relaxation from level $3'$ populates level 3, which can subsequently radiate in the visible on the $3 \rightarrow 1$ transition.

It is unusual for the $2 \rightarrow 1$ transition energy to be identical to that of a transition between levels 2 and $3'$. More often there is some excess energy or an energy deficit for which the lattice must compensate. Such an energy transfer is referred to as "phonon assisted" and the transfer rate is affected by the energy mismatch. Effective cooperative upconversion requires that the donor–acceptor ion pair be located near one another. For dipole–dipole interactions the energy transfer rate varies as r^{-6}, where r is the separation between the two ions. This underscores the need for high intensity pump light in the excitation volume. Other effects notwithstanding, the radial dependence of the dipole–dipole interaction suggests that a relatively high concentrations of rare earth ions will also increase the energy transfer rate. Another factor that influences the energy transfer rate is diffusion. If diffusion of excitation occurs, then energy will migrate among donor ions within the crystal lattice until a proximate acceptor ion is found. Since the donor–acceptor ion pairs with the shortest separation have the highest energy transfer rates, an excitation gradient may be established within the crystal. If no diffusion occurred the donor–acceptor pair density distribution would favor pairs with the largest radial separation; pairs with shorter separations would be more likely to undergo cooperative energy transfer. One manifestation of this would be non-exponential decay of fluorescence on the $3 \rightarrow 1$ transition, reflecting the different transfer rates for the different pair separations. However, in many crystal systems, the upconversion fluorescence decay for pulsed excitation is exponential, indicating rapid energy diffusion. In this case the spatial inhomogeneities are largely removed and the rate limiting step of direct energy transfer determines the time dependence of the fluorescence. These concepts are described in more detail in Ref. 2.

The kinetics of upconversion by cooperative energy transfer can be described for a three-level ion, assuming rapid relaxation from levels $2'$ and $3'$ to levels 2 and 3, respectively. The time dependent equation for the metastable level is

$$\frac{dn_2}{dt} = W_{12}n_1 - \frac{n_2}{\tau_2} - 2\gamma n_2^2 \tag{8}$$

while the time dependence of the fluorescing level is

$$\frac{dn_3}{dt} = \gamma n_2^2 - W_{31}n_3. \tag{9}$$

In the above equations γ is the ion pair cooperative upconversion rate coefficient and the factor of two in Eqn (8) is required to account for the fact that two energy quanta from level 2 are required to produce one ion in level 3.

In the steady state the fluorescence rate is equal to the cooperative energy transfer rate,

$$W_{31}n_3 = \gamma n_2^2 \tag{10}$$

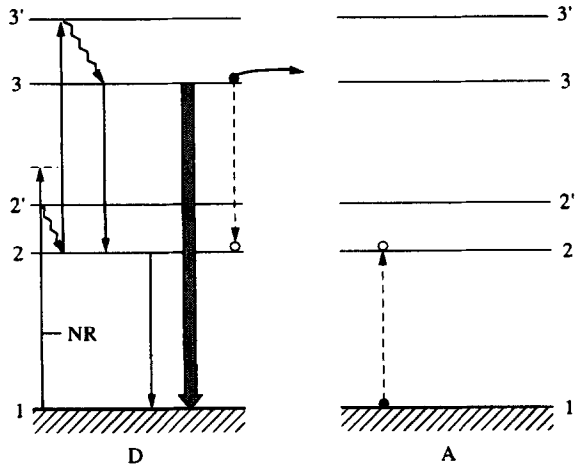

Fig. 5. Photon avalanche upconversion in modified three-level ions. The labels "D" and "A" refer to the donor and acceptor ions, respectively and the solid vertical arrows illustrate radiative transitions (absorption and emission). Three competing processes involving level 3 are illustrated. One involves energy transfer between level 3 of the D ion and level 1 of the A ion, resulting in both ions occupying level 2. The other two involve radiative decay from level 3 to level 1 or level 2. Radiative decay from level 2 is also shown. The arrow labeled "NR" illustrates non-resonant absorption from level 1 to level 2'.

By applying the steady state condition to Eqn (8) as well, it can be seen that for a given optical pump intensity (fixed W_{12}) the fluorescence emission rate increases with the metastable state lifetime since

$$2\gamma n_2^2 + \frac{n_2}{\tau_2} = W_{12} n_1 \tag{11}$$

If τ_2 increases, n_2 also increases, thereby increasing n_3.

2.4. *Photon avalanche upconversion*

Photon avalanche upconversion, sometimes called absorption avalanche, is among the most efficient types of upconversion. It is an unusual pump mechanism in that it is produced by absorption from an excited state of the ion. In photon avalanche pumping the pump photon wavelength is resonant with a transition from the intermediate metastable level to a more highly excited state. Since photon absorption directly populates the upper visible-emitting energy level, energy transfer must produce the population in the intermediate state that absorbs the pump flux. Without some mechanism for filling the metastable level, absorption and hence upconversion emission will cease. Energy transfer that replenishes the metastable state must involve downconversion or quenching since the level populated by photon absorption is higher in energy.

There are several aspects of photon avalanche upconversion that will be addressed in this section: One relates to the mechanism by which the metastable state population is initially established; another issue involves the energy transfer mechanism for replenishing the metastable level population. Typically several such mechanisms are possible. However, as the term "avalanche" implies, under certain conditions the pump flux produces a large increase in the steady state metastable population. It is therefore important to not only understand the energy transfer processes involved in photon avalanche but also the conditions under which avalanche occurs.

Figure 5 shows a schematic representation of a donor–acceptor ion pair involved in photon avalanche upconversion. Once again a modified three-level ion is used as the upconversion kinetics are far easier to understand. Analytical expressions can be derived for such a model and will be presented below. To unfold the sequence of events involved in photon avalanche, assume that the donor ion (ion D) is in metastable level 2 prior to turning on the pump flux. A neighboring acceptor ion (ion A) is in the ground state. Optical radiation resonant with the $2 \rightarrow 3'$ transition is then turned on and after rapid relaxation from level $3'$ the donor ion occupies level 3. In sequential two-photon absorption and cooperative energy transfer upconversion, decay from level 3 was discussed solely in terms of the $3 \rightarrow 1$ radiative transition. This transition produces visible emission and constitutes one of the steps in the photon avalanche upconversion process as well. However, an alternative decay mechanism involves energy transfer from the donor ion to a neighboring ground state ion. This non-radiative process is well-known and has several names, including ion pair relaxation, cross relaxation energy transfer and quenching. The result of this ion pair interaction is that the donor ion loses part of its energy to the acceptor, producing two ions in the metastable state.

The essence of the avalanche process is that one ion initially in the metastable state (ion D) produces two ions in this state as a result of photon absorption and subsequent energy transfer. Under appropriate pumping conditions, the two can produce four, the four eight and so on, giving rise to an avalanche of ion population occupying the metastable level. The avalanche process requires a minimum pump intensity and is characterized by a pump threshold. This threshold condition is unique among the three upconversion pump mechanisms and is a useful means of verifying experimentally that photon avalanche is indeed occurring.

The avalanche pumping described above assumes that some fraction of ion population is initially in the intermediate metastable level. While this might be true if the metastable level were thermally excited, photon avalanche upconversion can be observed at cryogenic temperatures. For an energy gap of a few thousand wavenumbers (cm^{-1}) and an operating temperature of 10°K, the thermal population in the metastable state is negligible. The most likely mechanism for producing an initial population in the metastable state is non-resonant absorption. This is illustrated in Fig. 5 by the arrow labeled NR. In this process a photon that is resonant with the $2 \rightarrow 3'$ transition promotes an ion from the ground state to level $2'$. Level 2 is then populated by relaxation from level $2'$. The non-resonant transition probability will depend on the energy difference between the $1 \rightarrow 2'$ resonant wavelength and the wavelength of the pump photons. From modelling results of photon avalanche upconversion the ratio of the transition probability for the resonant ($2 \rightarrow 3'$) to the non-resonant ($1 \rightarrow 2'$) transition is typically 5,000–10,000. However, even this low rate is sufficient to initiate the avalanche process.

Consideration of the non-resonant absorption step in the initial phase of photon avalanche upconversion underscores a similarity between this process and sequential two-photon absorption. Both processes utilize sequential absorption of two photons to populate the upper level. The difference in photon avalanche upconversion is the low pump efficiency of the non-resonant first step and the diminished importance of this process for pump intensities that exceed the avalanche threshold. Below the avalanche threshold, upconversion results from both sequential two-step absorption and ion pair relaxation as illustrated in Fig. 5. Above threshold the ion pair relaxation process accelerates and dominates the filling of the metastable level. Visible emission via the $3 \rightarrow 1$ transition then competes directly with the non-radiative ion pair interaction, as both processes deplete the n_3 population.

Following the calculations of Joubert *et al.*[4] the conditions for photon avalanche pumping can be articulated analytically. For this calculation we include the additional process of decay

from level 3 to level 2. The processes illustrated in Fig. 5 give rise to the following set of coupled population kinetics equations:

$$\frac{dn_3}{dt} = W_{23}n_2 - \frac{n_3}{\tau_3} - k_q n_1 n_3$$

$$\frac{dn_2}{dt} = W_{12}n_1 - W_{21}n_2 - W_{23}n_2 + 2k_q n_1 n_3 + W_{32}n_3$$

$$\frac{dn_1}{dt} = W_{31}n_3 + W_{21}n_2 - W_{12}n_1 - k_q n_1 n_3 \tag{12}$$

where k_q is the cross relaxation rate coefficient and W_{21} and W_{32} are the rate coefficients for the $2 \rightarrow 1$ and $3 \rightarrow 2$ transitions, respectively. The level populations are normalized so that $n_1 + n_2 + n_3 = 1$. Furthermore,

$$(W_{31} + W_{32})^{-1} = \frac{1}{\tau_3} \equiv W_3 \tag{13}$$

and the fraction of the level 3 population that decays to level 1 is designated as x while the fraction that decays to level 2 is $1 - x$.

Solving Eqn (12) under steady state conditions shows that when $k_q > xW_3$ two upconversion operating regimes can exist. These regimes are determined by the pump intensity and the pump intensity that produces the transition between the two regimes is defined as the threshold intensity for photon avalanche upconversion. Below threshold, population in level 2 results primarily from non-resonant absorption. The level 3 population and hence the upconversion emission intensity are therefore relatively low. Above threshold the population dynamics of level 2 are dominated by ion pair relaxation and the upconversion emission intensity increases by several orders of magnitude.

Photon avalanche upconversion cannot take place unless $k_q > xW_3$. This condition re-states the competition for level 3 population between ion pair relaxation and radiation. Unless ion pair relaxation is fast compared to decay from level 3, avalanche population of level 2 will not occur. For the model shown in Fig. 5 the threshold pump intensity can be obtained from the threshold rate coefficient W_{23}^{th}, which is

$$W_{23}^{th} = \frac{W_{21}(k_q + W_3)}{k_q - xW_3}. \tag{14}$$

The lowest photon avalanche thresholds will be associated with systems having high ion pair relaxation rate coefficients and long metastable state lifetimes. In the limit determined by $k_q \gg W_3$, the threshold pump rate coefficient is $W_{23}^{th} = W_{21}$. In this limit the avalanche threshold is at its lowest value determined by $W_{21} = 1/\tau_2$. This can be understood from the ion dynamics, where from Eqn (12) the filling of level 2 by ion pair relaxation competes directly with decay from this level. Upconversion emission depends on the population in level 3, but the $2 \rightarrow 3$ transition rate $W_{23}n_2$ depends directly on the population in level 2. In order to achieve a significant increase in the population of level 3, the $2 \rightarrow 3$ transition rate must be at least as fast as the decay rate from level 2. Otherwise the population produced in level 2 by ion pair relaxation will not be effectively promoted to level 3 and upconversion emission will not demonstrate an avalanche effect.

As a result of the unusual nature of photon avalanche-pumped upconversion fluorescence it is generally straightforward to verify experimentally that this process is taking place. Having first established that upconversion emission results by pumping a transition from the metastable state, one must observe either of two additional effects in order to positively identify photon avalanche. The first is the appearance of a threshold in the variation of upconversion fluorescence intensity with pump power. This is characterized by a large

increase in the upconversion fluorescence intensity at a specific value of the pump intensity. An example of the pump threshold behavior is shown schematically in Fig. 6. Below threshold the fluorescence intensity is due primarily to non-resonant two-photon absorption and increases quadratically (slope of 2 on a logarithmic plot). Well above threshold the slope is also 2, reflecting the two-photon pumping requirements for photon avalanche. The large increase in fluorescence intensity at threshold results from the additional level 2 population produced by photon avalanche upconversion pumping. The appearance of a threshold confirms the presence of this pump mechanism.

One cannot rule out the possibility that photon avalanche pumping is taking place even if a threshold is not observed in the fluorescence intensity variation measurement for a given crystal. In fact there are three different conditions that would produce this result. The first is that the avalanche threshold occurs at a very low pump intensity. In this case virtually all of the experimentally acquired fluorescence data points are above threshold and represent photon avalanche-pumped upconversion. The second alternative is that although photon avalanche upconversion can occur in the crystal, the threshold intensity requirement exceeds the available pump power. The third alternative is that photon avalanche upconversion is not possible at all due to the relative magnitudes of the coefficients for ion pair relaxation and the $3 \rightarrow 1$ fluorescence transition. In this case upconversion fluorescence due to both non-resonant sequential two-photon absorption and ion pair relaxation will be observed over the entire range of pump intensity used.

The possibility that threshold behavior is not observed because of a low threshold intensity requirement for photon avalanche can be distinguished from the other two alternatives by a time-dependent measurement. This measurement produces the second of the two phenomena that can be used to positively identify photon avalanche. The solution to the time dependent equations given in Eqn (12) indicates that the temporal dependence of the onset of photon avalanche-pumped upconversion fluorescence has a unique shape. In Fig. 7(a) the time dependence of upconversion fluorescence emission is shown for a system pumped with

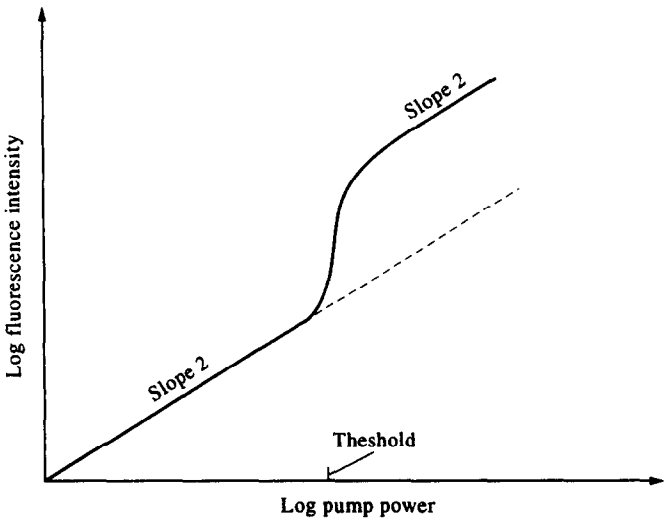

Fig. 6. Schematic illustration of the variation of upconversion fluorescence intensity with pump power for a rare earth ion-doped crystal pumped by photon avalanche upconversion. The curve is shown on a logarithmic plot and the threshold for photon avalanche is marked. At pump power levels below threshold the fluorescence intensity is seen to increase "linearly" with a slope of 2, corresponding to a quadratic dependence on pump power. At the threshold pump power the fluorescence undergoes a large increase in amplitude but eventually becomes quadratic again at higher pump power. The fluorescence intensity increase near threshold is typically several orders of magnitude.

an intensity below threshold. The pump waveform is a square pulse of duration equal to several times the metastable lifetime τ and the fluorescence increases as $1 - e^{-t/\tau}$ to its steady state value. Above threshold the time dependence of the upconversion fluorescence is markedly different as shown in Fig. 7(b). In this case the onset of upconversion fluorescence shows a concave region. The concave shape is a "signature" of photon avalanche upconversion and is due to the build-up time for the avalanche population in level 2. In addition, the transmission of the pump flux by the crystal will decrease as a function of time as the population in level 2 increases during the pulse. For non-resonant sequential two-photon absorption there is essentially no change in sample transmission with time. The temporal dependence of the optical transmission for a crystal undergoing photon avalanche upconversion is illustrated in Fig. 8.

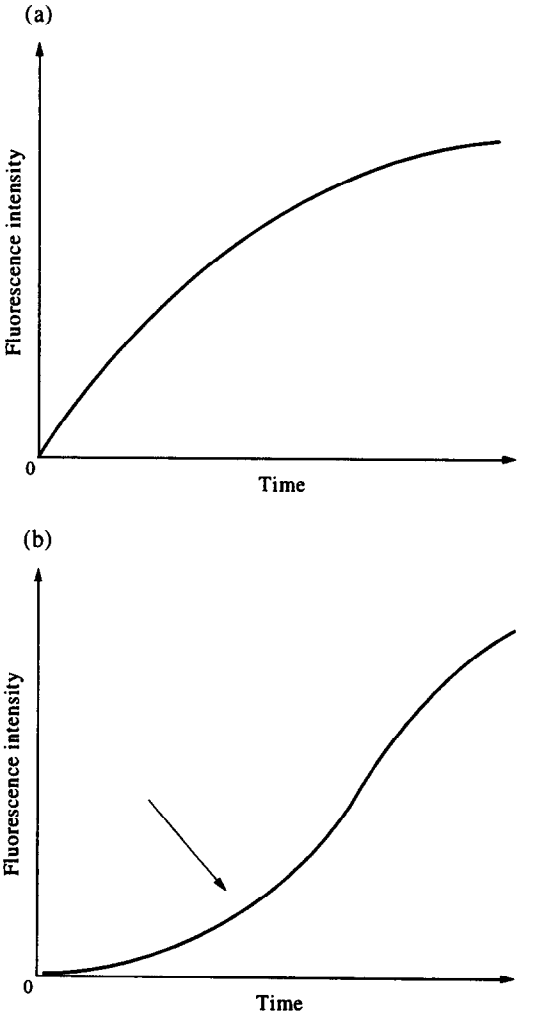

Fig. 7. (a) Temporal dependence of the upconversion fluorescence emission intensity for a square excitation pulse. The pulse duration exceeds the range of the time axis. The curve is shown schematically on linear axes and the shape is approximately given by $1 - e^{-t/\tau}$, where τ is the upper state lifetime. The leading edge of the excitation pulse occurs at $t = 0$. This type of temporal fluorescence curve is not representative of photon avalanche upconversion. (b) Temporal dependence of the upconversion fluorescence emission intensity under pulsed excitation conditions similar to Fig. 7(a), but for a crystal undergoing photon avalanche upconversion. Arrow indicates the concave rising portion of the fluorescence curve, which is a "signature" of photon avalanche upconversion.

Finally, it should be emphasized that despite its complexity photon avalanche upconversion can be highly efficient. One reason for this is the high density of acceptor (ground state) ions that naturally surround each donor ion. This is beneficial for dipole–dipole energy transfer, which as mentioned has an r^{-6} dependence on pair separation. In general, the major limitation to the efficiency of photon avalanche upconversion arises from the low absorption of pump flux due to the relatively low steady state density of absorbers in the metastable level. When the upconversion efficiency is based on the fraction of absorbed pump power it can be as high as 40%.

2.5. *Summary of upconversion processes*

In this section three types of upconversion processes have been described using three-level ions. One of the goals of this section is to describe sequential two-photon absorption upconversion, cooperative energy transfer upconversion and photon avalanche upconversion in a schematic manner. These are the pumping mechanisms that have produced upconversion laser emission. Numerous variations of these mechanisms have been observed in different rare earth doped crystals and will be described in more detail in the next section. Occasionally the terms describing the various types of energy transfer and upconversion pumping mechanisms are used inaccurately in the literature, making for confusing reading for the novice. By providing a basic discussion of upconversion processes in this section it is hoped that the reader will be better prepared for the ambiguities that seem to find their way into the literature on upconversion.

Finally, it is worth noting that there is an interesting symmetry in the three upconversion pumping mechanisms. Sequential two-photon upconversion relies on two photons at different wavelengths, "a" and "b", to populate the upper emitting level of the ion. Photon "a" promotes the ground state ion to the metastable intermediate state, while photon "b" promotes the ion from the metastable state to the upper, emitting level. Cooperative upconversion and photon avalanche upconversion are both related to, and distinct from, sequential two-photon absorption upconversion in that the former mechanism relies only on photons "a" while the latter mechanism relies only on photons "b".

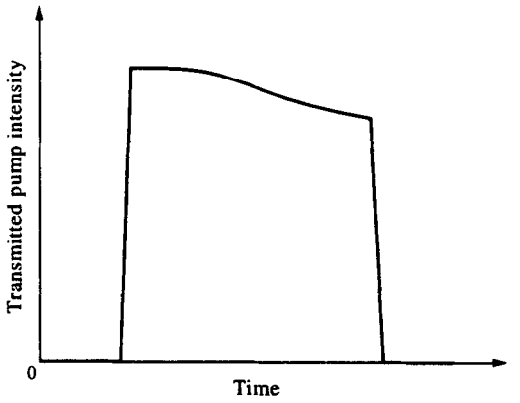

Fig. 8. Schematic representation of the temporal dependence of the pump intensity transmitted by a crystal undergoing photon avalanche upconversion. The pump wavelength is resonant with a transition from the metastable level. The population in this level increases with time as the photon avalanche process progresses, increasing the absorption of the pump flux.

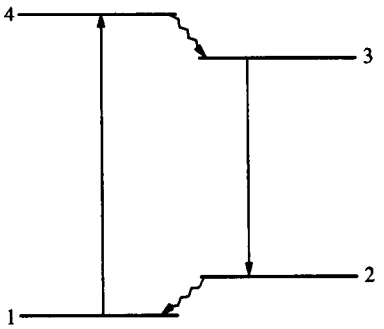

Fig. 9. Schematic representation of optical pumping and emission in a typical four-level ion.

3. UPCONVERSION LASERS

3.1. *Introduction*

In a conventional optically-pumped laser the pump photon energy is higher than that of the photons emitted by the laser. For an upconversion laser the reverse is true. Populating the upper laser level requires two or more pump photons and as a result the laser output may display a non-linear dependence on pump flux. In this section we will begin by describing the laser oscillation conditions for upconversion lasers. These criteria are largely similar to those for conventional lasers but the emphasis will be placed on discussing the unique requirements for upconversion lasers. Specific examples of upconversion lasers will then be described. Experimental results obtained with an Er:YALO upconversion laser are described in detail, followed by a more general discussion of the range of upconversion lasers that have been demonstrated to date. Power, mode of operation, operating temperature and output wavelengths will be addressed for numerous upconversion lasers.

3.2. *Laser oscillation conditions*

3.2.1. *Introduction.* Laser emission is produced by resonant feedback through an optical amplifying medium. The optical amplification occurs through stimulated emission and a condition for amplification is that a population inversion be established within the medium. A photon entering such a medium will stimulate additional photons to produce emission at the same wavelength, producing optical gain. The photons experience loss as well from a number of sources within the laser resonator. In order to experience net gain and, hence, produce laser emission the single pass unsaturated gain must exceed the loss.

Lasers are differentiated as three-level or four-level systems. In the former the terminal level for the laser transition is either the ground state or a long-lived metastable state. As a consequence of lasing the population in the terminal level builds up and the inversion eventually vanishes. Three-level lasers are therefore said to be self-terminating. A four-level system is quite different and is illustrated schematically in Fig. 9. Referring to the figure, the pump photons are resonant with the $1 \rightarrow 4$ transition. Rapid relaxation from level 4 populates level 3 and laser emission is produced by the $3 \rightarrow 2$ transition. If the energy gap between level 2 and level 1 is sufficiently large the equilibrium population in level 2 will be small. Therefore an inversion between levels 3 and 2 can be established with only a small population in level 3, producing gain in four-level lasers with very low pump power. On the other hand, rapid de-excitation of level 2 to level 1 is required to prevent the transition from being "blocked", so the energy gap between levels 2 and 1 should not be larger than a few times the phonon energy. If removal of population in the terminal laser level is slow, the laser transition will be self-terminating. Many laser systems are neither true three-level or four-level systems, and are sometimes referred to as "quasi-three-level" or "quasi-four-level" lasers.

The first observation of laser emission from a solid state gain element was made by Maiman in 1960. A pulsed ruby laser was used and since then coherent electromagnetic radiation has been generated from a diverse range of solid state materials. The first upconversion laser was reported[5] in 1971 in co-doped Ho,Yb:BaY_2F_8. The laser emission wavelength was 554 nm and the crystal was maintained at 77°C. Numerous other upconversion materials have been demonstrated over the past 25 years with operating temperatures ranging from cryogenic up to room temperature and wavelengths ranging from the near ultraviolet to the near infrared. The past decade has been a particularly active time for upconversion laser research due to both the development of efficient, tunable, near infrared pump lasers such as Ti:sapphire lasers and advances in crystal growth technology.

Efficient production of upconversion laser emission has somewhat different requirements than does a conventional laser. While the considerations regarding gain and loss are identical, upconversion pumping has certain unique characteristics. For example, population inversion requirements often dictate cryogenic operation. In 3.2.2 we will consider the gain and loss equations, while in 3.2.3 Q-switched operation of the upconversion laser will be addressed. In 3.2.4 the considerations regarding optimum pump optics and laser resonator design will be addressed. The equations describing laser oscillation and Q-switching will be described only briefly, as much of this information is available in detail in a number of widely used texts[6,7] on the subject.

3.2.2. *Gain and loss.* When an optical beam emerges from a medium with more photons than it had upon entering, the medium is said to have gain. Optical gain occurs at a specific wavelength or over a wavelength range. The same medium may also exhibit loss. What is typically measured by comparing the exiting beam intensity with the entering intensity in a small signal gain measurement is the net gain at the probe beam wavelength. The net gain represents the intrinsic gain minus the loss. From a practical point of view it is desirable to understand the variation of the threshold power and laser output power as a function of readily measured laser resonator parameters. This information can then be used to determine the appropriate design for the resonator and pump optics, issues that will be addressed in 3.2.4.

At cryogenic temperatures, many upconversion lasers can be represented by four-level or quasi-four-level models. The analysis below is based on a four-level laser. The threshold pump power P_{th} is given[8] by

$$P_{th} = \frac{L - \ln R}{G} \tag{15}$$

where L is the double-pass resonator loss and R is the reflectivity of the output coupler at the laser emission wavelength. G is a gain factor that is determined by the dependence of the double-pass gain on pump power and is given by $G = 2g_o\ell/P_{in}$, where g_o is the small signal gain coefficient, P_{in} is the pump power and ℓ is the length of the gain medium. In Eqn (15) the reflectivity of the rear reflector is assumed to be 1. If the loss and gain factor are known we can calculate P_{th} for a given output coupler reflectivity.

The parameters L and G can be determined directly from a Findlay–Clay[9] analysis of the threshold pump power variation with output mirror reflectivity. Rewriting Eqn (15)

$$-\ln R = GP_{th} - L \tag{16}$$

shows that a plot of $-\ln R$ as a function of P_{th} produces a line whose slope is G and ordinate intercept is $-L$. For an upconversion laser the use of the Findlay–Clay analysis brings up two issues. The first is whether the upconversion laser is four-level. In the Findlay–Clay model a four-level laser is defined as one where $n_3 \gg n_2$, where n_2 and n_3 refer to the densities in the upper and terminal laser levels, respectively (see Fig. 9). At the cryogenic temperature used for many upconversion crystal lasers the Boltzmann population factors for the terminal level

are small enough so that the criterion for a four-level laser transition can be easily met. Residual absorption due to thermal population in the terminal laser level simply adds to the passive loss.[10] Terminal level absorption is assumed to be non-saturable and independent of the pump power near threshold.

The second issue is related to the assumption, inherent in the Findlay–Clay model, that the threshold population of the upper laser level is linearly dependent on the pump intensity. While the laser output power for many upconversion pumped lasers depends non-linearly on the pump power, the threshold pump power dependence can under some circumstances be linear. This can be seen by using the model for cooperative upconversion as an example. Note that, although the following discussion is based on the pump dynamics of a nominally three-level ion model, this does not conflict with the Findlay–Clay four-level criterion. For the three-level model we expect that $n_3 \gg n_{1t}$ where n_{1t} refers to the population of the terminal Stark level of ground state level 1.

Equation (9) can be modified to include decay from level 3 by stimulated emission

$$\frac{dn_3}{dt} = \gamma n_2^2 - W_{31} n_3 - n_3 \frac{\sigma_{31} I}{h\nu_L} \tag{17}$$

where σ_{31} is the stimulated emission cross section, I is the intracavity laser intensity and $h\nu_L$ is the laser photon energy. In the steady state the cooperative energy transfer rate equals the emission rate from level 3

$$\gamma n_2^2 = n_3 \left(\frac{\sigma_{31} I}{h\nu_L} + W_{31} \right). \tag{18}$$

The intensity I is related to the double-pass small signal gain $g \equiv 2g_0\ell$ and L by

$$I = I_s \left[\frac{g}{L - \ln R} - 1 \right] \tag{19}$$

where I_s is the saturation intensity given by $I_s = h\nu_L/\sigma_{31}\tau_3$. Combining Eqns (18) and (19) leads to

$$\gamma n_2^2 = \frac{2\sigma_{31}\ell}{\tau_3 (L - \ln R)} n_3^2 \tag{20}$$

where $1/\tau_3 = W_{31}$ (Eqn 3) and g is replaced by $2n_3\sigma_{31}\ell$. Eqn (20) shows a linear dependence of the population in level 3 on that in level 2 under laser operation. From the steady state population in level 2 given by Eqn (11) it can be seen that the dependence of n_2 on the optical pump rate ($W_{12}n_1$) will be quadratic if $2\gamma n_2 \gg 1/\tau_2$, and linear if $2\gamma n_2 \ll 1/\tau_2$. Using a low loss laser resonator along with relatively high reflectivity output mirrors ($R > \sim 0.8$) to perform the Findlay–Clay measurements, both the threshold pump intensity and n_2 will be low. It follows then that the dependence of n_3 on the pump intensity will be approximately linear near threshold. From Eqn (11)

$$n_2 \approx W_{12} n_1 \tau_2 \tag{21}$$

where W_{12} is given by Eqn (6) and from Eqn (20)

$$\gamma n_2^2 = \frac{2\sigma_{31}\ell}{\tau_3 (L - \ln R)} n_3^2 \approx \gamma (W_{12} n_1 \tau_2)^2 \tag{22}$$

Equation (22) shows the linear relationship between the population in the upper laser level and the pump rate, consistent with the assumption in the Findlay–Clay analysis.

An alternative means of obtaining the passive loss is from the relaxation oscillation frequency. When a laser is pumped by a square pulse the initial increase in laser emission is not monotonic. Instead the onset of laser emission is characterized by oscillations or "ringing". These oscillations are damped and after several periods the laser produces a cw output. The passive round trip loss can be obtained from the relaxation frequency by[11]

$$L' = \frac{(2\pi f_r)^2 2\tau_3 \Sigma n_i \ell_i}{P_e c} \tag{23}$$

where f_r is the oscillation frequency, the n_i and ℓ_i refer to the refractive indices and lengths, respectively, of the various components (including air) within the laser cavity, and c is the speed of light. P_e is the "excess pump power" given by $P_e = (P_{in} - P_{th})/P_{th}$ where P_{in} is the pump power used to pump the material. L' includes both the round trip passive resonator loss (L) and the transmission of the output mirror. Comparable results for the loss calculated using Eqns (16) and (23) provides some indication that the approximation represented by Eqn (21) is reasonable.

Resonator losses arise from a variety of factors. Passive losses refer to those losses which are not induced by exciting the gain medium. Distributed passive loss includes absorption and bulk scattering, while non-distributed losses include reflections from anti-reflective (AR) coated surfaces and diffractive losses. The distinction between distributed and non-distributed losses is important as the former scales with the laser rod length. A gain medium exhibiting high distributed losses will not generally improve if the medium length is extended since the gain also scales with the rod length. On the other hand, increasing the length of the gain medium when non-distributed losses are dominant will generally improve the overall laser efficiency.

Active losses include effects such as beam distortion and thermal lensing due to pump-induced index inhomogeneities. Since most upconversion lasers are longitudinally pumped by lasers having high beam quality, index gradients transverse to the upconversion laser axis are generally not a problem. Another source of active loss is due to excited state absorption (ESA). ESA will occur if one of the excited ionic levels can be promoted to a higher excited state by resonant absorption at the upconversion laser emission wavelength. Since upconversion pumping populates one or more long-lived intermediate levels, ESA is a potential problem. However, for upconversion lasers operating at cryogenic temperatures the absorption linewidths are quite narrow and loss due to ESA would require an unlikely coincidence in transition energies. Note also that at these low temperatures there is significant population only in the lowest Stark component of each populated electronic manifold, further reducing the possibility of a coincidence.

On the other hand, for room temperature operation the absorption lines are much broader and the higher Stark levels of the various manifolds are occupied. Thus the possibility of ESA increases with temperature and in fact this is one reason why some crystalline upconversion materials cannot lase at room temperature. Many upconversion transitions terminate on a Stark component of the ground state and in general the Stark level should be located several times kT above the lowest Stark component. At cryogenic temperature the thermal population is generally quite low for Stark levels located only 30 cm^{-1} or more above the first Stark level of the ground state. For these lasers the terminal laser level typically lies within a few hundred wavenumbers of the first Stark level. At room temperature however the laser emission must terminate on a higher lying Stark component to reduce the absorption loss due to the equilibrium population in the terminal level. This red shifts the emission wavelength. In Er-doped materials the red shifted wavelength cannot lase at room temperature due to strong absorption by the metastable state ($^4I_{13/2} \rightarrow {}^2H_{9/2}$). On the other hand the shorter wavelength transition at cryogenic temperatures is not absorbed by any of the excited states involved in upconversion.

The resonator gain and loss also determine the laser output power and slope efficiency for a given pump power P_{in}. For conventional lasers the output power P_{out} is given by

$$P_{out} = \frac{T(\pi w_d^2) I_s}{2} \left[\frac{G P_{in}}{\frac{L}{2} + T} - 1 \right] \tag{24}$$

where w_d is the laser mode waist and T is the transmission of the output coupler. The slope of the power out as a function of input pump power, η_s, is

$$\eta_s = \left(\frac{h\nu_L}{h\nu_p} \right) \left(\frac{\sigma_L - \sigma_{ESA}}{\sigma_L} \right) \left(\frac{T}{T + L} \right) f_a \eta_p \tag{25}$$

where $h\nu_p$ is the pump photon energy, σ_L and σ_{ESA} are the cross sections for stimulated emission and excited state absorption, respectively, f_a is the fraction of incident pump power absorbed by the gain medium and η_p is the fraction of absorbed pump photons that populate the upper laser level. While some upconversion lasers display a linear dependence of the output power on pump power, many do not. In such cases Eqns (24) and (25) can be used in a qualitative manner to gauge the impact of changes in a specific resonator parameter on the upconversion laser output power.

The dependence of the upconversion laser output power on pump power can be obtained under pumping by cooperative energy transfer using the ion model illustrated in Fig. 4. As noted previously, the relative magnitudes of the cooperative energy transfer time, $(\gamma n_2)^{-1}$, and the lifetime of metastable level 2, τ_2, determine the exponent of the dependence of the metastable level population on optical pump flux. The energy transfer time is dependent on the population in level 2 while the metastable lifetime is not. Therefore the magnitude of the energy transfer time will decrease with increasing pump flux. In the limit of high cooperative energy transfer rates compared to the metastable state decay rate, Eqn (11) simplifies to

$$2\gamma n_2^2 = W_{12} n_1 \tag{26}$$

and from Eqn (18) the stimulated emission rate is determined by

$$\gamma n_2^2 = n_3 \left(\frac{\sigma_{31} I}{h\nu_L} + W_{31} \right) = \frac{1}{2} W_{12} n_1 \tag{27}$$

The dependence of the laser intensity I on the optical pump flux is approximately linear under these conditions. In general under high excess pump power conditions the stimulated emission rate is significantly higher than the spontaneous decay rate from the upper laser level ($\sigma I/h\nu \gg W_{31}$). Note also that n_3 is clamped at its threshold value. From Eqn (27) it can be seen that an increase in the pump rate W_{12} will increase the intracavity laser intensity I and hence the laser output power.

In the limit where the spontaneous emission from level 2 dominates the removal of metastable state population the metastable state density varies linearly with the pump intensity as shown in Eqn (21). Re-writing Eqn (9) to include the stimulated emission term,

$$\gamma n_2^2 = n_3 \left(\frac{\sigma_{31} I}{h\nu_L} + W_{31} \right) \approx \gamma (W_{12} n_1 \tau_2)^2 \tag{28}$$

and in this limit the dependence of the laser output power on pump flux is approximately quadratic.

3.2.3. *Q-switched operation*. The upper laser level of many upconversion crystals have long lifetimes. Under Q-switched operation these levels can store energy from the pump source and produce high peak power output pulses in the visible. While only a few upconversion lasers have been operated Q-switched there are numerous applications for short pulse visible lasers. These applications include precision machining, medical treatment and lithography. In this section several concepts basic to Q-switching will be described along with their application to upconversion lasers.

Q-switching refers to a technique where feedback within a laser resonator cavity is temporarily blocked (the cavity Q or quality factor is reduced). During the time that feedback is prevented the gain element is optically pumped. At the end of the pump cycle the population inversion in the gain element is significantly higher than the steady state inversion would have been had feedback not been blocked. At this time the cavity Q is restored, permitting feedback and resulting in a relatively high energy pulse of short duration. This Q-switched pulse can have a peak power that is many orders of magnitude higher than the cw or steady state output power and such pulses have been used successfully for such power dependent processes as non-linear frequency conversion or laser drilling.

Two Q-switching modes are widely used. The first produces low-repetition rate, high output energy pulses. Optical pumping is performed with a pulsed source such as a flashlamp. The lamp duration is approximately equal to the upper laser level lifetime and the Q-switch opening time is synchronized with the termination of the flashlamp pulse. This type of Q-switched laser typically emits 1 J or more per pulse at approximately 10 Hz.

As will be discussed below, flashlamps are not generally useful for pumping upconversion lasers. A Q-switching technique more appropriate for upconversion lasers is repetitive Q-switching. In this method the gain element is pumped cw and a rotating shutter or other suitable element is located within the laser cavity to alternately prevent and permit feedback. The shutter is closed for a period of time roughly corresponding to the upper state lifetime, allowing the cw pump flux to produce a relatively large population inversion. The shutter then opens, generating a high peak power Q-switched output pulse. This cycle is repeated at a frequency of about one per excited state lifetime, and for many solid state materials this corresponds to repetition rates in the multi-kHz range.

The difference between the two modes of Q-switching is that for repetitively Q-switched operation the energy per pulse is lower and the pulse duration tends to be somewhat longer. However, the average power for a well-designed repetitively Q-switched laser is identical to the cw output power that could be obtained under identical pumping conditions. The peak power of the repetitively Q-switched laser is generally several hundred times the cw power. The repetitive nature of the pulse train makes this type of output ideal for material processing applications where thermal diffusion might have an adverse effect on the processing efficiency. In addition, the beam quality from a repetitively Q-switched laser is generally as high as the underlying cw laser.

Q-switches for repetitive operation can take several forms, including mechanical rotating apertures, vibrating mirrors, or acousto–optic or electro–optic crystals. Repetitively Q-switched lasers generally have well-defined modes so that the Q-switch aperture can be fairly small. There are several requirements for efficient Q-switch operation. One is that the insertion loss be extremely low when the switch is open. Higher losses increase the laser threshold power and reduce the laser output power as discussed in the Section 3.2.2. In addition the holdoff should be high. Holdoff refers to the ability of given Q-switch to prevent feedback when the switch is closed and this issue is of particular concern when acousto–optic crystals are used. These materials introduce loss by diffraction and some intracavity flux can be transmitted when the switch is closed.

The theory of repetitively Q-switched lasers has been presented in detail elsewhere[12] and will be summarized briefly in this section. When the Q-switch is closed the pump flux can

build up a large population inversion. The specific pump mechanism for producing the excited state does not affect Q-switched operation and both upconversion four-level lasers and conventional four-level lasers behave identically.

Once the Q-switch opens, feedback can occur. The laser output power begins to build up exponentially from the noise but, as the intracavity intensity increases, the population inversion decreases. Once the population inversion is reduced below its threshold value there is no net gain in the system and the laser output power begins to decrease. The point in time where the net gain is zero marks the peak of the laser output pulse. Past the peak the laser output decays exponentially with a time constant determined by the photon lifetime in the cavity.[13]

At repetition rates that are low compared to the inverse of the upper laser level lifetime, the energy per pulse is independent of repetition rate. Increasing the repetition rate in this regime increases the average laser output power. On the other hand, at repetition rates that are high compared to the inverse of the upper laser level lifetime the average laser output power is independent of repetition rate. In this case the energy per pulse decreases monotonically with increased repetition rate.

For a given pump flux there is an output coupling that generates the highest Q-switched laser output energy and hence efficiency. Combining this pump intensity and output coupling produces an "optimally coupled" Q-switched laser. Simple analytical expressions have been derived for the pulse width, extraction efficiency, output energy and peak power of the optimally coupled laser.[14] The derivation assumes that the small signal gain coefficient, the resonator loss, the beam cross sectional area A and the stimulated emission cross section σ_L are all known. In addition, it is assumed that the population density in the upper laser level is linearly proportional to the pump excitation rate. As discussed in Section 3.2.2, with upconversion pumping this is often not the case. Nevertheless, it is worth examining the analytical expressions for the Q-switched output energy and pulse width. The qualitative dependence of these parameters on the resonator gain and loss is helpful in the design of Q-switched upconversion lasers.

Defining the parameter $z = 2g_o\ell/L$, which corresponds to the ratio of the round trip small signal gain to the round trip dissipative loss, the optimum output coupling R_o can be expressed as a function of the gain and loss

$$\ln\left(\frac{1}{R_o}\right) = L\left[\frac{z - 1 - \ln z}{\ln z}\right] \tag{29}$$

Using this optimum output coupling the Q-switched output laser energy E is

$$E = \frac{A\mathrm{h}\nu\mathrm{L}}{2\sigma_L\gamma_o}[z - 1 - \ln z] \tag{30}$$

where γ_o is an inversion reduction factor.[14] The expression in square brackets in Eqn (29) increases monotonically with z as shown in Fig. 10. The pulse length t_p for the optimally coupled laser is

$$t_p = \frac{t_r}{L}\ln z\left[\frac{1}{z - \left(\frac{z-1}{\ln z}\right)\left(1 + \ln\left(\frac{z\ln z}{z-1}\right)\right)}\right] \tag{31}$$

where t_r is the round trip cavity transit time. The pulsewidth decreases monotonically with increasing z and is shown in Fig. 11. The design of an optimally Q-switched laser using Eqns (29)–(31) can take several routes but assuming that the resonator loss is fixed the pump

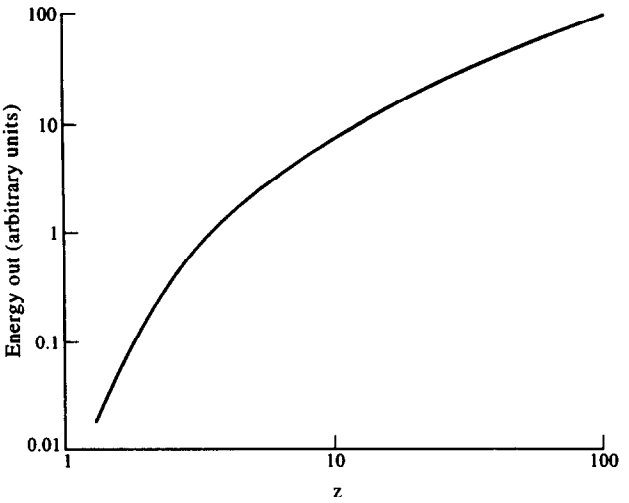

Fig. 10. Schematic representation of the output energy from an optimally coupled Q-switched laser as a function of the dimensionless parameter z. Plot is logarithmic, with an arbitrary scale for the ordinate. The parameter z is the ratio of the round trip resonator gain to the round trip dissipative loss.

intensity determines z. By adjusting the pump flux one can obtain a specific output energy or pulse width. Alternatively, Eqns (29)–(31) can be used to determine the maximum output energy and minimum pulse width that can be obtained when the pump flux is fixed at a specified intensity.

The pulsewidth in a Q-switched laser decreases with decreasing cavity length, increasing small signal gain (produced in a given material by increasing the optical pump intensity) and decreasing cavity loss. From Eqn (31) and Fig. 11 it is also clear that for a given upper laser level population the higher the stimulated emission cross section the shorter the output pulse. This is because $g_o\ell = \sigma_L n_3 \ell$ and is an important consideration regarding gain media selection for Q-switched operation. Finally, note that higher gain and lower loss are desirable for producing both shorter Q-switched pulse widths and higher Q-switched output pulse energies.

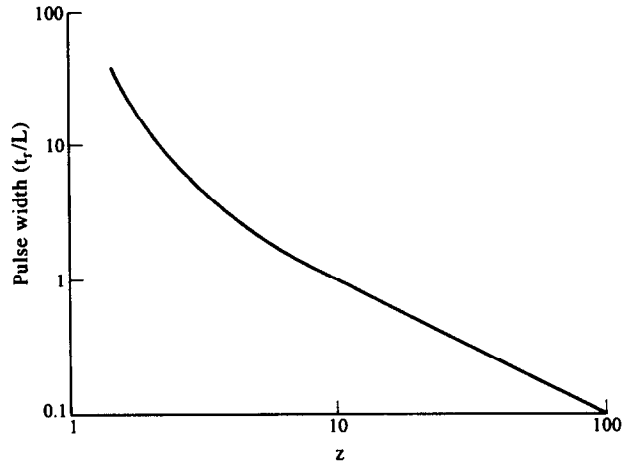

Fig. 11. Schematic representation of the full width at half maximum (FWHM) pulsewidth for an optimally coupled Q-switched laser. The plot is logarithmic with the ordinate in units of t_r/L. L is the double pass loss and t_r is the round trip transit time.

3.2.4. *Design considerations for optimum pump optics and upconversion laser resonator configuration.* In this section the design issues relevant to the pump optics and laser resonator for upconversion lasers will be discussed. The central issue in designing upconversion lasers for high efficiency is to produce high pump intensities within the resonator active volume. For all of the upconversion pump mechanisms described in Section 2, the pump efficiency is a strong function of the pump intensity. This is due to the two-photon nature of the pump mechanism and the limited lifetimes of the intermediate states involved in the energy transfer processes. In the case of sequential two-photon absorption upconversion for example, the higher the pump intensities for photon fields "a" and "b", the greater the probability that an ion in the intermediate metastable state will absorb a "b" photon before it decays back to level 1. For cooperative energy transfer upconversion the extreme radial dependence of the dipole–dipole energy transfer interaction (r^{-6}) dictates high metastable state densities for efficient upconversion pumping. For photon avalanche upconversion, a high density of ions in the metastable state coupled to an intense pump flux is beneficial for producing large upper level populations.

As a result of the intensity requirements for the pump flux the most efficient type of optical pumping is monochromatic longitudinal pumping (also called end-pumping). The sharp absorption features characteristic of rare earth-doped solids is one of the reasons why polychromatic sources such as filament lamps or flashlamps are not effective for upconversion laser pumping. Such lamps are often used to produce conventional lasing in rare earth doped crystals and in fact the first demonstration[5] of upconversion laser emission was accomplished with a flashlamp. However, the low f_a (see Eqn (25)) for these blackbody sources prevents the high density of excited states necessary for efficient upconversion pumping. Note also that the pump rate requirements for upconversion lasing are more severe than for upconversion fluorescence measurements. This is because the upper laser level population density must be maintained at its threshold value to produce stimulated emission.

An additional problem in using incoherent lamps for upconversion pumping is that their extended size prevents focusing the lamp emission to a small spot size. End-pumping with lamps is generally not practical. Instead, the most appropriate pump configuration is side-pumping. However, side-pumping for upconversion is not at all efficient as the absorption path length transverse to the laser rod is typically low. In addition an excitation gradient is created transverse to the rod axis due to Beer's law lamp flux attenuation. The highest density of excited states is near the edge of the rod closest to the lamps. Furthermore, with side pumping the resonator mode is generally a poor match to the excitation volume created by the lamp. This is particularly true for TEM_{00} laser operation. For cryogenic operation of the upconversion laser the lamp pumped geometry offers an additional challenge, as efficient coupling of the lamp energy into the rod while maintaining the rod in a temperature-controlled vacuum environment is quite difficult.

Finally, if flashlamp excitation was desired to produce laser emission in the visible, it would be far easier and is generally more efficient to pump the excited state directly. For most upconversion lasers the upper laser level can be pumped with a source of visible radiation that emits to the blue of the desired emission wavelength. (The terminal level for many upconversion lasers is the ground state.) The emission spectrum for a typical flashlamp operated at two different current densities is illustrated in Fig. 12. The relative spectral irradiance of the flashlamp depends on the blackbody temperature which is determined by the excitation current density. For the two excitation currents shown in Fig. 12, it is clear that a substantial amount of optical radiance is emitted in the visible. For green emission from Er excitation at wavelengths below 550 nm is required. There is substantially more radiance in this region than near 800 nm for the higher current lamp (blackbody temperature of approximately 9400°K). Since upconversion pumping requires 800 nm radiation, it can be concluded that, other considerations notwithstanding, the 9400°K flashlamp will be

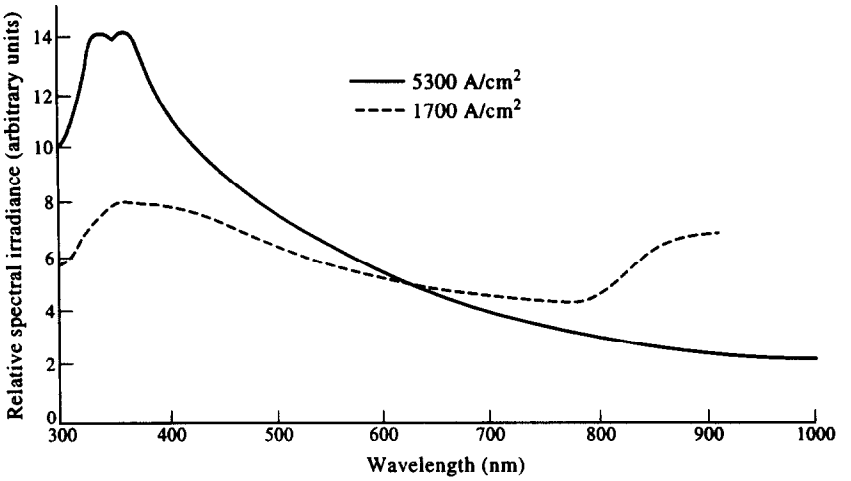

Fig. 12. Spectral emission of a flashlamp operated at the current densities indicated. The curves are smoothed for clarity. The blackbody temperatures are approximately 7000°K and 9400°K for the 1700 A cm^{-2} and 5300 A cm^{-2} current density operating points, respectively. The relative intensities are shown for each lamp. The irradiance of the 9400°K lamp is approximately five times higher than that of the 7000°K lamp.

more effective in populating the upper laser level directly than by upconversion energy transfer.

Monochromatic end-pumping produces a high density of excited states in an extremely small volume. In addition, the laser resonator can be designed so that the resonator mode matches, or coincides with, the inversion profile created by the pump beam. Mode matching ensures TEM_{00} operation by "gain aperturing". The alignment of the end-pumped optical configuration is adjusted so that the pump laser beam is focused into a small cylindrical volume along the laser resonator axis. The inversion profile created by the pump beam energy deposition coincides with the TEM_{00} laser resonator mode. Unlike a hard aperture, the excitation volume defines the gain region without diffractive losses. With ideal mode matching, none of the laser pump energy will be deposited in a region outside of the resonator volume. Energy deposited outside of the active volume is not normally extracted and represents a loss in pump efficiency. A typical pump optics arrangement is illustrated in Fig. 13.

The narrow absorption linewidths of rare earth doped crystals require tunable, monochromatic pump sources. The wavelength band appropriate for many two-photon upconversion pump processes is 700–900 nm and the Ti:sapphire laser is convenient for use in this wavelength range. For cw operation the Ti:sapphire laser can be excited by an argon ion laser, while for pulsed operation it is generally pumped with a doubled Nd:YAG laser.

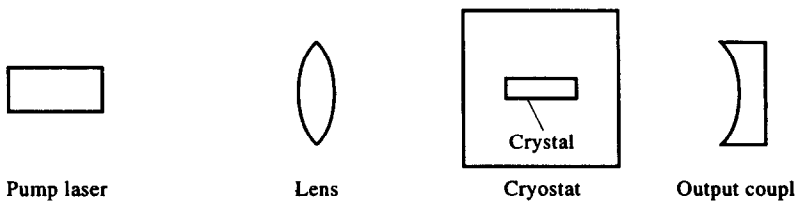

Fig. 13. General schematic of a simple end-pumped, nearly-hemispherical laser resonator used to produce upconversion laser emission. The pump laser and lens comprise the pump optics, while the laser crystal and output coupler comprise the laser resonator. The crystal is shown contained in a cryostat and the exterior face of the crystal is HR coated to form the rear reflector. The lens and output coupler may be located within, or attached to, the cryostat as described in the text.

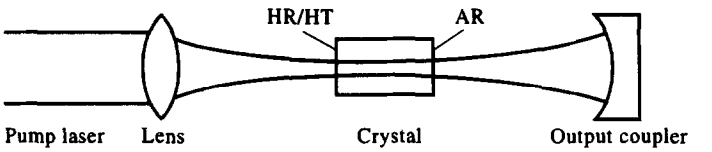

Fig. 14. Detail of the overlap between the resonator and pump modes for the nearly hemispherical laser resonator.

Flashlamp pumped Ti:sapphire lasers are also commercially available and unless Q-switched they produce output pulse widths of a few μs. The standard spectral bandwidth of a commercial cw Ti:sapphire laser is 40 GHz. This is usually narrow enough for most upconversion pumping but for even narrower linewidths, a single longitudinal mode Ti:sapphire ring laser may be used. Three-photon cooperative upconversion is produced with wavelengths further into the infrared. For three-photon cooperative upconversion in Er the pump wavelength is 1.5 μm.

The range of pump wavelengths used for upconversion is ideal for laser diode pumping. The cost, size and inefficiency of an argon ion laser capable of producing 1 W of Ti:sapphire laser pump power at 800 nm is an important impediment to the development of upconversion lasers for numerous applications. Laser diodes are relatively inexpensive, small and efficient. The electrical–optical conversion efficiency for a 1 W, 800 nm laser diode exceeds 30%. The diode operating lifetime is several hundred thousand hours compared to just a few thousand hours for an ion laser tube. Equally important, the laser diode output wavelength can be tuned to match the absorption resonance. By adjusting the diode temperature and drive current the output wavelength can be easily tuned over a range of several nm. For larger wavelength tuning ranges the diode can be operated in an external cavity resonator. Tuning ranges of 25 nm or more are routinely achieved in commercially-available external cavity laser diodes.

There are two basic considerations related to the efficient use of laser diodes as upconversion pump sources. The first is that the output power from a wide stripe, nominally 1 W laser diode is typically distributed among eight or so longitudinal modes spanning approximately 2.4 nm.[15,16] A rare earth-doped crystal will, therefore, absorb only a small fraction of the diode emission even when the peak of the absorption line is coincident with the wavelength of one of the longitudinal modes. The second consideration arises from the poor coherence of a typical gain-guided laser diode across its emitting aperture. This prevents achievement of the desired small pump spot size in the upconversion crystal using conventional diodes and pump optics. Single longitudinal mode, index guided laser diodes are presently available with output powers up to 200 mW and such devices can be as efficient as a Ti:sapphire laser in producing upconversion emission. Alternatively, line narrowing and beam profile control techniques[17] can be used to produce efficient, high power laser diode pump beams for upconversion lasers.

There are many types of laser resonator configuration but one of the most efficient for upconversion pumping is the nearly-hemispherical laser resonator. This design is shown schematically in Fig. 14 along with the pump beam. In its simplest form, the laser resonator consists of two components; the upconversion laser crystal and the output coupler. The exterior face of the crystal is coated with a dichroic coating that is highly reflective (HR) at the upconversion laser wavelength and highly transmissive (HT) at the pump wavelength. This coating serves as the HR rear laser reflector. The interior face of the crystal is coated AR at the upconversion laser wavelength. The output coupler is coated for partial reflectivity at the upconversion laser wavelength. The mirror is concave and has a relatively short radius of curvature (ROC). The separation between the mirror and the dichroic face of the laser crystal is approximately equal to the radius of curvature of the mirror.

The laser resonator mode contains a Gaussian waist or focus at the dichroic face of the laser crystal. Typically the mirror spacing is adjusted to produce a waist diameter of less than 50 μm. The resonator configuration defines the active volume and the pump optics must be aligned so that pump energy is deposited only within this volume. This can be readily accomplished for a Ti:sapphire pump laser by using a short focal length lens as shown in Fig. 14. Proper selection of the lens focal length and spacing between the lens and the dichroic-coated face of the crystal can produce the type of mode matching shown in the figure. The overlap obtained experimentally is often not as perfect as the ideal pictured in Fig. 14. However, good pump efficiency will be maintained as long as the pump beam deposition is confined to the active volume. In addition, the active volume dimensions are to be kept as small as possible, consistent with pump intensity and thermal loading considerations.

End-pumping provides the longest possible path length for the absorption of pump flux. This is particularly important in the case of photon avalanche upconversion where the absorbed fraction of pump flux is generally low due to the small fraction of ions in the metastable state. The active volume illustrated in Fig. 14 defines the TEM_{00} mode and confining pump energy deposition to this volume is important for gain aperturing as well as efficiency. Higher order transverse laser modes are often obtained when the pump mode is misaligned or mismatched with respect to the resonator mode.

As shown in Fig. 13 the upconversion laser crystal is contained within a cryogenic cooler. Closed cycle cryogenic chillers that produce temperatures as low as 5°K are commercially available. These devices are convenient to use as they are air-cooled and require only a source of AC current to operate. In addition, most have an internal heater allowing continuous adjustment of the crystal temperature between 5°K and room temperature. The technology used for closed cycle chillers is the same as that used for vacuum cryopumps and the compressors characteristically provide thousands of hours of maintenance-free operation.

The outer dimensions of the cooler chamber prevent the use of a focusing lens with a very short working distance. Placing such a lens inside the chiller chamber complicates the pump beam alignment. Using an external lens the shortest practical working distance that can be employed is approximately 50 mm and a lens of this type can produce an adequately small pump spot within the laser crystal. A second issue involving the chiller arises from the location of the laser output mirror. When placed external to the vacuum chamber one of the cryostat's optical vacuum windows is introduced into the laser resonator cavity. Although the window is AR coated, bulk scattering and residual reflective losses reduce the overall laser output power. An alternative would be to replace the intracavity window by placing the output mirror in a vacuum-tight housing attached to the cryostat. Such a housing would have to accommodate both translation as well as tilt for the critical output mirror alignment and is difficult to produce. A third issue is associated with the vibrations caused by the closed cycle chiller. Cryostat operation involves vibrations caused by the piston in the helium compressor. When the crystal and mirror are not mounted on the same bench one component vibrates with respect to the other. In the nearly hemispherical resonator configuration the mirror alignment is critical and the vibrations produce inadvertent, repetitive Q-switching of the upconversion laser output. Q-switching by means of a vibrating mirror is well-known, although in the present case it is undesirable. However, it is found that the average Q-switched laser output power is identical to the cw power. True cw operation can be obtained for example by momentarily turning off the chiller. Either mounting both the cryostat and the output mirror on the same optical bench or using a liquid He cryostat eliminates the pulsed output associated with the piston vibrations.

A monolithic upconversion laser crystal is an alternative solution to the problems caused both by the chiller vibrations and the intracavity cryostat window. Monolithic laser rods are machined with reflectively-coated end faces and form a complete, aligned laser cavity. Results obtained with monolithic lasers have not been as good as with the discrete element,

hemispherical resonator for several reasons. For one, most monolithic upconversion crystals use two curved end faces, producing a waist in the interior of the rod. Not only is the pump flux weaker when it reaches the waist location but the resonator waist is typically much larger than waists established in hemispherical resonators. The larger waists in monolithic rods are a result of the relatively large ROC of the end faces compared to the mirror separation, determined by the rod length. Producing accurate, short ROC ends on the rod is quite difficult and the sensitivity of the rod to end face misalignment is higher for shorter radius mirrors. The reduced pump intensity and larger active volume in the monolithic rods lowers the upconversion pump efficiency. While in principal a monolithic plano-convex rod could be fabricated to form a nearly hemispherical resonator, the severe tolerances would make fabrication impractical. Since the convex end would have a short ROC, the alignment of the curved end with respect to the flat end, as well as the separation between the two rod faces, would have to be nearly perfect. In addition, the length of the rod would be fixed and the resonator configuration would be optimum only for a specific pump intensity. It is found that at higher pump power it is desirable to increase the resonator mode waist to optimize the laser output power.

3.3. *Upconversion processes: experimental results*

3.3.1. *Introduction.* Among rare-earth ions that have demonstrated upconversion lasing, the Er^{3+} ion has been investigated extensively owing to its ability to produce efficient 550 nm green emission in a number of hosts. Er^{3+}:$YAlO_3$ (Er:YALO) is among the most efficient visible upconversion laser crystals demonstrated to date and is ideal for illustrating the upconversion pumping processes described in Section 2. This is because all three upconversion pumping mechanisms produce visible laser emission in Er:YALO. Selection among them is determined by the specific excitation wavelengths chosen within the 800 nm absorption band.

The configuration of the outermost electron shell of Er is $4d^{10}4f^{12}5s^25p^66s^2$. Er is incorporated in most crystals as a trivalent dopant, Er^{3+}. Trivalence indicates the loss of three electrons from the neutral atom. In the case of Er these electrons are the two $6s$ and one $4f$. The resulting $4f^{11}$ configuration represents a partially filled $4f$ shell and gives rise to 41 electronic states, 26 of which have been observed spectroscopically. Because the $4f$ orbits lie well inside the electronic shell, they are effectively screened from interactions with neighboring ions. One consequence of screening is the characteristic sharp crystal spectroscopic features. Another is that different crystal hosts do not strongly affect such spectroscopic properties as the absorption and emission spectra and the oscillator strengths.

The first cw upconversion laser was demonstrated[18] in Er^{3+}-doped yttrium orthoaluminate. This crystal host has the chemical formula $YAlO_3$ and is commonly referred to as YALO or YAP. YALO is similar[19] to YAG and superior to $YLiF_4$ (YLF) in terms of hardness and thermal conductivity. Upconversion at 550 nm in Er:YALO does not exhibit self-pulsing as had been observed[20] for 551 nm upconversion emission in Er:YLF. The terminal level for the laser transition is located 217.6 cm^{-1} above the lowest Stark level of the ground state manifold. A partial energy level diagram based on spectroscopic data reported by Donlan and Santiago[21] is shown in Fig. 15. The crystal field split Stark level locations are indicated for several of the electronic manifolds.

3.3.2. *Experimental apparatus.* The Er:YALO laser rod was 10 mm long, 6.4 mm in diameter and contained 1.5 at.% Er^{3+} ($\rho = 2.95 \times 10^{20}$ cm^{-3}). The end faces of the cylindrical rod were polished to better than $\lambda/10$ flatness and to 2 arc seconds parallelism. One face contained a dichroic coating that was HR at 550 nm and HT from 780 nm to 850 nm, while the other face was AR coated for 550 nm. The optical homogeneity of the polished rod was determined with a Twyman–Green interferometer at 633 nm. Less than $\lambda/10$ distortion was measured and an interferogram is shown in Fig. 16.

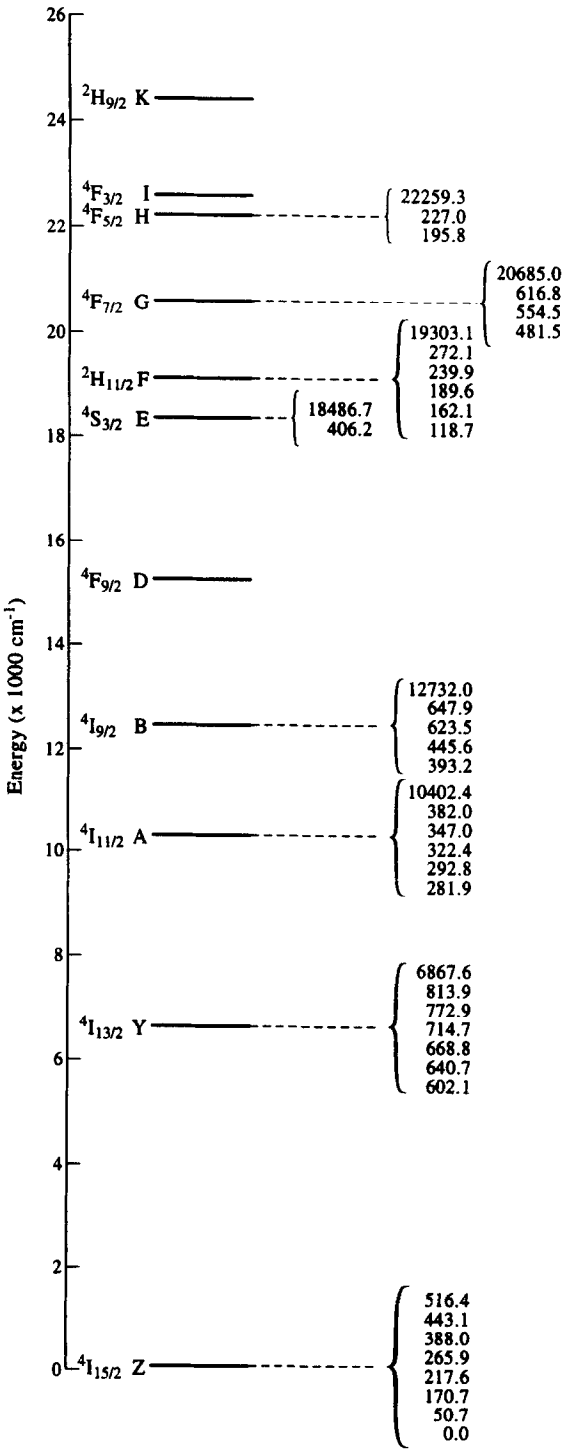

Fig. 15. Partial energy level diagram for Er:YALO. The energy of each Stark level within selected manifolds is given in cm^{-1} and listed to the right of the state. The letters Z, Y, A, etc. indicate standard notation for the various electronic states.

The axis of the Er:YALO laser rod is parallel to the crystallographic b axis. YALO is a negative biaxial crystal having a distorted perovskite structure. The unit cell is orthorhombic and the two optic axes are in the ac plane at an angle of 70°. The axes of the indicatrix are parallel to the crystallographic axes with $a = z$, $b = y$ and $c = x$. The acute bisectrix of the optic axes is the c axis.[22,23] Optical excitation was performed with a Ti:sapphire laser. It was found that rotating the plane of polarization of the pump laser 360° about the laser rod axis changed the absorbed power slightly, producing a ratio at 785 nm of 0.93 for the minimum absorbed pump light to the maximum. The pump polarization was oriented to produce maximum absorption.

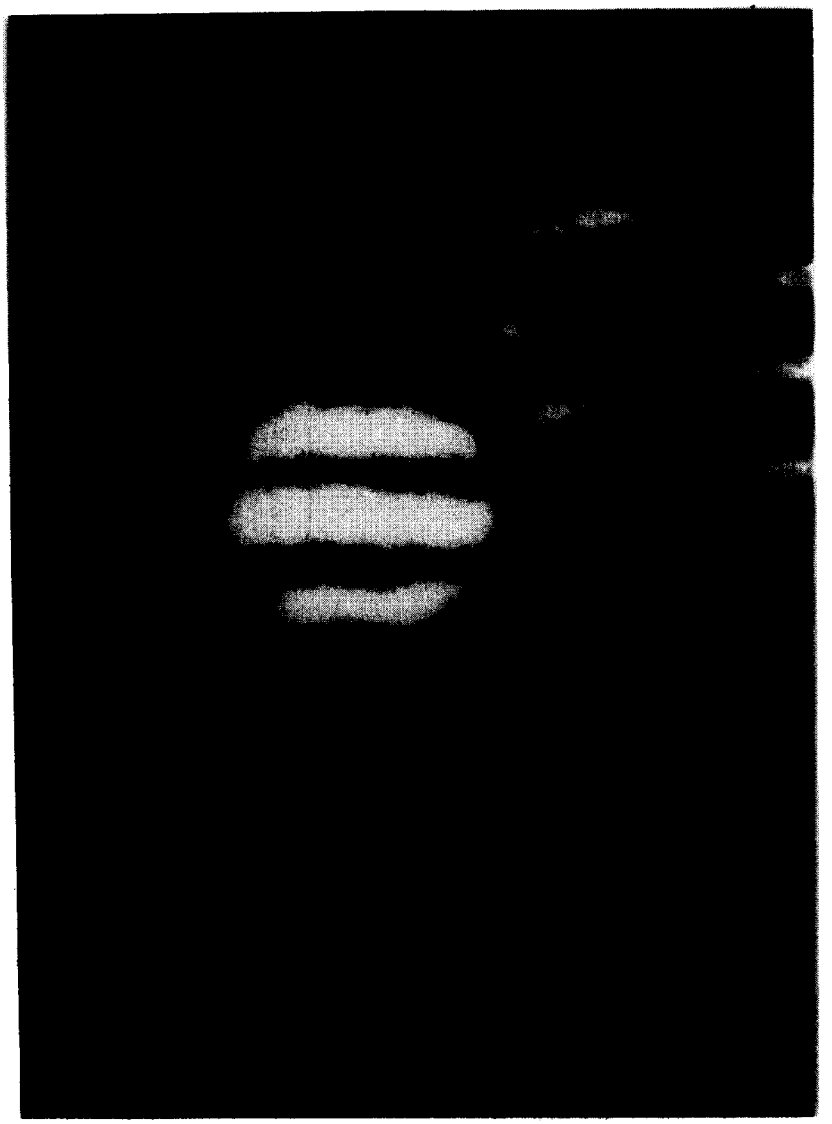

Fig. 16. Twyman–Green interferogram of the Er:YALO laser rod used in this work. For this measurement both faces of the laser rod had broadband AR coatings.

Two different Ti:sapphire lasers were employed to pump the Er:YALO crystal. For most of the measurements reported below a commercial laser was used. As much as 1.08 W of output power could be produced at 807 nm when the Ti:sapphire laser was pumped with a 6 W argon ion laser. The output bandwidth was measured to be less than 0.02 nm (0.31 cm^{-1}). For sequential two-photon absorption upconversion pumping, a dual wavelength Ti:sapphire laser[24] was used. Typically this laser produced over 400 mW of total power when operated at wavelength pairs suitable for sequential two-photon absorption upconversion pumping of Er:YALO (785 nm and 840 nm). The laser bandwidth could be adjusted between 0.03 nm and 0.7 nm. This laser is uniquely suited for sequential two-photon absorption upconversion pumping and is described in some detail below.

The dual wavelength Ti:sapphire laser resonator is shown schematically in Fig. 17. The resonator design is based on a Ti:sapphire laser reported by Schulz.[25] By inserting a high dispersion prism between the gain element and the HR flats, separate feedback paths are established for each wavelength. The use of a Brewster angle prism in minimum deviation provides low insertion loss while minimizing the amount of astigmatism introduced. The resonator mode is collimated as it passes through the prism. Angular rotation of one of the HR flats allows tuning of one wavelength while leaving the other unaffected. Alternately, tuning may be achieved by rotating the prism. This changes both wavelengths simultaneously while maintaining a constant separation between the two. An important feature of the resonator is that both wavelengths emerge from the output coupler simultaneously collimated and spatially overlapped. In addition, the mode shape and size for each wavelength are similar.

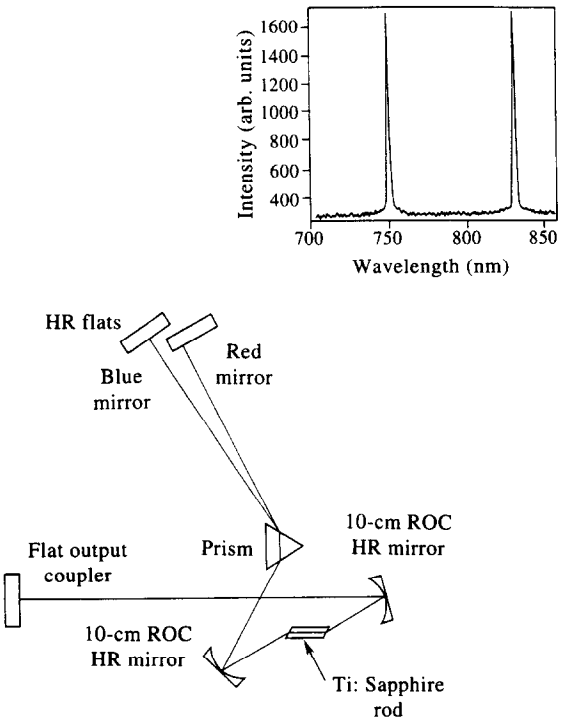

Fig. 17. Laser resonator used to obtain dual wavelength operation in Ti:sapphire. The two coupled cavities overlap between the Ti:sapphire crystal and the flat output coupler. The mirror that produces feedback at the shorter wavelength is labeled "blue", while the longer wavelength mirror is labeled "red". A spectral trace of dual wavelength output at 750 nm and 830 nm is shown in the inset. The trace was acquired with an optical multichannel analyzer.

The importance of the region of the resonator where the wavelengths are spatially separated is that perturbations can be introduced that affect only one of the wavelengths. For example, the polarization of one wavelength may be rotated relative to the other. A modulator can be inserted to provide amplitude modulation at one wavelength, or modulators for both wavelengths can be introduced to generate arbitrary phase and frequency relationships between the two outputs. In addition, etalons may be inserted to reduce the linewidth at only one of the wavelengths, or attenuators may be introduced to reduce the intracavity power at either wavelength. An alternative method of reducing the intracavity power is to replace one of the HR flats with a partial reflector.

Using a 5 W argon ion laser pump, simultaneous operation at two frequencies was demonstrated over the wavelength range of 710–940 nm. The maximum total output power was over 800 mW for wavelength pairs near the peak of the gain curve. To achieve these results with a 5 W pump laser, a 0.1% doped high figure of merit (~ 1000) Ti:sapphire crystal was used. In order to verify that both wavelengths were produced simultaneously, the laser output was dispersed by a diffraction grating and each wavelength was detected with a separate photodiode. Stable, simultaneous dual-wavelength cw output was observed over a wide range of wavelengths.

Line narrowed operation was obtained by inserting an etalon pair in the collimated region of the resonator between the prism and one of the two HR flats. The etalons were 0.5 and 10 mm thick. The resulting linewidth measurement of 450 MHz was resolution limited. The linewidth at the second wavelength was unaffected. It is also possible to narrow the linewidths of both wavelengths simultaneously by introducing the etalon pair in the collinear region of the resonator. Narrow linewidth operation at each wavelength can be maintained at higher output power levels than for a traditional single longitudinal mode standing wave laser. Spatial hole burning will be reduced owing to the simultaneous oscillation of two resonant wavelengths in the same gain volume and as a consequence, the threshold for additional longitudinal modes will be increased.

Spatial overlap between the mode axes for the two wavelengths inside the cavity is obtained only in the region of the resonator between the output mirror and the face of the Ti:sapphire crystal closest to this mirror. Owing to dispersion the mode axes do not coincide in the gain element although the beam diameters are large enough to produce significant overlap. The spatial overlap of the two pump simultaneously-emitted output wavelengths was measured outside the cavity using a commercial laser beam diagnostic system. The results are shown in Fig. 18 for simultaneous operation at 785 nm and 840 nm. The traces show the 785 nm output obtained by blocking the feedback mirror for 840 nm, the 840 nm output obtained by blocking the feedback mirror for 785 nm and the composite output in which both wavelengths are produced simultaneously. The data for the output beams were obtained close together in time to ensure that the detector array was not moved between frames. Comparable size, power and Gaussian intensity profiles were measured for the three beams shown in the figure. The overlap of the two emitted wavelengths is within 4 μm in the vertical plane and 1 μm in the horizontal plane. This type of laser clearly minimizes the alignment problems associated with using two separate lasers for sequential two-photon absorption upconversion.

The Er:YALO rod was placed in a closed cycle helium cryostat. The cryostat had four optical windows oriented 90° with respect to one another. The lowest temperature that could be achieved was 6.7°K and temperature control to 0.1°K could be maintained. Fluorescence excitation spectra were taken by pumping the crystal along the b axis with a Ti:sapphire laser and observing emission at 90° with respect to the excitation axis. The emission was detected with an end-on photomultiplier tube (PMT) located behind a blue–green optical filter. No imaging optics were used. The fluorescence excitation spectrum records the intensity of the 550 nm Er fluorescence as a function of the excitation wavelength. The output of the PMT was digitized, normalized to the Ti:sapphire laser output power and stored in a computer.

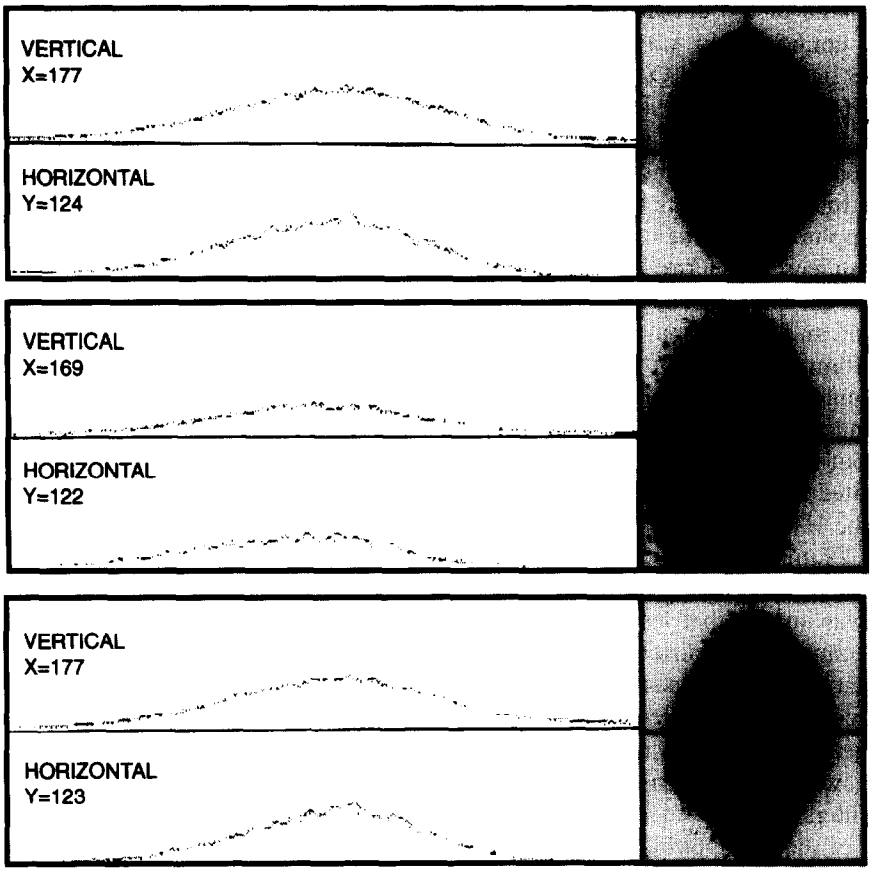

Fig. 18. Beam profiles of the output of the dual wavelength Ti:sapphire pump laser. The top trace is the 785 nm output, the middle trace is the 840 nm output and the lower trace is the beam profile of both wavelengths operating simultaneously. The image on the right of each profile indicates with shades of grey the contours of equal beam intensity. The axes on the contour map intersect at the centroid of the intensity pattern and the two curves to the left of each contour map indicate the intensity variation along the vertical and horizontal axes. The Gaussian fits to the data have correlation coefficients that range between 0.95 and 0.98 for the six curves. The x and y values indicated on each beam profile give the coordinates of the centroid relative to an arbitrarily chosen origin. The magnification of the detection system was selected so that each coordinate unit is approximately 1 μm.

The normalization algorithm provides accurate corrections for small variations in the Ti:sapphire laser output power.

The Ti:sapphire laser output wavelength was determined with a commercial wavemeter interfaced to the computer. The wavemeter, which also contained a power meter, was positioned to monitor the optical flux that leaks through the HR rear reflector of the Ti:sapphire laser. The wavemeter was calibrated and is accurate to 1 part in 10^4. The resolution of the fluorescence excitation measurements is determined by the size of each wavelength step, which was 0.18 nm. In general the wavelengths reported for Er:YALO are vacuum wavelengths. The vacuum wavelength is calculated from the experimentally measured wavelength using the well-known relationship $\lambda_V = 1.0002926\lambda_A$, where λ_V is the vacuum wavelength, λ_A is the wavelength measured in air and 1.0002926 is the refractive index[26] of air. For wavelengths near 800 nm the vacuum wavelength is approximately 0.23 nm higher than the measured wavelength.

A schematic of the upconversion laser and pump optics is shown in Fig. 19. The laser resonator configuration was nearly hemispherical. A small resonator mode waist was established in the Er:YALO rod using a 10 cm radius of curvature output coupler separated from the HR/HT coated crystal face by a distance slightly in excess of the mirror ROC. The resonator design required the use of an intracavity cryostat window. The intracavity window was AR coated and the combined reflectivity for both surfaces at 550 nm was less than 0.4%. Several output mirrors were used with reflectivities ranging from 59.6% to HR (>99.9% R). The Ti:sapphire laser emission was focused onto the face of the Er:YALO rod with a 50 mm focal length lens. The term "incident pump power" as used below refers to the pump power incident on the focusing lens. Approximately 87% of the incident pump power is transmitted into the rod and approximately 98% of this power is absorbed. As discussed in Section 3.2.4, it is important to use as short a focal length as possible for the focusing lens in order to obtain the maximum pump power density in the laser rod. Maintaining a high activator ion doping density and using a pump wavelength that is strongly absorbed improve the upconversion laser output for similar reasons. The pump beam enters the cryostat through a window that is AR coated and is 96.4% transmissive at the pump wavelength. The diameter of the pump spot on the HR face of the rod was measured to be 21 μm for the commercial Ti:sapphire laser and 28 μm for the dual wavelength laser.

In order to determine the temporal dependence of the upconversion laser emission a chopper was inserted between the pump laser and the focusing lens. The chopper repetition rate was continuously variable up to 3 kHz. The upconversion laser emission was observed with a fast photodiode connected to a 500 MHz oscilloscope. To measure the temporal dependence of the upconversion fluorescence the crystal emission along the excitation axis was imaged onto a 0.3 m monochromator. An S-1 PMT was used to detect the 960 nm radiation, while a high sensitivity modified S-20 PMT was used to detect emission in the visible. Filters were placed in front of the entrance slit of the monochromator to block the detection of the Ti:sapphire pump laser emission. The output of the PMT was sent to a fast oscilloscope. In all cases the electronic response of the measurement system exceeded the desired time resolution by one or more orders of magnitude.

To obtain repetitively Q-switched operation the Er:YALO crystal was pumped cw and the chopper[27] was located inside the upconversion laser cavity adjacent to the cryostat window as shown in Fig. 19. Switching rates up to 3 kHz were used and the chopper aperture was 1.5 mm. The resonator mode diameter at the chopper blade was under 1 mm and based on the linear speed of the blade, approximately 32 μs were required to traverse the full mode diameter. However, the Q-switch opening time[27] is only a small fraction of the traversal time and short Q-switched pulses were obtained.

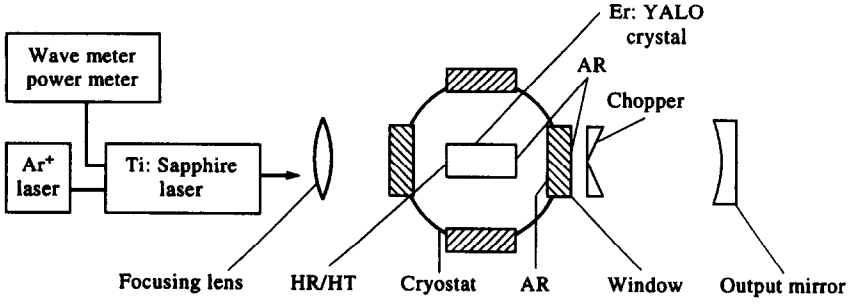

Fig. 19. Schematic of the laser resonator and pump optics used to demonstrate upconversion laser emission in Er:YALO. The intracavity cryostat window is AR coated. A commercial wavemeter/power meter is positioned to monitor the optical flux that leaks through the HR rear reflector of the Ti:sapphire laser. The position of the intracavity chopper used as a Q-switch is shown.

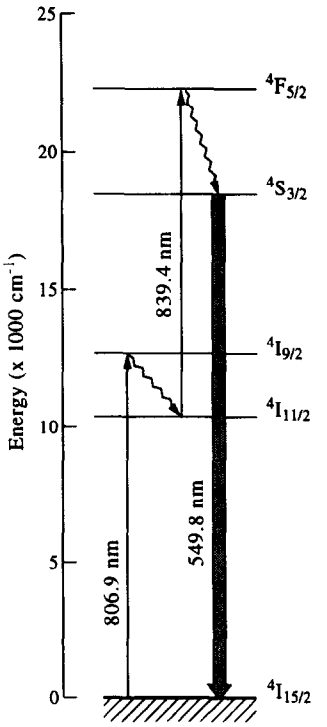

Fig. 20. Sequential two-photon absorption upconversion in Er:YALO. Only electronic states involved in the laser and optical pumping transitions are shown. The wavelengths indicated for absorption represent transitions between the lowest Stark components of the respective manifolds. Stimulated emission is marked with a heavy arrow and the laser wavelength is indicated. Laser emission originates in the lowest Stark level of the $^4S_{3/2}$ state and terminates on the fourth Stark level of the $^4I_{15/2}$ state.

The fluorescence spectrum was taken by imaging the crystal emission onto a 0.3 m monochromator equipped with an optical multichannel analyzer detector (OMA). The OMA records the entire 550 nm emission spectrum at one time without mechanical scanning. The monochromator entrance slit was adjusted to 10 μm and the center-to-center spacing of adjacent detector elements on the OMA array was 25 μm. With a 1200 groove mm^{-1} grating the resolution of the fluorescence spectrum was approximately 0.06 nm. The OMA integration time was set to 0.8 s to average the small amount of amplitude jitter.

3.3.3. *Sequential two-photon absorption upconversion in Er:YALO.* The first demonstration of upconversion laser emission in Er:YALO was obtained[18] by sequential two-photon absorption upconversion. The energy flow dynamics for this process are illustrated in Fig. 20. The shorter wavelength photon populates the $^4I_{9/2}$ state and rapid non-radiative decay from the $^4I_{9/2}$ state populates the $^4I_{11/2}$ state. The $^4I_{11/2}$ state is metastable with a lifetime[28] of 1.2 ms. The longer wavelength photon promotes an ion from the $^4I_{11/2}$ state to the $^4F_{5/2}$ state. Rapid multiphonon relaxation from the $^4F_{5/2}$ state produces population in the $^4S_{3/2}$ upper laser level. Non-radiative decay can occur through the $^4F_{7/2}$ and $^2H_{11/2}$ states, which are intermediate in energy between the $^4F_{5/2}$ state and the $^4S_{3/2}$ state. The $^4S_{3/2}$ upper laser level lifetime is 160 μs. In this section the results obtained by Silversmith *et al.*[18] for sequential two-photon absorption upconversion are summarized. In that work two separate lasers were used to pump a monolithic Er:YALO laser crystal. A description of more recent results obtained for pumping with a dual wavelength Ti:sapphire laser are also reviewed.

Two narrow bandwidth, cw dye lasers were used in Ref. 18, one emitting at 792 nm and the other at 840 nm. The maximum pump power available from each laser was about 300 mW. The outputs from the dye lasers were polarization-combined into a single pump beam. The dual-wavelength pump beam was focused onto the face of a monolithic Er:YALO laser crystal located inside a temperature-controlled cryostat. The crystal was 3 mm long and each end face was convex with a 2 cm ROC. The doping level was 1%.

Laser threshold was obtained with approximately 100 mW of incident power from each of the dye lasers. The fraction of pump power absorbed at the longer wavelength is dependent on the pump power from the other dye laser, as the latter produces the population of longer wavelength absorbers. The crystal absorbed about 30% of the power at the shorter wavelength and 15% of the power at the longer wavelength was absorbed when irradiating the crystal with 200 mW of pump power at the shorter wavelength.

Using a 0.99 R output coupler, the maximum upconversion laser output power was 0.8 mW at 549.8 nm. With the pump power at the shorter wavelength held constant, the dependence of the laser output power on the longer wavelength pump power was linear. However when the longer wavelength power was fixed and the shorter wavelength power varied, saturation of the laser output power was observed. This indicates saturation of the $^4I_{11/2}$ population. Coupled with the fact that Silversmith *et al.* could not obtain laser emission by cooperative upconversion pumping via the $^4I_{11/2}$ state (cooperative upconversion is normally quite efficient in Er:YALO as will be discussed below), the data suggest that impurity quenching limited the $^4I_{11/2}$ state population in the Er:YALO sample used in Ref. 18.

The performance of the upconversion laser was reported to depend critically on the spatial overlap of the pump beams from the two dye lasers. Small shifts in the position of one of the pump beams with respect to the other, or a mismatch in the radial intensity distribution of the two dye laser beams was found to result in a reduction of the laser output power. As the reported pump waist was approximately 15 μm and the focal length of the lens used to produce this waist was 85 mm, small deviations in the alignment of the two pump beams produce large reductions in the laser output efficiency. In order to demonstrate improved upconversion laser efficiency using two-photon absorption pumping, the dual wavelength Ti:sapphire laser described in Section 3.3.2 was used. Several different wavelength pairs corresponding to different Stark levels of the $^4I_{9/2}$ and $^4F_{5/2}$ states were used to produce upconversion laser emission. The resonator and pump configurations that were employed for pumping with the dual wavelength Ti:sapphire laser are those described in Section 3.3.2 above.

It proved to be more difficult to demonstrate sequential two-photon absorption upconversion with this laser than had originally been anticipated. The laser threshold power requirements for cooperative energy transfer upconversion via the $^4I_{11/2}$ state were so low that using the dual wavelength Ti:sapphire laser to pump the Er:YALO crystal with any of the excitation wavelengths corresponding to the individual Stark levels of the $^4I_{15/2} \rightarrow {}^4I_{9/2}$ transition produced laser emission independent of the presence of the second, longer pump wavelength. This was verified by blocking the "red" feedback mirror in the dual wavelength Ti:sapphire laser cavity while continuing to observe upconversion laser emission at 549.8 nm.

To observe sequential two-photon absorption upconversion under these conditions requires low pump flux at the shorter wavelength. The resulting small population in the $^4I_{11/2}$ level will then be insufficient to produce the $^4S_{3/2}$ threshold population by cooperative energy transfer upconversion pumping. Unfortunately, this cannot be readily accomplished with the dual wavelength Ti:sapphire laser. Gain competition in this laser has been described elsewhere[24,29] and prevents completely independent, continuously variable amplitude control of the two simultaneously-operating wavelengths. In order to produce enough Ti:sapphire laser output power at both wavelengths to exceed threshold for sequential two-photon absorption upconversion a relatively large argon ion laser pump power is required. At this

operating level, however, the output power at the shorter wavelength is greater than the single wavelength threshold power requirement for cooperative energy transfer upconversion pumping. To produce upconversion by two-photon absorption using the dual wavelength laser, the section of the Ti:sapphire laser resonator producing the shorter wavelength was slightly misaligned. This increased the emission bandwidth to approximately 0.7 nm. Since in this case relatively little of the shorter wavelength pump emission is absorbed by the crystal, broadening the pump bandwidth has the same effect as reducing the pump power.

In spite of this somewhat inefficient pumping method, 8 mW of upconversion laser output was achieved with a total of 445 mW of incident pump power. The pump wavelengths were 785 nm and 840 nm, although any of the five wavelengths corresponding to transitions to the $^4I_{9/2}$ Stark levels could be used to initiate the two-photon pumping process. The Er:YALO crystal was maintained at 34°K and a 0.90 R output mirror was used. The spectral composition of the pump beam consisted of approximately 195 mW at 785 nm and 250 mW at 840 nm. The upconversion laser output power is an order of magnitude more power than that previously reported[18] when the crystal was pumped with 195 mW at 792 nm and 250 mW at 840 nm. More importantly, no evidence of saturation of the laser output power with pump power was observed.

The results obtained with the dual wavelength Ti:sapphire laser demonstrate that stimulated emission can be achieved using a number of wavelength pairs. For each pair, one wavelength must correspond to one of the $^4I_{15/2}(1) \rightarrow {}^4I_{9/2}(n)$ transitions while the other corresponds to one of the $^4I_{11/2}(1) \rightarrow {}^4F_{5/2}(n)$ transitions. The use of the dual wavelength Ti:sapphire pump laser, which emits both wavelengths in a single beam, simplifies this type of pumping. Simplification arises from the natural overlap of the two wavelengths in terms of both spatial position and radial intensity distribution, as well as from the elimination of the requirement for an additional pump laser for the second wavelength. The laser output efficiency obtained with dual wavelength pumping is not as high as that obtained with single wavelength upconversion but relative to the results presented in Ref. 18, the output power and efficiency are significantly improved. This is due in part to the longer path length and higher doping density of the laser rod, as well as to the substantially lower passive loss of the Er:YALO laser crystal. In addition, improved operation results from applying the concepts discussed in Section 3.2.4 regarding the design of the resonator and pump optics of the upconversion laser.

3.3.4. *Cooperative energy transfer upconversion in Er:YALO*. Cooperative energy transfer upconversion is the most efficient upconversion pump mechanism in Er:YALO and indeed the optical conversion efficiency obtained for 549.8 nm emission is the highest reported for any upconversion laser crystal. Cooperative energy transfer upconversion in Er:YALO is illustrated in Fig. 21. As in sequential two-photon absorption, the upconversion pump process is initiated by the promotion of an ion from the ground state to the $^4I_{9/2}$ state. The metastable $^4I_{11/2}$ state is populated by rapid non-radiative decay. Cooperative transfer involves two neighboring ions in the metastable state, one termed the energy donor and the other the acceptor. In the energy transfer interaction the donor ion relaxes to the ground state while the acceptor ion is promoted to the $^4F_{7/2}$ state. Rapid relaxation populates the $^4S_{3/2}$ upper laser level. Although illustrated in the figure as direct non-radiative decay from the $^4F_{7/2}$ state, multiphonon relaxation may occur through the intermediate $^2H_{11/2}$ state.

As mentioned above, one of the great advantages of cooperative upconversion pumping compared to sequential two-photon absorption is that a single pump wavelength is required. Before describing the laser results in detail it is instructive to review some of the basic features of low temperature spontaneous emission and infrared absorption in Er:YALO. Single wavelength excitation in the $^4I_{15/2} \rightarrow {}^4I_{9/2}$ band was used to produce the spectroscopic data, with wavelengths in the range 785–807 nm. The fluorescence spectrum is shown in Fig. 22. The crystal temperature was 7°K and the excitation wavelength in this case was 806.9 nm.

The sharp peak at 549.8 nm represents the laser emission wavelength and is due to the $^4S_{3/2}(1) \rightarrow {}^4I_{15/2}(4)$ transition. This is the strongest line in the green emission band. Identical fluorescence spectra were obtained for excitation wavelengths corresponding to the other Stark levels of the $^4I_{9/2}$ state.

The dependence of the green fluorescence intensity on pump power was measured and is shown in Fig. 23. To obtain the data, the laser crystal was placed in the cryostat. The fluorescence normal to the excitation (*b*) axis was imaged onto the entrance slit of a 0.3 m monochromator and detected with an end-on PMT. The PMT signal was digitized and stored in a computer, which also controlled and recorded the monochromator wavelength. The monochromator wavelength was calibrated with several low pressure spectral calibration lamps. For the data shown in Fig. 23 the monochromator was set to 550 nm and the excitation wavelength was 790.6 nm, corresponding to the $^4I_{15/2}(1) \rightarrow {}^4I_{9/2}(4)$ transition. The resolution of the monochromator was 1 nm. Measurements were performed at both 295°K and 7°K. The linear regression fits to the data provide a slope of 1.95 for the 295°K data points and 2.05 for the 7°K data. The linear fit on the full logarithmic plot in Fig. 23 indicates a power-law dependence of the fluorescence intensity on pump power with the exponent given by the slope of the line. The slopes for both temperatures obtained from the linear regression fit indicate that the dependence is quadratic. The coefficients of determination are 0.999 and 0.966 for the 295°K and 7°K data, respectively. There is no indication of saturation of the 550 nm emission at either temperature up to a pump power of approximately 700 mW.

The fluorescence excitation spectrum is shown in Fig. 24. The incident pump power was approximately 7 mW (2 kW cm^{-2}) and seven peaks are observed. The fluorescence excitation spectrum contains several features in common with an absorption spectrum taken at the same

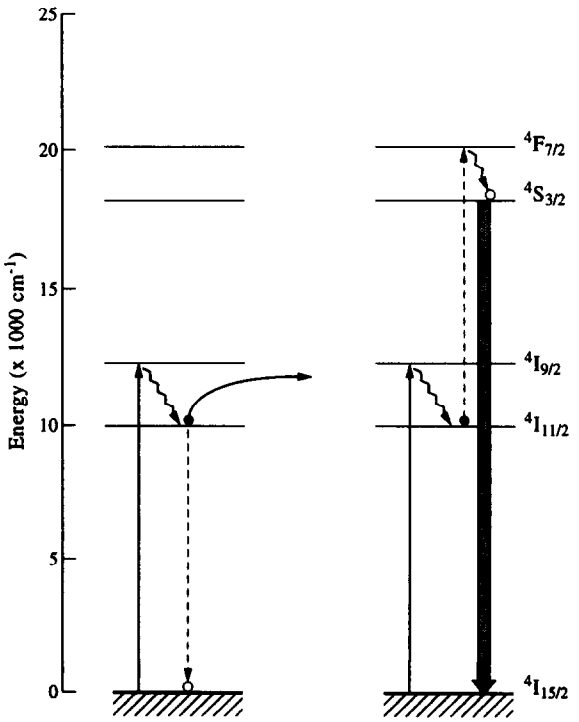

Fig. 21. Cooperative energy transfer upconversion in Er:YALO. Only the electronic states directly involved in the laser and upconversion pumping transitions are shown. The solid circles represent population prior to the energy transfer interaction, while the open circles represent the ion population after energy transfer has taken place.

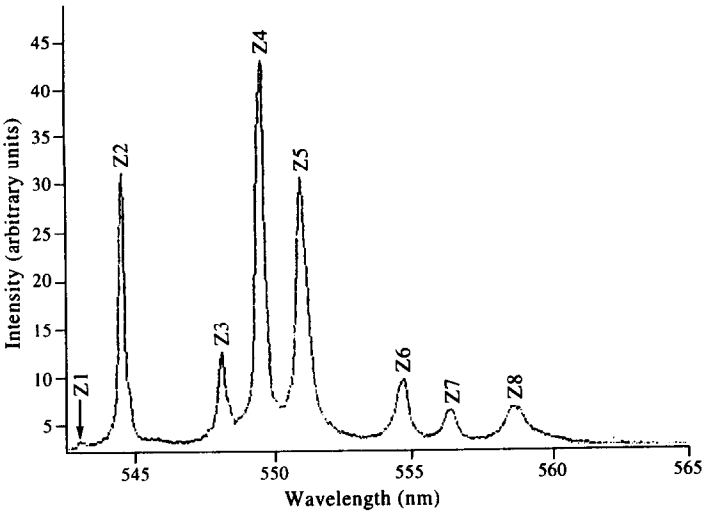

Fig. 22. Fluorescence spectrum of Er:YALO excited by a Ti:sapphire laser operating at 806.9 nm. The spectrum is recorded with an OMA over a period of approximately 0.8 s. The spectral resolution is 0.06 nm and the crystal temperature is 7°K. To obtain the data the fluorescence emitted along the pump axis is imaged onto a 0.3 m monochromator. Eight emission lines are observed corresponding to the eight Stark levels of the $^4I_{15/2}$ ground state. Emission originates from the lowest Stark level of the $^4S_{3/2}$ state and the terminal Stark level in the $^4I_{15/2}$ (Z) state is labeled in the figure for each emission line.

temperature. If the efficiency of producing 550 nm emission is independent of the specific Stark level that is initially excited in the manifold of $^4I_{15/2} \rightarrow {}^4I_{9/2}$ transition lines, then the 550 nm emission intensity measured in the fluorescence excitation spectrum is a direct reflection of the absorption strength of the pump transition. The five strongest fluorescence

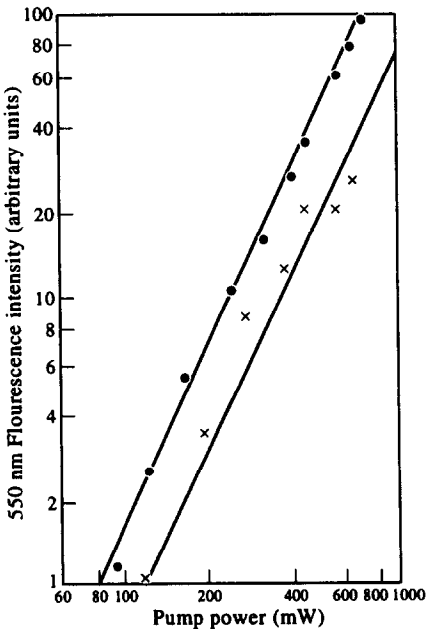

Fig. 23. Dependence of the 550 nm fluorescence intensity on the incident pump power for Er:YALO. The • indicate data for 295°K operation and the x indicate 7°K data. The lines are linear regression fits to the data and have slopes of 1.95 and 2.05 for the 295°K and 7°K data, respectively. The pump wavelength is 790.6 nm. Note the logarithmic axes.

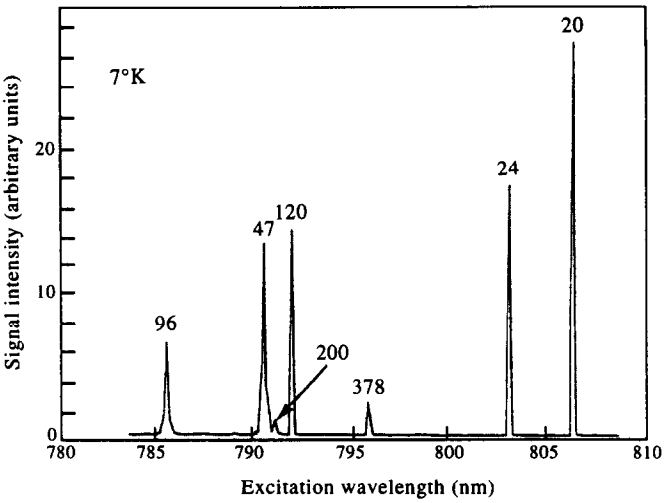

Fig. 24. Fluorescence excitation spectrum for Er:YALO at 7°K. The 550 nm fluorescence intensity is plotted as a function of pump wavelength. The numbers above the fluorescence excitation lines indicate the incident threshold power (in mW) for 549.8 nm upconversion lasing. An HR output mirror was used for the threshold measurements. The abscissa represents λ_A.

excitation lines correspond to transitions from the lowest Stark level of the ground state to the five Stark levels of the $^4I_{9/2}$ state. The small peak at 796.1 nm corresponds in wavelength to the $^4I_{15/2}(3) \rightarrow {}^4I_{9/2}(5)$ transition as well as the $^4I_{13/2}(1) \rightarrow {}^2H_{11/2}(2)$ transition. The Boltzmann factor for population of the third Stark level of the ground state, which is located 171 cm^{-1} above the lowest Stark level, is $\sim 10^{-16}$ at 7°K. It is far more likely that this fluorescence excitation line is due to absorption from the $^4I_{13/2}$ state. The smallest line occurs at 791.3 nm and is due to the $^4I_{13/2}(1) \rightarrow {}^2H_{11/2}(4)$ transition.

Based on the assignment of two of the fluorescence excitation lines to transitions from the $^4I_{13/2}$ state, the probable mechanism for green emission when pumping with 791.3 nm or 796.1 nm radiation is not cooperative energy transfer but photon avalanche upconversion. Photon avalanche upconversion in Er:YALO will be discussed in more detail in Section 3.3.5. Like the $^4I_{11/2}$ state, the $^4I_{13/2}$ state in Er:YALO is metastable with a lifetime[30] of 7.2 ms.

Laser performance measurements were taken using the nearly hemispherical resonator and end-pumping configuration described in Section 3.3.2. The seven excitation wavelengths obtained in the fluorescence excitation spectrum shown in Fig. 24 produced laser emission at 549.8 nm when the resonator was operated with an HR output mirror. The pump wavelengths are 806.9 nm, 803.5 nm, 796.1 nm, 792.2 nm, 791.3 nm, 790.6 nm and 785.4 nm. The pump power required to reach threshold varied for the different excitation wavelengths and the incident threshold pump power is indicated for each line in Fig. 24. The threshold power generally scales inversely with the fluorescence excitation intensity. Some uncertainty in the relative peak heights results from the difficulty of tuning the Ti:sapphire laser output wavelength to the central wavelength of each narrow absorption line but the large deviation from inverse scaling for the 792 nm line may arise from orientational effects. It is well-known[31,32] that the relative intensities of Nd^{3+}:YALO luminescence lines depend on the direction of both the excitation and observation axes relative to the crystallographic axes. The discrepancy in the threshold power scaling for the 792 nm line may be understood by noting that the axis for laser emission is parallel to the pump propagation *b* axis while the fluorescence excitation spectrum is observed normal to this axis. The threshold power should depend inversely on the 550 nm emission intensity along the crystallographic *b* axis, and this is not necessarily identical to the 550 nm emission intensity recorded along the axis of

observation. Orientational effects may also explain the high threshold power for the 796 nm line, although the threshold power for laser emission pumped by photon avalanche upconversion is not generally related in a simple manner to the fluorescence intensity obtained with a low power pump source. In addition, much of the incident pump power is not absorbed by the crystal since the population density in the $^4I_{13/2}$ state is relatively low.

To investigate whether the upconversion laser output saturates with pump power, the variation of the laser output power was measured for pump powers up to 1 W. An HR output mirror was used and the crystal temperature was maintained at 7°K. Saturation was not observed for any of the seven excitation wavelengths for which fluorescence excitation peaks were obtained. For the five wavelengths corresponding to the $^4I_{9/2}$ state the laser output power depended quadratically on the pump power up to the maximum pump power.

To optimize the 549.8 nm output power several different output mirrors were used. The best output power was obtained with a 0.90 *R* mirror. With 893 mW of 806.9 nm pump power absorbed by the Er:YALO laser crystal at 7°K, 91 mW of 550 nm output was produced. The laser output was highly polarized. The temperature dependence of the laser output power was measured to determine the optimum crystal temperature and the results are shown in Fig. 25. For 743 mW of absorbed pump power the highest output power was 80 mW, produced at 34°K. The maximum temperature for laser operation was 63°K. For all measurements the laser operated in the TEM_{00} mode.

Using the 0.90 *R* output mirror the dependence of the upconversion laser power on pump power was once again measured. Measurements were performed both at 7°K and 34°K. The five excitation lines corresponding to the $^4I_{15/2}(1) \rightarrow {}^4I_{9/2}(n)$ transitions were used to pump the Er:YALO crystal. The data for pumping at 806.9 nm are shown in Fig. 26. Lines of slope 2 (quadratic dependence) are illustrated and provide a good fit to the low power data for both temperatures but at higher pump power the dependence deviates from quadratic. The pump power dependence for wavelengths corresponding to the other $^4I_{15/2}(1) \rightarrow {}^4I_{9/2}(n)$ transitions is similar to that illustrated in Fig. 26. The data shown in the figure were obtained with the resonator and pump optics optimized for threshold operation.

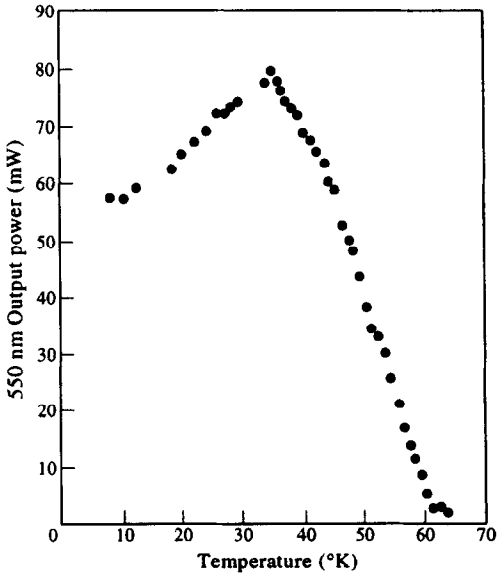

Fig. 25. Dependence of the 549.8 nm Er:YALO upconversion laser output on crystal temperature. The • represent data obtained with a pump wavelength of 806.9 nm. The maximum absorbed pump power for this measurement was 743 mW. Laser emission could not be achieved at temperatures above 63°K.

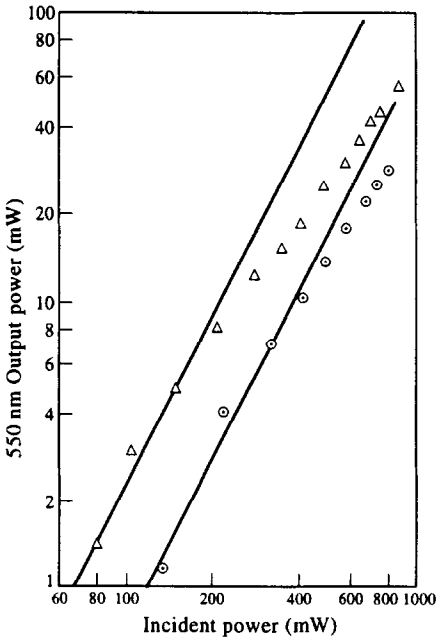

Fig. 26. Er:YALO laser output power dependence on the incident pump power. Both 7°K data (⊙) and 34°K data (△) are shown. The lines illustrate a slope of 2. The resonator and pump optical alignment were adjusted for minimum threshold power using a 0.90 R output mirror. Once the optimum threshold configuration was determined the pump power was increased and the laser output power measured without further adjustments to the laser resonator and pump optical alignment.

When the optical alignment is repeatedly adjusted to maximize the laser output power for each pump power data point the result is somewhat different as shown in Fig. 27. The data in Fig. 27 are shown for excitation at 806.9 nm and are typical of those observed for excitation to the other Stark levels of the $^4I_{9/2}$ manifold. In this case the data sets at both 7°K and 34°K fit well to a straight line (power fit) over the entire range of pump power used. For the 7°K data the laser output power dependence on the pump power is quadratic. The 34°K data exhibit a dependence that is less than quadratic. However, no indication of saturation of the green emission is observed up to a pump power of more than 900 mW. As will be discussed below the deviation from quadratic for the dependence, shown in Figs 26 and 27, indicates a change in the laser dynamics. The maximum output power shown in Fig. 27 was obtained for excitation at 34°K. The laser output power was 121 mW and the absorbed pump power was 918 mW.

The inset in Fig. 27 shows the photon avalanche upconversion laser output power dependence on pump intensity for excitation at 791.3 nm. A 0.99 R output mirror was used and the Er:YALO crystal temperature was 7°K. The dependence of the output power on pump intensity is similar to that observed[33] for photon avalanche upconversion fluorescence from Pr:$LaBr_3$. Near threshold the emission is highly sensitive to pump intensity but the dependence becomes quadratic at higher pump intensities. Photon avalanche upconversion will be described in more detail in the following section.

The fluorescence excitation spectrum was taken for Er:YALO at 34°K and is shown in Fig. 28. The incident pump power used to obtain the data was 7 mW. The five lines representing excitation to the $^4I_{9/2}$ manifold, as well as the two photon avalanche-pumped lines that were observed in the 7°K spectrum, are clearly visible in the 34°K spectrum. Two additional small photon avalanche lines are observed at 789.1 nm and 787.3 nm and are assigned to transitions from the lowest Stark level of the $^4I_{13/2}$ manifold to the fifth and sixth

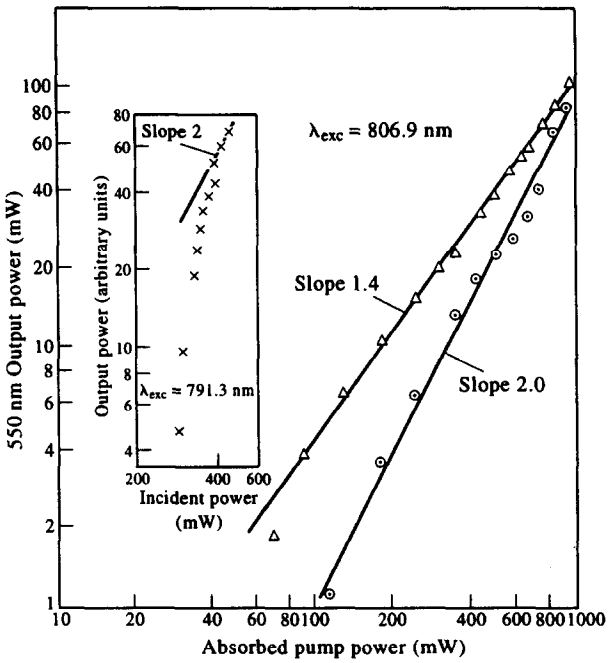

Fig. 27. Dependence of the 550 nm Er:YALO laser output power on the absorbed pump power using a 0.90 R output mirror. The data shown are for 7°K (⊙) and 34°K (△). The straight lines are linear regression fits to the data points and the slopes are indicated for each line. Note the logarithmic axes. For the data shown the resonator and pump optical alignment were adjusted for maximum laser output power at each pump power level. The pump wavelength is 806.9 nm. The inset shows the variation of laser output power (in arbitrary units) with incident pump power in mW for excitation at 791.3 nm. The data for the inset were obtained at 7°K and a 0.99 R output mirror was used. A line of slope 2 is shown for reference near the maximum pump laser power.

Stark levels, respectively, of the $^2H_{11/2}$ state. These lines are also observed in the 7°K fluorescence excitation spectrum but are extremely weak.

The additional lines in the 34°K fluorescence excitation spectrum are due to thermal population of the second Stark levels of the $^4I_{15/2}$ and $^4I_{13/2}$ states. These levels are 50.7 cm^{-1}

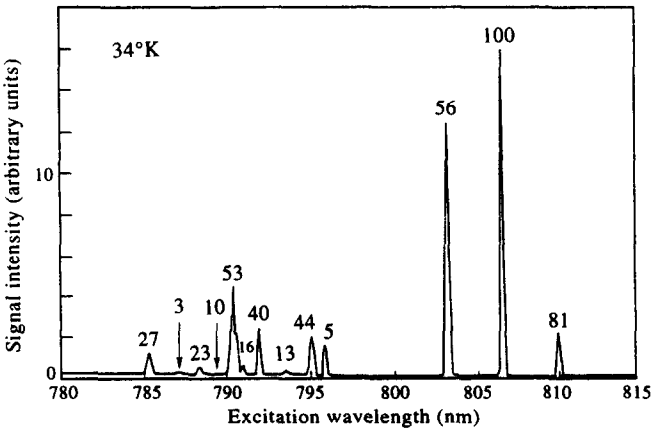

Fig. 28. Fluorescence excitation spectrum for Er:YALO at 34°K. The number above each excitation peak indicates the 550 nm laser output power in mW obtained when pumping the crystal at the excitation wavelength. The incident pump power used was approximately 800 mW. The abscissa represents λ_A.

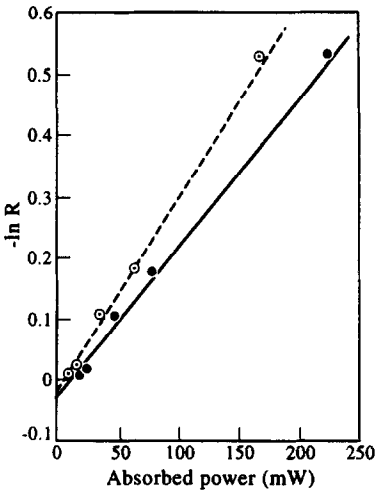

Fig. 29. Plot of the absorbed threshold power as a function of the negative log of the output mirror reflectivity, $-\ln R$, for the Er:YALO upconversion laser. Data for 7°K operation are shown as • and the solid line represents the linear regression fit to this data. The 34°K data are indicated as ○ and the linear regression fit is represented by the dashed line.

and 38.6 cm^{-1} above the first Stark level of the ground state and metastable state, respectively. The strong lines at 810.2 nm and 795.4 nm are due to transitions from the $^4I_{15/2}(2)$ level to the first and third Stark levels, respectively, of the $^4I_{9/2}$ state. The transition to the fifth Stark level is observed at 788.6 nm but the transitions to the second and fourth levels of the $^4I_{9/2}$ state are masked by fluorescence excitation lines at 806.9 nm and 793.7 nm that originate from the $^4I_{15/2}(1)$ level. The small peak at 793.7 nm is due to photon avalanche upconversion initiated by the $^4I_{13/2}(2) \rightarrow {}^2H_{11/2}(4)$ transition.

All of the wavelengths that generated fluorescence excitation peaks at 34°K produced laser emission at that temperature when operating the resonator with a 0.90 R output coupler. The laser output power for each pump wavelength is indicated on the figure. The output power does not scale with the intensity of the fluorescence excitation lines for reasons discussed above. Five of the 13 lines shown in Fig. 28 are due to photon avalanche and it should be noted that the efficiency of this pump mechanism is quite high when based on absorbed power. For example, pumping the 791.3 nm line with 111 mW of absorbed power produces 33 mW at 549.8 nm, giving an optical conversion efficiency of 30%. The absorbed power required to reach threshold is 42 mW. However, the incident pump power required to produce the 33 mW laser output power is approximately 850 mW.

The upconversion laser output wavelength was measured for each excitation wavelength using a commercial wavemeter. Emission at 7°K and 34°K was measured. In Er:YLF different excitation wavelengths in the 800 nm band produce different upconversion output wavelengths in the green. However, under all excitation conditions the Er:YALO emission wavelength remained fixed at 549.8 nm.

The variation of pump threshold power with output coupling was measured to determine the passive loss of the laser resonator. The Findlay–Clay analysis was performed both at 7°K and 34°K with an excitation wavelength of 806.9 nm. The data are shown in Fig. 29. Note the low threshold pump powers obtained at both temperatures for upconversion laser emission pumped by cooperative energy transfer. Using an HR output mirror ($\ln R \approx 0$) the absorbed threshold powers were 11 mW and 20 mW at 34°K and 7°K, respectively. For a 0.90 R output mirror ($-\ln R \approx 0.1$) the threshold powers are 35 mW and 47 mW at 34°K and 7°K, respectively. The linear regression fit for the 7°K points provides a slope of $2.4 \times 10^{-3}\, P^{-1}$, where P is the absorbed power in milliwatts, an intercept of 2.5×10^{-2}, and

a coefficient of determination of 0.996. For the 34°K data, the slope, intercept and coefficient of determination are $3.2 \times 10^{-3}\ P^{-1}$, 1.97×10^{-2} and 0.999, respectively. No saturation of the absorbed power was observed. The slope and intercept of the linear regression fit provide the round trip small signal gain and passive loss for the resonator, respectively, as discussed in Section 3.2.2. The small difference in loss for the 34°K and 7°K data is due to experimental uncertainty.

The relaxation oscillation frequency was determined for the Er:YALO laser at both temperatures to provide an additional determination of the resonator passive loss. The round trip passive loss can be obtained from the frequency by Eqn (23). Using 1.96 for the refractive index of YALO, the term containing the lengths and refractive indices in Eqn (23) is 12.59 cm. A value of 160 μs was used for τ, although this may be too high owing to concentration quenching[34] of the $^4S_{3/2}$ state in the 1.5% Er:YALO crystal. At 34°K the measured f_r was 330 kHz and P_e was 4.7, giving a value for L′ of 12.28×10^{-2}. For the 7°K measurement f_r was 300 kHz and P_e was 3.6, yielding 13.25×10^{-2} for L′. Subtracting the output coupling of 9.96×10^{-2} produces round trip losses of 2.32×10^{-2} and 3.29×10^{-2} for 34°K and 7°K operation, respectively. These values are in reasonable agreement with the passive loss obtained from the Findlay–Clay analysis and the difference in the passive loss for the two temperatures is within experimental error. The experimental uncertainty of the passive loss determination using Eqn (23) is magnified by subtracting the relatively large output coupling term from L′ and in general this method is more precise when performed with low output coupling ($R \approx 1$). Only a small fraction of the loss is expected to be distributed, as most involves residual reflections and bulk scattering from the intracavity cryostat window. For comparison, the loss for the 3 mm long monolithic Er:YALO laser rod[18] used by Silversmith *et al.* to demonstrate two-photon absorption upconversion was 9%.

To verify that cooperative energy transfer is the optical excitation pathway for the five pump wavelengths corresponding to the $^4I_{15/2} \rightarrow {}^4I_{9/2}$ transitions, the pump beam was chopped and the temporal variation of the upconversion laser output was measured. Temporal measurements were performed at 7°K, 34°K and 52°K using a 0.90 R output mirror. Representative traces are shown in Fig. 30. In each oscillogram, two traces are recorded. The lower trace monitors the pump pulse and a negative signal indicates that the shutter is open. The upper trace in each oscillogram shows the 549.8 nm upconversion laser output, where emission produces a positive signal. To obtain the appropriate temporal resolution only 125 μs of the pulse is shown before the shutter closes. The chopper requires approximately 20 μs to completely traverse the pump beam and upconversion laser emission is observed well beyond termination of the pump pulse. It can also be seen quite clearly that the steady state output is purely cw, showing no evidence of amplitude spikes. The excitation wavelength was 806.9 nm and the cw output power at 34°K was 63 mW.

Repetitively Q-switched upconversion emission was demonstrated with several output mirrors at both 7°K and 34°K. The pump power and output mirror reflectivity were selected to obtain optimal coupling under Q-switched operation as described in Section 3.2.3. An oscilloscope trace of the Q-switched pulse is shown in Fig. 31. With an absorbed power of 692 mW at 806.9 nm the shortest pulse width achieved was 40 ns. At 7°K the average Q-switched power at 3 kHz was 9.6 mW and represented 25% of the cw power obtained with the intracavity Q-switch turned off. Somewhat higher ratios of Q-switched to average power were measured at 34°K using lower reflectivity output mirrors. The best ratio of Q-switched to cw power obtained was 0.29 and the highest average Q-switched power obtained was 11 mW. Based on the lifetime of the $^4S_{3/2}$ state the maximum Q-switch rate of 3 kHz is not fast enough[12] to produce ratios approaching one. Repetitively Q-switched operation of an upconversion laser had been demonstrated[35] for the first time in Er:YLF, where 6 mW of average power was reported.

The excitation wavelength band for single wavelength upconversion pumping, ranging from 785 nm to 807 nm, is readily accessible by AlGaAs laser diodes. To demonstrate diode pumping, a wide stripe (200 μm) laser diode was used to pump the Er:YALO laser road. The pump geometry was modified to include a polarization beam combiner cube. In this manner both the Ti:sapphire laser and laser diode could pump the crystal simultaneously. The diode wavelength was temperature tuned and produced 1 W of output power at 803.5 nm. However, diode pumping was not successful. Although low threshold laser operation was produced with

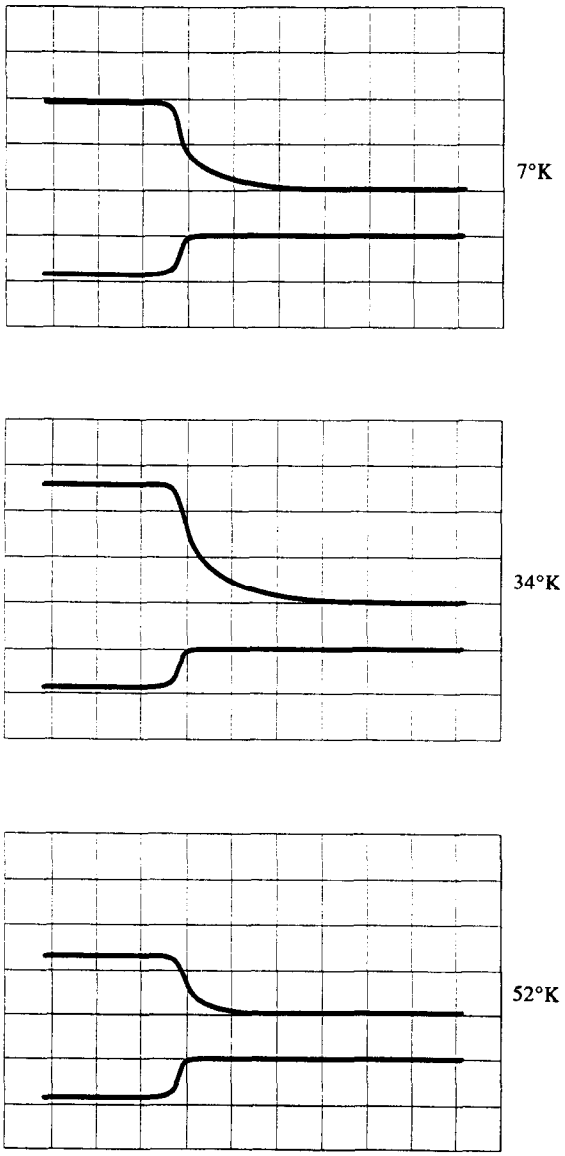

Fig. 30. Oscilloscope traces of the 549.8 nm Er:YALO upconversion laser output obtained with a pump beam chopped at 200 Hz. The pump wavelength is 806.9 nm. Each trace shows the temporal region beginning approximately 125 μs prior to the closing of the shutter. The upper oscillogram represents 7°K operation, while the middle and lower oscillograms are 34°K and 52°K, respectively. For each oscillogram there are two traces. The upper trace corresponds to the upconversion laser output and the lower trace tracks the pump laser output. Light incident on the detector used for the upper trace produces a positive signal, while a negative signal is produced for the detector used in the lower trace. The time scale for all traces is 50 μs per division.

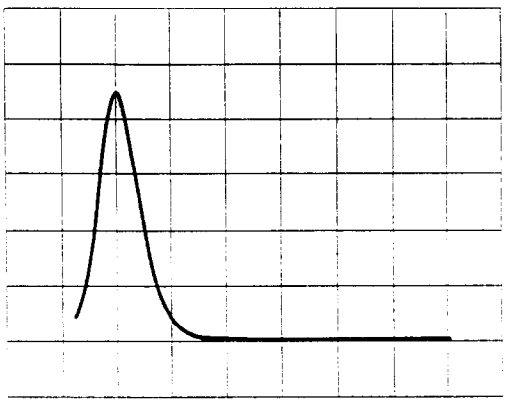

Fig. 31. Oscilloscope trace of the repetitively Q-switched Er:YALO upconversion laser output pulse. The pump wavelength is 806.9 nm, the average Q-switched power was 9.6 mW, the crystal temperature was 7°K and the output mirror was 0.90 R. The horizontal scale is 50 ns per division.

the Ti:sapphire laser pump, the laser diode could not sustain laser oscillation in the Er:YALO crystal with the Ti:sapphire laser blocked.

The difficulties associated with laser diode pumping of upconversion lasers at cryogenic temperatures was discussed in Section 3.2.4. The laser diode used was a gain-guided semiconductor with an output bandwidth of approximately 2.4 nm. As can be seen from the fluorescence excitation spectrum shown in Fig. 24, the absorption bandwidths of the Er:YALO lines are quite narrow. The crystal can therefore absorb only a small fraction of the incident diode pump power even if the wavelength of one of the diode longitudinal modes coincides with an absorption line of the upconversion crystal. Another problem associated with the use of this type of laser diode for upconversion pumping arises from the poor coherence of the gain-guided laser diode across the emitting aperture. An 8 mm focal length, high numerical aperture collimating lens was used to collect the emission from the laser diode and relay the pump flux to a 50 mm focusing lens. The inherent magnification of the pump optics is 6.25. The pump spot size on the exterior face of the laser crystal is many times diffraction-limited due to the poor spatial coherence of the diode and the pump spot size at the HR/HT face of the Er:YALO rod measured 200 μm by 700 μm. Using a shorter focal length focusing lens can reduce these dimensions but the spot size will remain many times diffraction-limited. As mentioned previously, single longitudinal mode, index guided laser diodes or line narrowing and beam profile control techniques for wide stripe gain-guided laser diodes can be used to produce upconversion laser emission as efficiently as a Ti:sapphire laser.

The experimental results obtained for the Er:YALO upconversion laser presented in Figs 22–31 can be discussed in terms of the modified three-level ion model presented in Section 2. The temporal dependence of the laser output power shown in Fig. 30 follows the behavior expected for upconversion pumping by cooperative energy transfer. Laser emission for as long as 150 μs after the termination of the pump pulse indicates that the upper laser level is populated by a long-lived intermediate state. This intermediate state acts as a reservoir for pump excitation and continues to feed the $^4S_{3/2}$ upper laser level after termination of the pump pulse.

The temperature dependence of the laser output shown in Fig. 25 can also be understood within the context of the three-level ion model for cooperative energy transfer upconversion. The build-up of the $^4S_{3/2}$ population n_3 is given by Eqn (17), where level 3 is the $^4S_{3/2}$ state, level 2 is the $^4I_{11/2}$ state and level 1 is the $^4I_{15/2}$ state. With the exception of stimulated emission, all radiative and non-radiative single ion decay processes from the $^4S_{3/2}$ state are included in the term W_{31}. The steady state condition expressed by Eqn (18) suggests that factors that

enhance the cooperative energy transfer rate increase the laser output intensity but only if the population in the terminal laser level remains relatively low.

The temperature dependence of the output power above 34°K is dominated by increased passive loss resulting from increased thermal population in the terminal laser level. To determine the effect of temperature on the passive loss, note that at 7°K the Boltzmann factor for the terminal laser level population is $\sim 10^{-20}$, while at 34°K it has a value of $\sim 10^{-4}$ and at 52°K it is $\sim 10^{-3}$. An estimate of the minimum $^4I_{15/2}(4)$ terminal level population for which the laser intensity is affected can be made using the Findlay–Clay loss. The intensity is related to the round trip small signal gain and loss by Eqn (19). The absorption cross section[18] for the $^4I_{15/2}(4) \rightarrow {}^4S_{3/2}(1)$ transition at 549.8 nm is 2×10^{-19} cm^2. A density of 5×10^{16} cm^{-3} in the terminal laser level will approximately double the round trip passive loss relative to its value at 7°K. This density of population in the $^4I_{15/2}(4)$ level represents 1.7×10^{-4} of the total Er^{3+} ion population and is achieved at 36°K.

Another way of reaching a similar conclusion is from an analysis of the gain. At 7°K the round trip small signal gain near threshold (~ 50 mW of absorbed pump power) is 0.12. Since the small signal gain is $2\sigma N\ell$, the inversion density N that produces this gain is 3×10^{17} cm^{-3}. This value of N represents 1×10^{-3} of the total Er^{3+} ion density. At low temperature N is approximately equal to the population density in the $^4S_{3/2}(1)$ level but as the temperature increases beyond approximately 34°K absorption due to population in the terminal laser level begins to lower the gain and dominate the temperature dependence. Based on the Boltzmann factors, the population density in the $^4I_{15/2}(4)$ level will be approximately 10% of the $^4S_{3/2}$ population at 34°K and approximately 20% at 37°K.

Based on the above discussion, at temperatures greater than 34°K the decrease in the cw output power shown in Fig. 25 as well as the decrease in the steady laser output shown in Fig. 30 are a result of increased passive loss due to thermal population in the terminal laser level. On the other hand the increase in laser output observed between 7°K and 34°K is due to an increase in the cooperative energy transfer rate γn_2^2 as shown by Eqn (18). However, it is not clear whether γ or n_2 increases with increasing temperature. Increasing either of these quantities increases the laser intensity. At 34°K there is an increase in the population of the second and third Stark levels of the $^4I_{11/2}$ manifold but cooperative energy transfer between ions in the higher Stark levels is not more efficient based on the level energetics. That is, cooperative energy transfer from the second or third Stark level requires that more excess energy be removed by the lattice than does cooperative energy transfer from the lowest Stark level. In fact for cooperative energy transfer processes that populate the $^4F_{7/2}$ state, the first Stark level produces the lowest excess energy (9 cm^{-1}) of any of the Stark levels of the $^4I_{11/2}$ manifold. Therefore if the cooperative energy transfer rate coefficient γ were responsible for the observed initial increase of laser output power with temperature, factors other than level energetics would have to be responsible.

The possibility that the observed increase in laser output with temperature is due to an increase in the steady state population n_2 would require that the multiphonon relaxation rate from the $^4I_{9/2}$ state to the $^4I_{11/2}$ state increase, or that the relaxation rate from the $^4I_{11/2}$ state to the $^4I_{13/2}$ state decrease, as the temperature increases from 7°K. Multiphonon relaxation rates are indeed affected by temperature and a comparison of the[36] 300°K and the[28] 77°K lifetimes for the $^4I_{11/2}$ state show a significantly shorter lifetime at 300°K. This is indicative of a faster relaxation rate from the $^4I_{11/2}$ state which of course would reduce the steady state n_2. However, if the relaxation rate from the $^4I_{9/2}$ state increases more rapidly with temperature, the steady state n_2 would show a net increase.

It is interesting to note that Silversmith *et al.*[18] observed a maximum in the dependence of the laser emission on temperature near 30°K under sequential two-photon absorption upconversion pumping of Er:YALO. The cooperative energy transfer rate coefficient is an irrelevant factor in two-photon upconversion but an increase in the $^4I_{11/2}$ state density will

positively affect the laser output produced by two-photon upconversion. This suggests that the increased laser output intensity observed between 7°K and 34°K is due to an increase in the steady state $^4I_{11/2}$ population density.

In Fig. 27 the dependence of the laser output power on pump intensity at 7°K is quadratic while the exponent for the dependence at 34°K is 1.4. Some insight into this scaling difference can be obtained by referring to the model developed in Section 2 and focusing on the pump power dependence shown in Fig. 26. The advantage of using Fig. 26 instead of Fig. 27 is that in the former data set the alignment is fixed, keeping the pump intensity and resonator extraction efficiency constant as the pump power is increased. The steady state condition for Eqn (8) is given by Eqn (11), while the steady state condition for the $^4S_{3/2}$ level is given by Eqn (18). Note that W_{12} is simply a constant times the pump intensity. The exponent in the power-law dependence of the laser output power on the pump power depends on the relative magnitudes of the cooperative energy transfer and single ion decay rate from the $^4I_{11/2}$ state. In the limit where cooperative energy transfer dominates the population dynamics of the $^4I_{11/2}$ state, the stimulated emission rate is given by Eqn (27). Under these conditions the dependence of the laser intensity on the optical pump power is approximately linear. In the limit where spontaneous emission and non-radiative decay from the $^4I_{11/2}$ state dominate the level 2 population dynamics, the metastable state density varies linearly with the pump intensity. In this case the dependence of the laser output power on the pump power is approximately quadratic. Note that n_3 is clamped at its threshold value.

The pump power scaling shown in Fig. 26 can be discussed in terms of the relative magnitudes of the cooperative energy transfer and single ion decay rates. The quadratic dependence observed for the low power data indicates that single ion decay processes such as spontaneous emission and multi-phonon relaxation dominate the n_2 population dynamics. As the pump power increases, n_2 increases and the cooperative energy transfer rate becomes more competitive with single ion decay from the $^4I_{11/2}$ state. In this case the pump power dependence will be less than quadratic. The deviation from quadratic dependence shown in Fig. 26 occurs at a lower pump power for the 34°K data than the 7°K data and implies that γn_2 is larger at 34°K for the same pump power. As mentioned above, this is due to the beneficial effect of temperature on the steady state $^4I_{11/2}$ population.

An implication of the two different scaling exponents shown in Fig. 27 is that the Er:YALO crystal temperature that optimizes the output power is dependent on the pump power. That is, at sufficiently high pump power the 7°K output will exceed the 34°K output if the laser emission does not saturate. Extrapolation of the linear regression fits for the two data sets shown in the figure indicates that the cross-over point will occur when the absorbed power is approximately 1200 mW.

The use of the fit parameters from the Findlay–Clay analysis to generate gain and loss values for the Er:YALO upconversion laser was described in Section 2. The issues are whether the upconversion laser is four-level and whether the threshold upper level population is linearly dependent on the pump power. At both 7°K and 34°K the Boltzmann population factors for the terminal laser level are small enough that this transition can accurately be portrayed as four-level. The linear dependence of the upper level population on pump power is shown by Eqn (22) to hold since $2\gamma n_2 \ll 1/\tau_2$ near threshold. As described above, the quadratic dependence of the laser output power with pump power, illustrated in Fig. 26 for low pump power levels, is further support that $2\gamma n_2 \ll 1/\tau_2$ near threshold.

The good agreement between the passive loss obtained from the Findlay–Clay analysis and that calculated from the relaxation oscillation frequency provides additional support for using the Findlay–Clay results. The loss obtained from the relaxation frequency measurement depends on the value of the $^4S_{3/2}$ state lifetime. It is likely that concentration quenching of the $^4S_{3/2}$ state by ion-pair interactions is substantial for the 1.5% Er-doped sample. The 160 μs lifetime used in Eqn (23) had been measured for a 0.1% doped sample. The decay for a 2%

doped crystal was reported[34] to be non-exponential with a 1/e decay time of about 50 μs. A shorter lifetime used in Eqn (23) would lower the calculated round trip loss.

In the discussion of the Findlay–Clay results it was pointed out that when $2\gamma n_2 \ll 1/\tau_2$ the dependence of the laser output power on the pump power is quadratic while the dependence of the upper laser level population on the pump power is linear. These seemingly contradictory results are derived from the three-level model and can be understood by recognizing that under laser operation n_3 is clamped at its threshold value. Therefore the stimulated emission rate and hence laser intensity, does not depend on the upper laser level population density. The dependence of the laser intensity on the pump power under these conditions is given by Eqn (28). Under these same conditions, the threshold population in level 3 depends linearly on the pump power as shown in Eqn (22).

Pumping the upconversion laser at 806.9 nm produced the most efficient results. At 34°K 166 mW of output power was produced in Er:YALO. The optical conversion efficiency was 17% based on an absorbed pump power of 970 mW. The incident pump power was 1.08 W and the 549.8 nm laser output was TEM_{00} under all conditions. The output power for this crystal is among the highest reported for any upconversion laser. Of the three upconversion pump mechanisms that are known to produce laser emission, cooperative energy transfer provides the highest output power and optical conversion efficiency in Er:YALO. The optimum temperature for upconversion emission was 34°K. At higher temperature thermal population of the terminal laser level reduces the laser output, while at lower temperature the cooperative energy transfer rate is less efficient.

The Er:YALO laser output of 166 mW represents more than a two order-of-magnitude increase compared to that previously reported[18] for upconversion laser emission in Er:YALO and was obtained with only a factor of two higher pump power. In fact the optical conversion efficiency is higher than any reported previously for an upconversion laser. Given the non-linear dependence of the laser output power on pump power, the optical conversion efficiency should continue to increase with increasing pump power. The improved performance is due in part to the high quality laser crystal used as well as to an advantageous resonator design. It is significant that the upconversion laser output power is not observed to saturate with increasing pump power. Replacing the ion laser-pumped Ti:sapphire laser with laser diodes can provide excellent electrical efficiency, although the laser diode output must be tuned to the proper wavelength. Tuning the diode output can be achieved by a number of means, including junction temperature control or using an external cavity. Additional details of the performance of the Er:YALO upconversion laser pumped by a dual wavelength Ti:sapphire laser to produce sequential two-photon absorption upconversion and by a single wavelength commercial Ti:sapphire laser to produce efficient cooperative energy transfer upconversion are available in the literature.[37]

3.3.5. *Photon avalanche upconversion in Er:YALO.* Photon avalanche-pumped fluorescence was first observed[33] in 1979 but was not identified as the dominant pump mechanism for visible upconversion lasers until $Pr^{3+}:LaCl_3$ laser emission was reported[38] in 1990. Shortly afterwards, photon avalanche pumping was reported for $Nd^{3+}:YLiF_4$(Nd:YLF[39]) and $Tm^{3+}:YLiF_4$(Tm:YLF[40]) lasers. The energy transport and photon processes involved in photon avalanche upconversion in Er:YALO are illustrated in Fig. 32. This pump mechanism involves several different steps, including production of both the small initial population and the higher avalanche population in the metastable state, and the promotion of ions from the metastable state to the upper laser level. Following the notation used in Fig. 5, level 3 is the $^4S_{3/2}$ state, level 2 is the $^4I_{13/2}$ state and level 1 is the $^4I_{15/2}$ state. The initial population in the $^4I_{13/2}$ metastable state is produced by non-resonant absorption of the single wavelength pump flux by ions in the $^4I_{15/2}$ ground state. For pump wavelengths in the 800 nm band the state nearest in energy to the pump photon energy is the $^4I_{9/2}$ state. Rapid relaxation from the $^4I_{9/2}$ state produces population in the $^4I_{11/2}$ state and subsequent radiative and non-radiative decay

from the $^4I_{11/2}$ state populates the $^4I_{13/2}$ state. The pump flux then excites the $^4I_{13/2} \rightarrow {}^2H_{11/2}$ transition. This is followed by rapid relaxation to populate the $^4S_{3/2}$ upper laser level.

As illustrated in Fig. 32, two processes compete for the population in the $^4S_{3/2}$ state. The first is radiative decay to lower lying states. In Fig. 32 radiation to only the ground state is shown, as this transition produces the 549.8 nm laser emission. However, radiative transitions from the $^4S_{3/2}$ state to other levels have been observed in Er:YALO. The second process is cross relaxation energy transfer, in which energy is transferred between the donor ion in the $^4S_{3/2}$ state and a neighboring acceptor ion in the $^4I_{15/2}$ ground state. Cross relaxation promotes the ground state ion to the $^4I_{13/2}$ metastable state, while the donor ion decays to the $^4I_{11/2}$ intermediate state. This is shown by the dashed lines in Fig. 32. Radiative and non-radiative decay from the $^4I_{11/2}$ state populate the $^4I_{13/2}$ state. Starting with one ion in the metastable state, the absorption of a photon followed by cross relaxation energy transfer produces two ions in the metastable state. As described in Section 2.4 this multiplicative effect is the basis of photon avalanche upconversion.

The branching between radiation from the $^4S_{3/2}$ state and cross relaxation energy transfer from this state determines both the intensity of the 549.8 nm emission as well as the steady state $^4I_{13/2}$ population for a given pump power. One complication in modelling the Er:YALO upconversion laser is that there are two metastable states, the $^4I_{11/2}$ and the $^4I_{13/2}$. The lifetimes are 1.2 ms and 7.2 ms for the $^4I_{11/2}$ and $^4I_{13/2}$ states, respectively. In the absence of significant cooperative energy transfer upconversion from the $^4I_{11/2}$ state the population in this state will decay to the $^4I_{13/2}$ state. In fact, the 2.7 μm Er:YALO laser operates on the radiative $^4I_{11/2} \rightarrow {}^4I_{13/2}$ transition. However, the model of photon avalanche upconversion illustrated in Fig. 5, which shows a short lived level 2′ decaying rapidly to level 2, is not quite correct for Er:YAO.

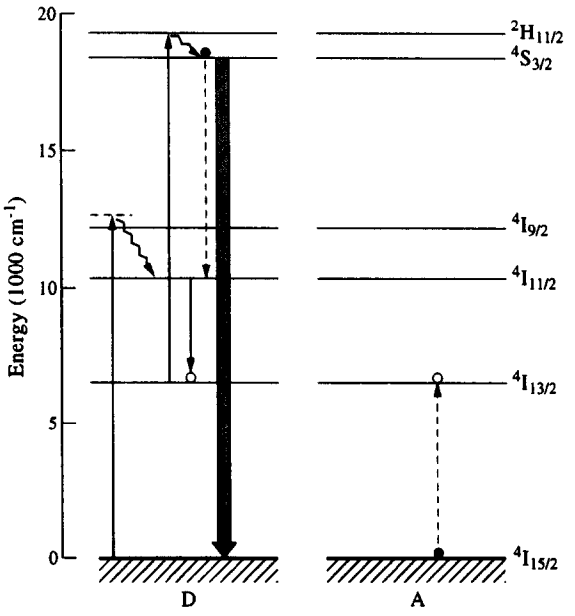

Fig. 32. Schematic representation of photon avalanche upconversion pumping in Er:YALO. Only selected states involved in the pump process are shown. Solid vertical lines correspond to radiative transitions, while wavy lines indicate non-radiative decay. Dashed vertical lines show the energy flow for cross relaxation energy transfer in the donor (D)–acceptor (A) ion pair. Filled circles represent population in the ion pair prior to cross relaxation, while open circles represent the population after relaxation.

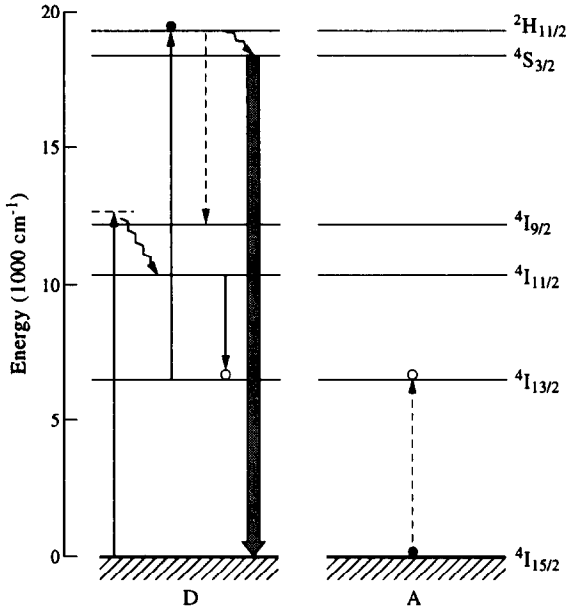

Fig. 33. Schematic representation of an alternative photon avalanche pumping mechanism in Er:YALO. Solid, wavy and dashed arrows have meanings identical to those in Fig. 32. Only selected states involved in upconversion are shown.

The "mirror image" of the energy transfer process shown in Fig. 32 is an equally important process in cross relaxation. In this case the acceptor ion is promoted to the $^4I_{11/2}$ state while the donor ion decays to the $^4I_{13/2}$ state. For either process the excess energy for the ion pair interaction is approximately 1500 cm^{-1}. An alternative path for cross relaxation energy transfer involves the $^2H_{11/2}$ state and is illustrated in Fig. 33. In this process the initial population in the $^4I_{13/2}$ state occurs through non-resonant absorption and relaxation processes identical to those described above. Absorption from the $^4I_{13/2}$ metastable state promotes the ion to the $^2H_{11/2}$ state. However, cross relaxation energy transfer involves the $^2H_{11/2}$ state directly, producing ions in both the $^4I_{13/2}$ and $^4I_{9/2}$ states. The ion in the $^4I_{9/2}$ state decays to the $^2H_{11/2}$ state (not shown in Fig. 33) and a second decay produces the $^4I_{13/2}$ state, completing the photon avalanche cycle as described in reference to Fig. 32. Alternatively, population in the $^2H_{11/2}$ state can decay non-radiatively to the $^4S_{3/2}$ state, populating the upper laser level. In this alternative photon avalanche pumping mechanism non-radiative decay and cross relaxation energy transfer compete for population in the $^2H_{11/2}$ state. An important aspect of this upconversion process is that the cross relaxation energy transfer is almost resonant, producing only 4.3 cm^{-1} of excess energy.

In this section the details of photon avalanche-pumped laser performance of Er:YALO are presented. The section begins by providing experimental evidence for photon avalanche upconversion. This consists of a series of parametric measurements of upconversion fluorescence. Upconversion laser operation is then described. Threshold performance, the dependence of the laser output power on crystal temperature, and the optical conversion efficiency will be discussed for this unusual pumping mechanism.

Experimental evidence for photon avalanche upconversion in Er:YALO was obtained in a manner consistent with the general procedure for identifying photon avalanche upconversion outlined in Section 2.4. The first step is to verify that the pump wavelength promotes ions from the metastable state. In Fig. 34 the 7°K fluorescence excitation spectrum is displayed. This figure is a reproduction of the data shown in Fig. 24 but the pump transition associated with each of the nine fluorescence excitation lines is labelled in Fig. 34 using

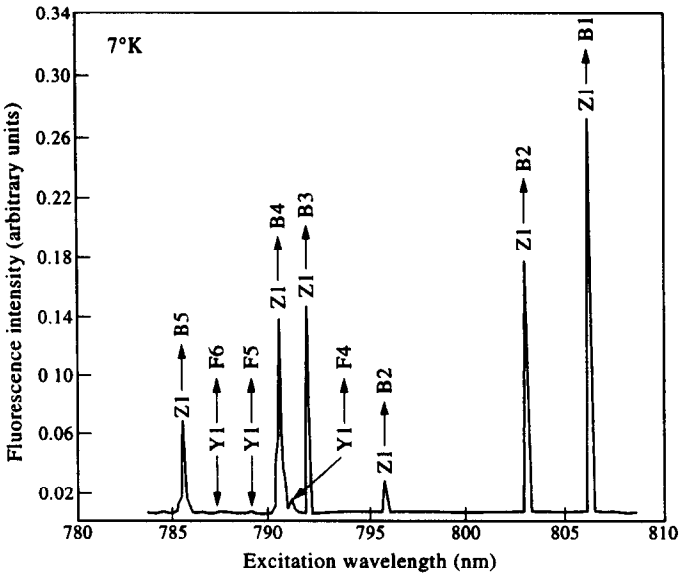

Fig. 34. Fluorescence excitation spectrum for Er:YALO at 7°K. The 550 nm fluorescence intensity is plotted as a function of pump wavelength. The labels of the nine lines correspond to the absorption transition responsible for producing the visible emission. The incident pump power was 7 mW.

conventional notation.[41] The five spectral lines representing Z1 → Bn(n = 1–5) transitions are clearly visible and the four weaker lines are due to absorption from the Y1 level. Some of the weakest lines are difficult to see in Fig. 34. The pump power was limited to 7 mW to avoid saturating the PMT on the stronger lines, but at higher pump power these lines become more prominent. The two weakest fluorescence excitation lines were also verified by their appearance in the 34°K excitation spectrum (Fig. 28).

No fluorescence excitation lines originating from higher ($n \geqslant 2$) Stark levels were observed at 7°K. The Boltzmann factors for the first three Stark levels of the ground and metastable states are given in Table 1. The transition wavelengths for absorption from the first two Stark levels of the ground state and the first Stark level of the metastable state are listed in Table 2.

The assignment of the fluorescence excitation lines in Fig. 34 is based on the thermal population of the Stark levels and the spectroscopic data of Donlan and Santiago.[21] The Boltzmann factors listed in Table 1 indicate that only transitions from the lowest Stark level of the $^4I_{15/2}$ or $^4I_{13/2}$ state will appear in the 7°K fluorescence excitation spectrum. By referring to Table 2 it can be seen that fluorescence excitation lines due to ground state absorption are easily distinguished from transitions originating in the metastable state. While no fluorescence excitation lines from the second Stark level of either the ground state or metastable state appear in the 7°K spectrum, three Z2 and one Y2 transitions were observed at 34°K (Fig. 28). These transitions do not overlap the Y1 transitions.

Table 1. Boltzmann population factors for selected Stark levels

Level	7°K	34°K
Z1	1	1
Z2	2.95×10^{-5}	1.17×10^{-1}
Z3	5.78×10^{-16}	7.29×10^{-4}
Y1	1	1
Y2	3.58×10^{-4}	1.95×10^{-1}
Y3	1.11×10^{-6}	5.95×10^{-2}

Table 2. Transition wavelengths for Er:YALO

Transition	Vacuum wavelength (nm)
Z1 → B1	806.89
Z1 → B2	803.50
Z1 → B3	792.17
Z1 → B4	790.65
Z1 → B5	785.42
Z2 → B1	810.21
Z2 → B2	805.78
Z2 → B3	795.37
Z2 → B4	793.83
Z2 → B5	788.56
Y1 → F1	798.94
Y1 → F2	796.18
Y1 → F3	794.44
Y1 → F4	791.28
Y1 → F5	789.08
Y1 → F6	787.35

Having established that four of the excitation lines in Fig. 34 are due to absorption from the metastable state, additional evidence is required to positively identify photon avalanche as the dominant upconversion pump mechanism. This is because $^4I_{13/2}$ state absorption is associated with both photon avalanche and non-resonant sequential two-photon absorption upconversion. The sequence of events for non-resonant two-photon absorption upconversion is: non-resonant absorption of the pump flux from the $^4I_{15/2}$ ground state, followed by relaxation from the $^4I_{9/2}$ state to the $^4I_{13/2}$ metastable state and then resonant absorption from the metastable state to the $^2H_{11/2}$ state. Relaxation to the $^4S_{3/2}$ state produces population in the 550 nm–emitting level. Since photon avalanche does not occur below the threshold pump power defined by Eqn (14), upconversion fluorescence at low pump power results primarily from non-resonant two-photon absorption. However, it should be pointed out that cross relaxation energy transfer processes of the type illustrated in Figs 32 and 33 occur at pump powers below the avalanche threshold. These processes also contribute to the production of 550 nm emission at low pump power.

As noted in Section 2.4, positive identification of photon avalanche requires that either the threshold in the pump power dependence of the upconversion fluorescence be detected (see Fig. 6), or the appearance of a concave region in the initial portion of the temporal fluorescence dependence under pulsed pumping must be observed (see Fig. 7(b)).

The first set of measurements performed to verify photon avalanche recorded the variation of the upconversion fluorescence output power on pump power. The measurements were taken as described in Section 3.3.2 and consisted of detecting the fluorescence emitted by the sample along the excitation axis. The sample was placed in a cryostat and the emission was imaged onto a monochromator set to detect 550 nm radiation. The four wavelengths identified from the fluorescence excitation spectrum as being resonant with transitions from the $^4I_{13/2}$ state were used to excite the crystal. For all wavelengths no discernible deviation from a quadratic dependence of the fluorescence emission intensity could be observed up to a pump power of approximately 600 mW. The pump power was focused onto the crystal with a 50 mm lens so that the pump intensities used in this measurement are comparable to those used to demonstrate laser operation (reported below). A representative plot of the fluorescence emission intensity dependence on the pump power is shown in Fig. 35. The excitation wavelength was 791.3 nm and the crystal temperature was 7°K. Note the similarity of the data in Fig. 35 to that shown in Fig. 23 for Er:YALO upconversion pumped by cooperative energy transfer.

As indicated in Section 2.4, there are several phenomena that can produce fluorescence data that do not display threshold behavior. One possibility is that the absence of a distinct threshold of the type shown in Fig. 6 is due to a low threshold pump power requirement for photon avalanche upconversion. With this in mind, a second set of measurements were performed to determine the temporal evolution of the 550 nm upconversion. These measurements were taken in the same manner as the fluorescence intensity variation measurements. The pump beam was focused onto the face of the Er:YALO crystal, and the fluorescence emitted along the excitation axis was directed onto a 0.3 m monochromator. The Er:YALO sample was maintained at 7°K and the pump power was 400 mW.

Typical oscilloscope traces are shown in Figs 36(a) and 36(b). Figure 36(a) displays the pump pulse as well as the fluorescence waveform. The small square wave is the pump pulse. A positive signal indicates that the pulse is on and the baseline for this trace is aligned with the horizontal grid line containing the vertical ticks that is located in the center of the trace. The other trace represents the fluorescence signal. The polarity of the PMT produces a negative signal when light is detected. The horizontal scale is 2 ms per division and the chopper repetition rate is 54 Hz.

Figure 36(a) shows the fluorescence waveform for pumping at 806.9 nm. The relatively steep rise of the fluorescence indicates that photon avalanche is not taking place. For this pump wavelength upconversion occurs exclusively by cooperative upconversion and the long decay time following pulse termination is expected for this type of upconversion. Unlike the decay of the laser output illustrated in Fig. 30, the time scale for upconversion fluorescence emission is somewhat longer. Figure 36(b) shows the fluorescence waveform for pumping at 798.9 nm. There are three important differences between this fluorescence signal and that shown in Fig. 36(a). The first is the long rise time of the fluorescence signal. The rise time is comparable to the 7.2 ms lifetime of the $^4I_{13/2}$ state and confirms the participation of the metastable state in the upconversion process. The second difference is the more rapid decay of the fluorescence signal after pulse termination, while the third is the clearly concave region

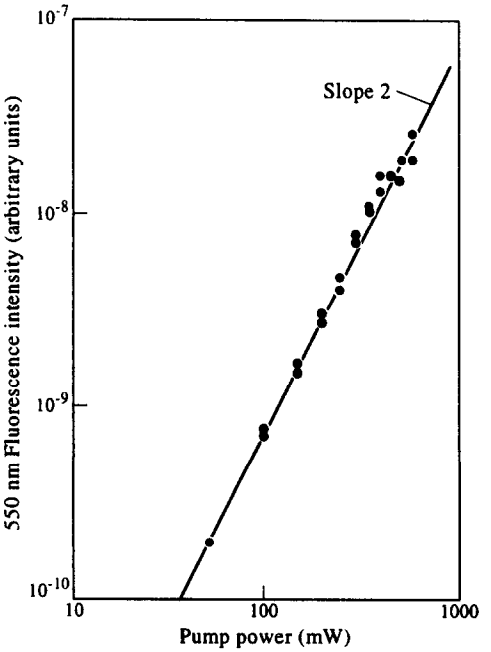

Fig. 35. Variation of the Er:YALO fluorescence intensity with pump power for pumping at 791.3 nm. The crystal temperature was 7°K. The dots represent data, and the line is drawn to illustrate a slope of 2.

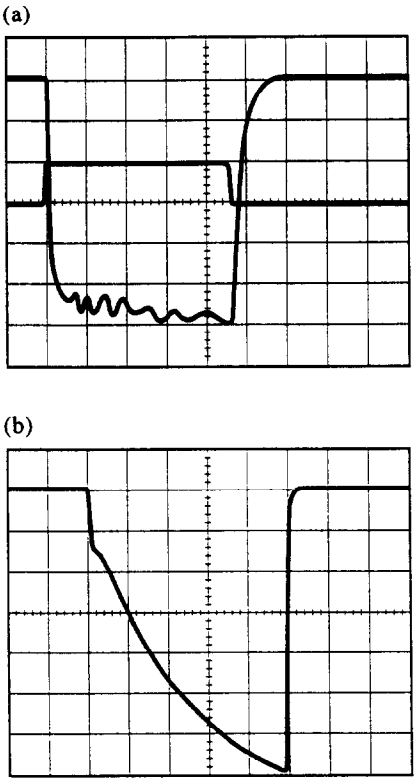

Fig. 36. (a) Typical oscilloscope trace of the temporal dependence of the upconversion fluorescence in Er:YALO. The oscillogram contains two traces. The small square wave is the pump pulse, obtained by chopping the cw pump beam from a Ti:sapphire laser. A positive signal indicates that the pulse is on; the baseline for this trace is aligned with the horizontal grid line containing the vertical ticks located in the center of the trace. The other trace represents the fluorescence signal. The polarity of the PMT produces a negative signal when light is detected. The oscillations in the fluorescence signal are not reproducible and are due to noise. The horizontal scale is 2 ms per division, the chopper repetition rate is 54 Hz, the pump wavelength is 806.9 nm and the pump power is 400 mW. The crystal temperature was maintained at 7°K. (b) Oscilloscope trace of the Er:YALO upconversion fluorescence emission for pumping at a wavelength of 798.9 nm. The pump pulse is not shown, but other experimental conditions are identical to those specified for Fig. 36(a).

of the fluorescence spectrum observed at about 300 μs into the pulse. An unusual feature of the trace is the initial steep rise in the fluorescence signal. This feature is reproducible and has a rise time similar to the fluorescence shown in Fig. 36(a). This steep rise is due to residual population in the $^4I_{13/2}$ state at the start of the pulse and masks part of the concave portion of the trace.

The residual population results from the long lifetime of the metastable state relative to the time between excitation pulses. At 54 Hz about 7% of the $^4I_{13/2}$ state population remains from the previous excitation pulse when the chopper opens again. By slowing the chopping rate to approximately 15 Hz the fast rise portion of the fluorescence is completely gone. However, this rate proved too slow relative to the pump beam diameter. The fluorescence waveform was a convolution of the chopper opening time and the temporal dependence of the upconversion fluorescence.

While the fluorescence trace in Fig. 36(b) appears to identify photon avalanche as the upconversion pump mechanism, additional observations remove the possibility that upconversion is pumped by non-resonant sequential two-photon absorption. The first is that non-resonant absorption is not efficient enough to support laser operation. Non-resonant sequential two-photon absorption pumping produces upconversion fluorescence at low pump

power but to effectively sustain laser operation the excitation rate would have to be at least as large as the stimulated emission rate. The stimulated emission rate is $n_3\sigma_{31}I/h\nu_L$, where n_3 is the population in the $^4S_{3/2}$ state. For the 549.8 nm laser transition pumped at 791.3 nm, $\sigma_{31}/h\nu_L$ is 0.55 cm^2 $Joule^{-1}$, I is 9.5×10^4 W cm^{-2} at 33 mW of output power, n_3 is approximately 6×10^{17} cm^{-3} and the stimulated emission rate is 3.1×10^{22} cm^{-3} sec^{-1}. The non-resonant pump rate is R_1n_1, where R_1 is the pump intensity-dependent rate coefficient for ground state absorption and n_1 is the ground state population density. Using $R_1 \approx 1$ s^{-1}, as was reported[4] for Nd:YLF and taking $n_1 \approx \rho = 2.95 \times 10^{20}$ cm^{-3}, the non-resonant pump rate is less than 0.01 of the minimum required for upconversion lasing. The difference between the wavelengths for absorption from the $^4I_{13/2}$ state and the nearest ground state absorption wavelength varies from 0.7 nm (for 791.3 nm pumping) to 4.0 nm. Modelling indicates that the ratio of the resonant to the non-resonant absorption rate coefficient is between 5000 and 10,000[42] for several different crystals. This ratio is independent of pump intensity.

To determine the efficiency of the non-resonant absorption step the monochromator was set to monitor the fluorescence from the $^4I_{11/2} \rightarrow {}^4I_{15/2}$ transition at 973 nm. Since non-resonant absorption populates the $^4I_{11/2}$ state subsequent to relaxation from the short-lived $^4I_{9/2}$ state, the intensity of the 973 nm emission under conditions where upconversion does not occur is a good gauge of the efficiency of the non-resonant step. The pump wavelength was de-tuned by less than 0.1 nm from resonance with the $^4I_{13/2} \rightarrow {}^2H_{11/2}$ transition. Since the small de-tuning does not affect the non-resonant absorption rate but eliminates resonant absorption from the metastable state to the $^2H_{11/2}$ state, promotion of ground state ions produced by non-resonant absorption of the pump flux should lead to radiation at 973 nm. With the pump wavelength slightly de-tuned relative to each of the four photon avalanche absorption lines detected in fluorescence excitation, no 973 nm radiation was observed within the detection limits of the measurement system.

Another measurement performed to evaluate the participation of non-resonant two-photon absorption was the temporal dependence of the Er:YALO crystal transmission at each of the four pump wavelengths that had been observed to produce photon avalanche upconversion. A representative trace for pumping at 791.3 nm is shown in Fig. 37. The baseline is near the bottom of the oscillogram and the polarity of the PMT produces a positive signal proportional to the amplitude of the light detected. It can be seen that the crystal transmission drops with time in a manner similar to the schematic example illustrated in Fig. 8. It was shown[43] by Joubert *et al.* for the three-level ion model illustrated in Fig. 5 that in the absence of photon avalanche upconversion the crystal transmission remains constant in time. However, under photon avalanche pumping the slow build-up in $^4I_{13/2}$ population produces the observed temporal increase in absorption.

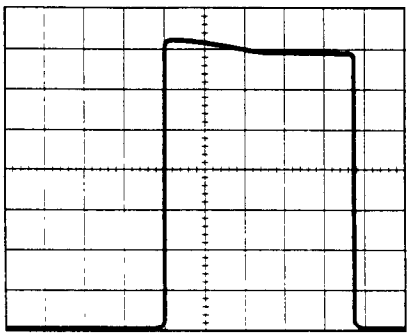

Fig. 37. Temporal dependence of the Er:YALO crystal transmission at the pump wavelength. The crystal temperature is 7°K, the pump wavelength is 791.3 nm, the chopper frequency is 54 Hz and the horizontal scale is 2 ms per division. The polarity of the detector produces a positive signal when light is detected.

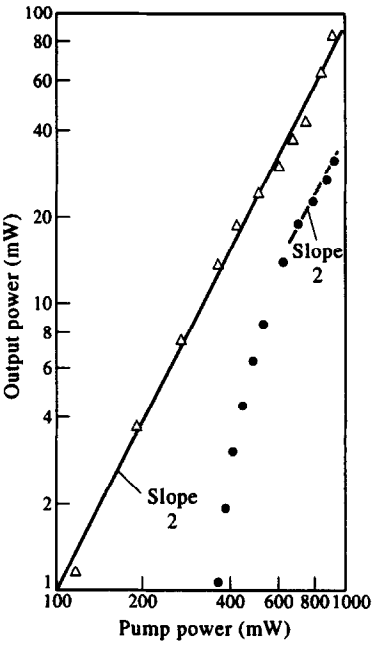

Fig. 38. Er:YALO upconversion laser output power as a function of the incident pump power at wavelengths of 791.3 nm (●) and 806.9 nm (△). The output mirror reflectivity is 0.90 R and the Er:YALO crystal temperature is 7°K. The solid lines are drawn to illustrate a slope of 2.

Laser performance was evaluated using the nearly hemispherical resonator and end-pumping configuration described in Section 3.3.2. All of the wavelengths that generated fluorescence excitation peaks at 7°K produced laser emission at that temperature. With an incident power of approximately 900 mW and an output coupler reflectivity of 0.90, between 6 mW and 33 mW of 549.8 nm laser output power were obtained for the Y1 transitions. The four pump wavelengths that produced photon avalanche laser emission are 787.4 nm, 789.1 nm, 791.3 nm and 796.2 nm. In addition, pumping at 793.7 nm produced photon avalanche laser emission at temperatures above 30°K, as this transition (Y2 → F4) requires thermal population of the second Stark level of the $^4I_{13/2}$ state. Among the excitation wavelengths corresponding to absorption from the metastable state, 791.3 nm produced the highest output power. The data reviewed below are for excitation at this wavelength.

The variation of the laser output power with pump power is shown in Fig. 38. The output is highly sensitive to the 791.3 nm pump power near laser threshold but the dependence becomes quadratic at higher pump power. The 791.3 nm data are substantially different from the laser output power variation when upconversion pumping is by cooperative energy transfer upconversion. The latter pump mechanism dominates when the pump wavelength is 806.9 nm. As can be seen in Fig. 38, this dependence is quadratic over the entire range of pump power used. Note that the axes in Fig. 38 are logarithmic and a slope of 2 corresponds to a quadratic dependence. The difference in laser threshold power for the two pump wavelengths is due to the low fraction of pump power absorbed at 791.3 nm.

The greater-than-quadratic increase in laser output power with pump power was observed for pump wavelengths resonant with other metastable state transitions. On the other hand, even near laser threshold the output power dependence is quadratic for pump wavelengths that produce upconversion by cooperative energy transfer. These contrasting pump power-dependent characteristics are shown in Figs 39(a)–(d) for pump wavelengths corresponding to metastable state absorption, and Figs 39(e)–(h) for ground state absorption.

With 853 mW of pump power incident on the Er:YALO crystal, 33 mW of laser output power was obtained. The optical conversion efficiency was 3.9%. Only a small fraction of the incident power is absorbed, as the steady state population in the $^4I_{13/2}$ state is relatively low. The absorption coefficients for the Y → F transitions are comparable[43] to the Z → B transitions. The fraction of absorbed light is pump power dependent since the pump power determines the steady state population of absorbers. At the maximum pump power only about 13% of the incident power is absorbed, so that the optical conversion efficiency is 30% based on the absorbed power. Over 90% of the incident power is absorbed when pumping by cooperative energy transfer and the best output power was obtained with a pump wavelength of 806.9 nm. As mentioned in Section 3.3.4, at 34°K over 160 mW of output was produced with an optical conversion efficiency of 17%.

The variation of the output power with crystal temperature was measured and is shown in Fig. 40. The laser output drops monotonically with crystal temperature, in contrast to the variation of the laser output power for pumping at 806.9 nm. In the latter case, shown in Fig. 25 and also in the inset in Fig. 40, the temperature dependence is governed by the competing processes of thermal population of the terminal laser level and the increase in the cooperative energy transfer rate. The temperature dependence of cooperative energy transfer upconversion was described in Section 3.3.4. For either pump mechanism the laser output wavelength was not affected by changes in the crystal temperature.

The temperature dependence shown in Fig. 40 is consistent with photon avalanche pumping. It is well known that absorption lines broaden[44] as the temperature increases. If the pump mechanism were non-resonant two-photon absorption, line broadening would produce improved laser emission near 7°K. This assumes that non-resonant absorption is the rate limiting step and factors that affect this rate dominate the overall upconversion efficiency. Instead, the laser emission intensity decreases monotonically with temperature. Since ground state absorption initiates rather than sustains photon avalanche upconversion, increasing the non-resonant absorption rate will not affect the steady state laser output power achieved under photon avalanche pumping. Although Fig. 40 represents pumping at 791.3 nm, similar

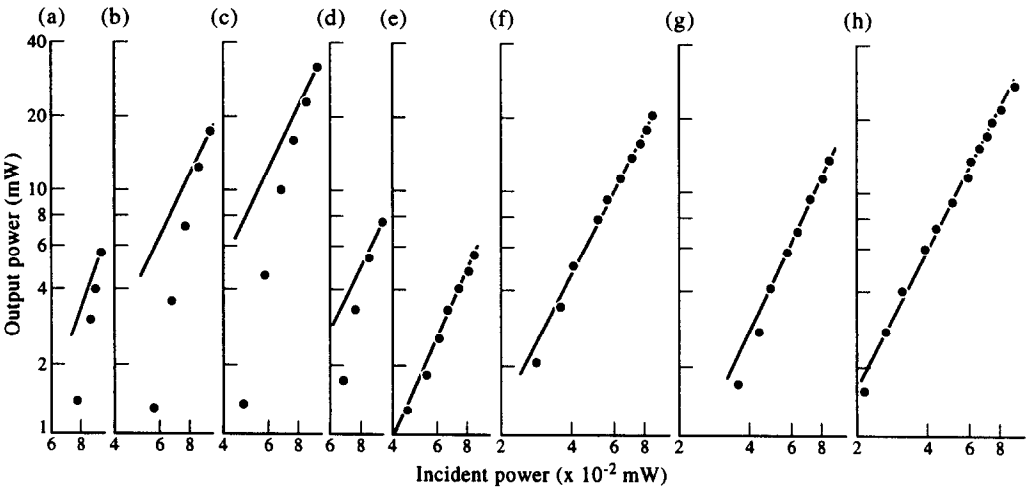

Fig. 39. Er:YALO laser output power dependence on pump power for pump wavelengths that produce upconversion by photon avalanche pumping (a)–(d) and cooperative energy transfer (e)–(h). The pump wavelengths are (a) 787.4 nm; (b) 789.1 nm; (c) 793.7 nm; (d) 796.2 nm; (e) 785.4 nm; (f) 790.6 nm; (g) 792.2 nm; (h) 803.5 nm. All data were obtained at 7°K except (c), which was taken at 34°K. The output coupler for curves (a)–(d) was 0.90 *R*, while for curves (e)–(h) it was 0.98 *R*. Straight lines illustrate a slope of 2. For each data set the abscissa extends to 1 W of incident power. The final tick mark coincides with the vertical line comprising the right hand side of each frame but the 1 W call-out was omitted for clarity.

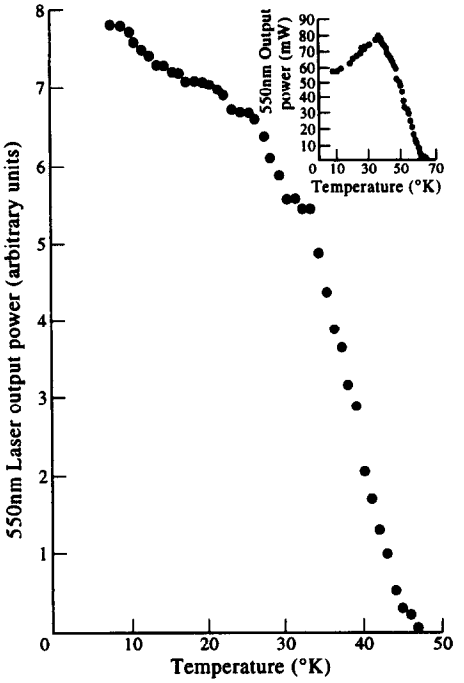

Fig. 40. Temperature dependence of the Er:YALO upconversion laser emission. The pump wavelength is 791.3 nm, the output coupler is 0.90 R and the incident pump power is 772 mW. Laser emission was observed up to 47°K. The inset shows the temperature dependence when cooperative energy transfer is the dominant pump mechanism. The pump wavelength used to obtain the data shown in the inset was 806.9 nm.

temperature dependent data were obtained for wavelengths corresponding to other transitions from the $^4I_{13/2}$ state.

Photon avalanche-pumped upconversion has been previously observed in other Er^{3+}-doped and related materials. McFarlane[45] discussed photon avalanche lasing in several Er-doped halide crystals, while room temperature photon avalanche upconversion laser emission in Er-doped ZBLAN glass was recently reported.[46] In addition, photon avalanche pumping produced[47] laser emission in Tm:YALO. There is little evidence in the literature to support the concept of upconversion laser emission pumped by non-resonant two-photon absorption. Brede *et al.*[48] have shown that for several Er-doped fluorides at room temperature two-photon absorption can produce upconversion laser emission in spite of weak ground state absorption. However, the ratio of the metastable state to ground state absorption coefficients was estimated to be 10, suggesting that although weak, the ground state absorption transition is resonant with the pump wavelength. At room temperature the Er^{3+} absorption lines are broad and the bandwidth of the pump source used in Ref. 48 was 5 nm.

The data reported for upconversion in Er:YALO do not permit an unambiguous assignment of the specific pathway for cross relaxation energy transfer. A consideration for evaluating the viability of a given energy transfer interaction is that cross relaxation must be competitive with other decay processes from the excited state involved in the transfer. For the nearly resonant process ($^2H_{11/2}(1) \rightarrow {}^4I_{9/2}(2)$, $^4I_{15/2}(1) \rightarrow {}^4I_{13/2}(3)$) the dominant decay mechanism from the upper state in the absence of cross relaxation is non-radiative decay to the $^4S_{3/2}$ state. Based on the 632 cm^{-1} energy gap between the $^2H_{11/2}$ and $^4S_{3/2}$ states, the decay time will be shorter[28] than 1 μs. The rate constant for the nearly resonant cross relaxation energy transfer process may not be fast enough to dominate the avalanche kinetics. The "mirror image" energy transfer process from the $^2H_{11/2}$ state, $^2H_{11/2}(1) \rightarrow {}^4I_{13/2}(3)$,

$^4I_{15/2}(1) \rightarrow {}^4I_{9/2}(2)$, is identical to the cross relaxation mechanism described above in that only 4.3 cm^{-1} of excess energy is produced.

Ion pair energy transfer from the $^2H_{11/2}$ state had been discussed[49] by Breguet *et al.* in the context of a room temperature investigation of the 2.7 μm $^4I_{11/2} \rightarrow {}^4I_{13/2}$ laser transition in Er:YALO. Population in the $^4I_{13/2}$ terminal laser level diminishes the laser efficiency and it was found that by preventing direct excitation of the $^2H_{11/2}$ state the threshold power requirement for 2.7 μm laser emission was reduced. The implication of this observation is that the $^2H_{11/2}$ state is highly effective in populating the $^4I_{13/2}$ state by cross relaxation. However, at 298°K there is a sizable steady state population in the $^2H_{11/2}$ state due to thermal excitation from the $^4S_{3/2}$ state. The cross relaxation energy transfer kinetics at 7°K, where the steady state population in the $^2H_{11/2}$ state is low, may be substantially different.

Breguet *et al.*[49] noted that at 298°K cross relaxation from the $^4S_{3/2}$ state, $^4S_{3/2}(1) \rightarrow {}^4I_{9/2}(1)$, $^4I_{15/2}(1) \rightarrow {}^4I_{13/2}(1)$, is also effective in producing population in the metastable state. The energy deficit of 589 cm^{-1} makes this mechanism unlikely at 7°K, but the $^4S_{3/2}(1) \rightarrow {}^4I_{11/2}(6)$, $^4I_{15/2}(1) \rightarrow {}^4I_{13/2}(7)$ cross relaxation process produces about 1100 cm^{-1} of excess energy. The longer lifetime of the $^4S_{3/2}$ state relative to the $^2H_{11/2}$ state makes cross relaxation from the former state more likely. As mentioned in Section 3.3.4, however, the fluorescence lifetime of the $^4S_{3/2}$ state in the 1.5% doped Er:YALO crystal is shortened[34] to 50 μs as a result of concentration quenching. In addition, under laser operation decay from the $^4S_{3/2}$ state occurs through stimulated emission as well as fluorescence. For a cavity intensity of 9.5×10^4 W cm^{-2} the stimulated emission lifetime is 19 μs.

In photon avalanche pumping of Tm:YLF, cross relaxation was reported[50] to originate from the upper laser level. The production of 1100 cm^{-1} of excess energy by cross relaxation from the $^4S_{3/2}$ state does not necessarily imply a smaller energy transfer rate coefficient relative to the nearly resonant process from the $^2H_{11/2}$ state. Recent modelling[51] shows that for Tm:LaF_3 the cross relaxation rates are similar for two processes which produce as little as 30 cm^{-1} and as much as 1000 cm^{-1} of excess energy, respectively. However, in doubly-doped Y_2O_3 it was reported[2] that the energy transfer rate decreases exponentially with the excess energy. A similar result is obtained for multiphonon relaxation; in Y_2O_3 the effective phonon energy is 420 cm^{-1}.

In an attempt to distinguish between the two upconversion pump processes shown in Figs 32 and 33, an experiment was performed to determine whether the upconversion fluorescence intensity would be affected if the $^2H_{11/2}$ state were not populated. Pumping the Er:YALO crystal at wavelengths corresponding to the $^4I_{13/2} \rightarrow {}^4S_{3/2}$ transitions in the 847 nm band produces no population in the $^2H_{11/2}$ state. Under these pump conditions no upconversion emission was detected. While possibly representative of the reduced non-resonant absorption rate R_1 at the longer wavelengths, this observation casts some doubt on the participation of the $^4S_{3/2}$ state in the cross relaxation energy transfer process illustrated in Fig. 32. Based on results reported by Auzel and Chen[52] the non-resonant absorption coefficient depends on $e^{-x\Delta E}$ where x is a constant and ΔE is the difference in energy between the pump photon and the nearest electronic state. ΔE for pumping at 847 nm is approximately a factor of 10 greater than ΔE for pumping the $^4I_{13/2} \rightarrow {}^2H_{11/2}$ transitions in the 800 nm band. In concluding the discussion of pump mechanisms, it is noteworthy that for both Tm:YLF[50] and Tm:LaF_3[51] two photon avalanche channels operate simultaneously. It is possible that cross relaxation from both the $^2H_{11/2}$ and $^4S_{3/2}$ states contribute to photon avalanche upconversion in Er:YALO as well.

Cross relaxation energy transfer from either the $^2H_{11/2}$ or the $^4S_{3/2}$ state involves cascade relaxation and it is worthwhile to briefly review some of these processes. The $^4S_{3/2}$ state can populate intermediate states by both radiation[53] and relaxation.[36] Radiative processes include decay to the $^4I_{13/2}$ state, which is the basis for the 840 nm Er:YALO laser. The radiative[34] rate is 935 s^{-1}. The radiative transition to the $^4I_{9/2}$ state produces 1.66 μm laser

emission and radiative decay to the $^4I_{11/2}$ state has been observed[36] as well. The multiphonon relaxation rates for the $^4S_{3/2}$ and $^4F_{9/2}$ states are[28] $3.6 \times 10^3\ s^{-1}$ and $4.9 \times 10^4\ s^{-1}$, respectively, so that the non-radiative decay rates are competitive with radiative rates. Fluorescence from the $^2H_{11/2}$ state has not been observed.

Ions in the $^4F_{9/2}$ and $^4I_{9/2}$ states decay by multiphonon relaxation to the $^4I_{11/2}$ state. The lifetime of the non-fluorescing $^4I_{9/2}$ state is less[36] than 20 μs. Ions in the $^4I_{11/2}$ state populate the $^4I_{13/2}$ state both by relaxation and radiative decay. The lifetime of the $^4I_{11/2}$ state is[28] 1.2 ms. The multiphonon relaxation rate for the $^4I_{11/2}$ state is[28] $5.9 \times 10^2\ s^{-1}$ and as noted above, the $^4I_{11/2} \rightarrow {}^4I_{13/2}$ radiative transition is the basis for the 2.7 μm Er:YALO laser.[49,54] The radiative lifetime of the $^4I_{11/2}$ state was calculated[28] to be 4.4 ms. Decay from the $^4I_{13/2}$ metastable state occurs primarily through radiation, as the multiphonon relaxation rate for this state is low. While high steady state population in the $^4I_{13/2}$ level is desirable for efficient photon avalanche upconversion, excited state absorption (ESA) at wavelengths longer than 556 nm promotes ions from the $^4I_{13/2}$ state to the $^2H_{9/2}$ state. As mentioned in Section 3.2.2, ESA is responsible[43] for preventing laser emission into the higher lying Stark levels of the $^4I_{15/2}$ state, thereby eliminating the possibility of cw lasing at room temperature.

A basic model[55] of the photon avalanche laser dynamics can provide a basis for discussing the dependence of the laser output power on pump flux. The steady state $^4I_{13/2}$ metastable population n_m is given by

$$n_m = \alpha[(Y/Y_c) - 1] \tag{32}$$

where α is determined by the rate constants and Y, Y is $W_p/(W_p + 1/\tau_u)$, W_p is the pump rate for optical absorption from the $^4I_{13/2}$ state to the upper laser level, τ_u is the lifetime of the upper emitting state and Y_c is the threshold value for Y. In the steady state the pump rate is equal to the decay rate from the upper laser level. In the simplest case we can assume that the only means of populating the upper laser level is through the process represented by W_p and that stimulated emission dominates decay from this level. In that case

$$W_p n_m = n_u \frac{\sigma I}{h\nu} \tag{33}$$

where n_u is the upper laser level population density, σ is the stimulated emission coefficient and $h\nu$ is the laser photon energy. The laser intensity is then related to the intracavity flux given by

$$I = \frac{W_p n_m h\nu}{\sigma n_u}. \tag{34}$$

Combining Eqns (32) and (34) leads to

$$I = \alpha[(Y/Y_c) - 1]\left[\frac{W_p h\nu}{\sigma n_u}\right] \tag{35}$$

and from Eqn (35) it is evident that the laser output power will increase rapidly with pump power near $Y/Y_c \approx 1$.

The approximations made to produce Eqns (32)–(35) oversimplify the pump dynamics. For example, near threshold the stimulated emission rate is not dominant over the other decay rates from the upper laser level. Therefore we do not expect quantitative results from this model. However, the basic concept illustrated in Eqn (34), which shows that the laser intensity depends directly on the metastable state population under photon avalanche pumping, will be true even with a more complicated kinetics model. As the metastable state population increases rapidly near the avalanche threshold, the laser emission intensity would be expected to mimic this behavior if the pump power required to reach laser threshold is only slightly larger than the photon avalanche pump power.

The expression for n_m given in Eqn (32) is a good qualitative description of the photon avalanche-pumped threshold behavior usually observed for upconversion fluorescence (see Fig. 6). To reach threshold for upconversion laser operation requires several hundred mW of incident pump power, depending on the output coupling. If the rapid increase in laser emission near the laser threshold is due to pumping the crystal at a power near the avalanche threshold power (Y_c) as given by Eqn (35), the implication is that the threshold power for photon avalanche is several hundred mW. However, the data shown in Fig. 35 suggest an extremely low threshold for photon avalanche upconversion. If the photon avalanche threshold pump power is very small, then another explanation is required for the variation of the laser intensity near laser threshold. Additional details of the photon avalanche upconversion process in Er:YALO have been reported[56] in the literature.

As can be seen in Fig. 6, well above threshold the dependence of the photon avalanche upconversion emission on pump power is approximately quadratic. If the model given by Eqns (32)–(35) is qualitatively correct, then the dependence of the laser emission on pump power will be quadratic over the entire range of operation if the laser threshold is substantially higher than the threshold for photon avalanche. The steep increase in stimulated emission intensity near laser threshold will not be observed. An example of this was reported for photon avalanche-pumped laser emission[50] in Tm:YLF.

3.4. *Other rare earth doped crystalline upconversion lasers*

3.4.1. *Introduction.* In this section we will summarize the laser performance reported for a wide range of upconversion lasers. Upconversion materials include both crystalline and amorphous hosts, while the dopants are primarily the trivalent rare earth ions Pr^{3+}, Nd^{3+}, Er^{3+} and Tm^{3+}. The three general types of upconversion pumping have been demonstrated for numerous gain media and operational temperatures range from cryogenic up to 298°K. Although many different crystalline hosts have been demonstrated to produce efficient upconversion laser output, the fluorides have been of particular interest. The low phonon frequencies in fluoride hosts keep the multiphonon relaxation rates low, increasing the lifetimes of the intermediate metastable and upper laser levels. This is important for efficient upconversion. However, fluorides have several well-known disadvantages as laser host crystals, including thermal lensing and fracturing under high average power operation. In those cases where rare earth ion-doped hosts such as garnets or perovskites demonstrate efficient upconversion emission, they are more desirable from a laser operational point of view.

In Section 3.4.2 upconversion laser results will be summarized for singly doped crystals. The laser parameters that will be summarized in this section are mode of operation, temperature, type of pump mechanism, output power, and output wavelength. Section 3.4.3 describes results obtained with doubly doped crystals. These laser gain elements are doped with a sensitizer ion which absorbs the pump light and transfers the excitation energy to the co-doped acceptor ion. Co-doped lasers are more interesting from an historical point of view and only two of these lasers will be described in detail. Amorphous host materials suitable for upconversion lasers are typically optical fibers. These glasses are fluoride-based and will be discussed briefly in Section 3.5.

The sections that follow are written to provide the reader with an overview of the many different types of upconversion lasers that have been demonstrated. The summaries are intended to offer an appreciation of the range and depth of this fascinating field but the review is not encyclopedic in scope. It is by no means comprehensive and many interesting studies have not been included due to space constraints.

3.4.2. *Singly doped crystals.* This section is organized in terms of dopant ion. The four dopant ions discussed are trivalent Pr, Nd, Er and Tm. Upconversion in Ho has been

obtained in both a co-doped crystal and a fiber host and is described in Section 3.4.3 and Section 3.5, respectively. Tables 3 and 4 at the end of this section summarize the laser results obtained with singly doped crystalline upconversion lasers.

3.4.2.1. *Pr^{3+}-doped upconversion lasers*

The earliest report[38] of photon avalanche pumped upconversion laser emission was in Pr-doped $LaCl_3$. The energy level diagram and pump mechanism are shown schematically in Fig. 41. A cw dye laser at 677 nm is used to pump the $^3F_3 \rightarrow {}^3P_1$ transition, and following relaxation to the $^3P_0$ state laser emission is observed on the $^3P_0 \rightarrow {}^3F_2$ transition. Laser action was observed up to 210°K, and for a 7% doped crystal the optical conversion efficiency was 25%. The dependence of the laser output power on pump power was approximately linear.

3.4.2.2. *Nd^{3+}-doped upconversion lasers*

Nd^{3+}-doped lasers have demonstrated upconversion both by sequential two-photon absorption and photon avalanche.[39] Sequential two-photon absorption is illustrated in Fig. 42 for Nd:LaF_3. The first absorption step requires a pump wavelength of 790 nm to excite the $^4I_{9/2} \rightarrow {}^4F_{5/2}$ transition. Relaxation populates the $^4F_{3/2}$ level, which is the upper laser level for the 1.06 μm laser transition in Nd-doped lasers. However, in two-photon absorption this level acts as the intermediate state for upconversion pumping, having a lifetime in LaF_3 of 700 μs. The second absorption step utilizes a pump wavelength at 590 nm to populate the

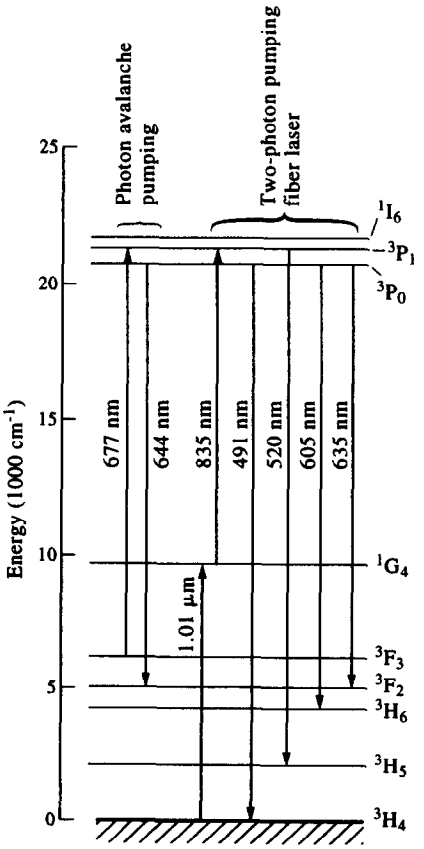

Fig. 41. Partial energy level diagram of Pr^{3+}:$LaCl_3$ showing the pump and laser emission transitions for upconversion. The maximum output power reported for this laser under photon avalanche pumping was 240 mW at 80°K. Sequential two-photon absorption pump transitions and emission for Pr-doped ZBLAN fiber lasers are also shown.

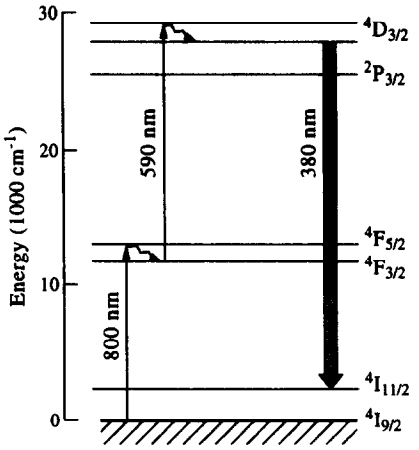

Fig. 42. Partial energy level diagram for Nd:LaF_3, illustrating one of the sequential two-photon absorption upconversion mechanisms used to obtain laser emission at 380 nm.

$^4D_{3/2}$ upper laser level, producing upconversion emission on the $^4D_{3/2} \rightarrow {}^4I_{11/2}$ transition at 380 nm. Lenth and Macfarlane[39] also demonstrated two-photon absorption in this crystal using a single pump wavelength at 578 nm, but found that the single wavelength process was less efficient.

In Nd:YLF excitation into the $^4D_{3/2}$ state produces emission at 413 nm on the $^2P_{3/2} \rightarrow {}^4I_{11/2}$ transition. The pump wavelength is 604 nm. Less than 10 μW of output power was achieved in this laser but 30 mW of 730 nm output power was obtained on the $^2P_{3/2} \rightarrow {}^2H_{9/2}/{}^4F_{5/2}$ transition. While originating in the same upper level as the 413 nm transition, the 730 nm transition terminates on a higher lying state. The 730 nm emission does not represent upconversion in the sense that the emission wavelength is longer than the pump wavelength. However, population of the upper laser level for either transition occurs through photon avalanche pumping. The pump wavelength at 604 nm is resonant with transitions from the metastable $^4F_{3/2}$ state, which in YLF has a lifetime of 525 μs. At a pump intensity of 50 kW cm^{-2}, approximately 30% of the pump flux is absorbed by ions in the intermediate $^4F_{3/2}$ state. The avalanche pumping mechanism populates the intermediate state by cross relaxation from the $^2P_{3/2}$ state.

3.4.2.3. *Er^{3+}-doped upconversion lasers*

Upconversion in Er-doped lasers has been demonstrated by sequential two-photon absorption, cooperative energy transfer and photon avalanche. In the case of YALO, all three mechanisms have produced upconversion in the same crystal. Er upconversion hosts have been primarily fluorides, with YALO being the notable exception. One of the most efficient of the fluoride upconversion laser hosts is YLF.

The majority of the upconversion laser demonstrations in Er-doped materials have been based on cooperative energy transfer in Er:YLF. The primary emission transition is $^4S_{3/2} \rightarrow {}^4I_{15/2}$ at 551 nm, although 470 nm emission has been observed as well. The energy levels of Er:YLF are similar to those shown for Er:YALO in Fig. 15. The first report[57,58] of upconversion laser emission in Er:YLF was based on cooperative energy transfer pumping at 800 nm. Photon absorption to the $^4I_{9/2}$ state is followed by rapid relaxation to populate the $^4I_{11/2}$ state. The $^4I_{11/2}$ state has a lifetime of 2.9 ms in YLF, more than twice that of YALO due to the lower phonon frequencies in the fluoride host. Cooperative upconversion between two neighboring ions in the $^4I_{11/2}$ state produces an ion in the $^4S_{3/2}$ state, similar to the process described for Er:YALO. Emission at 551 nm originates from the $^4S_{3/2}$ state, which has a lifetime of 400 μs in YLF. Pumping the crystal at 802 nm, 5 mW of green emission was

obtained at 50°K. The optical conversion efficiency was 2%, and the dependence of the laser output power on pump power was linear. As mentioned in Section 3.3.1, the observed emission was not purely cw but consisted of random amplitude spikes at repetition rates ranging from tens to hundreds of kHz (termed "self-pulsing").

McFarlane[20] achieved the highest upconversion laser output power recorded to date through cooperative energy transfer upconversion in 5% doped Er:YLF. Pumping with a 4.4 W Ti:sapphire laser at 49°K, 467 mW of 551 nm emission was obtained. The optical conversion efficiency was approximately 11% and the measured dependence of the output power on pump power was linear in this work as well. Self-pulsing of the Er:YLF upconversion laser output was also observed by McFarlane, who reported repetition rates of hundreds of kHz. Unlike the monolithic resonator design used in Refs 57 and 58, the high power Er:YLF laser was operated in a nearly hemispherical resonator using a discrete output coupler.

Several diode-pumped demonstrations of upconversion laser emission in Er:YLF are noteworthy. The first demonstration[59] of a visible upconversion laser pumped by laser diodes was reported for the 551 nm transition in Er:YLF. A monolithic laser crystal doped with 1% Er^{3+} was used in conjunction with a wide stripe 500 mW laser diode. The diode bandwidth was approximately 3 nm and with the crystal at 77°K only 15% of the pump light was reported to be absorbed. Approximately 100 μW of output power was achieved. The incident power was 350 mW, 50 mW of which was absorbed. Subsequently, a substantially improved diode-pumped upconversion laser was demonstrated by using[60] a single mode semiconductor laser pump source. Operating the diode at 802 nm to pump a 1% Er-doped monolithic laser, 2.3 mW of 551 nm emission was obtained. The incident pump power was 100 mW, leading to an optical conversion efficiency of 2%. The crystal temperature was 50°K and approximately 60% of the incident pump light from the diode was reported to be absorbed. Using a dye laser to pump the crystal at 797 nm, the authors were able to show that upconversion laser emission at 544 nm or 561 nm could be produced by adjusting the pump wavelength or crystal temperature.

The highest diode-pumped upconversion laser output reported[17] to date was for an Er:YLF crystal pumped by a wide stripe gain-guided semiconductor laser. The key to this work was the use of beam shaping and mode tailoring techniques that allowed the normally broadband emitting laser diode to operate as a narrowband, coherent pump source. The authors used a nominal 3 W laser diode. This device had an emitting aperture of 1 μm by 500 μm and produced output with a 1.6 nm bandwidth. By aligning the pump diode in a manner that permitted selective, spectrally narrow feedback, the diode operating characteristics were altered. The resulting laser diode output bandwidth was reduced to less than 0.1 nm. Tuning the diode wavelength was accomplished by changing the center wavelength used for feedback and over 1.75 W of narrowband pump power could be delivered to the crystal.

In addition to control of the emission wavelength and bandwidth, an anamorphic focusing lens system was used to produce a small pump waist in the upconversion laser crystal. The pump focal spot dimensions were 290 μm by 85 μm. A 5% doped monolithic laser crystal was used to produce 100 mW of 551 nm emission. The optical conversion efficiency was 6%. Although not linear over the entire range of pump power used, the dependence of the output power on pump power was linear at the higher pump powers used. The slope efficiency in this region was 8%.

Cooperative energy transfer upconversion in Er:YLF has also been demonstrated[61] using three photons at 1.55 μm, the so-called "trio upconversion". Emission at 544 nm was produced at 9°K with a slope efficiency of 16%. The dependence of the output power on pump power was approximately linear. With 400 mW of pump power, 34 mW of output power was achieved, giving an optical conversion efficiency of 8%. At higher crystal temperatures the laser emission wavelength red-shifted to 551 nm. The output wavelength was

independent of the specific pump wavelength in the 1.45–1.55 μm band. The authors also reported pure cw output in Er:YLF under trio upconversion pumping. This is in sharp contrast to the self-pulsed output reported by others using shorter wavelength pump bands. Using trio upconversion pumping, Q-switched and mode-locked operation of an Er:YLF laser was also reported.[35] Pulse widths of approximately 100 ns were obtained under Q-switched operation, while pulses as short as 200 ps were obtained with mode-locking. The maximum average mode locked power was 2 mW for 450 mW of incident power.

The $^2P_{3/2} \rightarrow {}^4I_{11/2}$ upconversion transition in Er:YLF has been demonstrated.[62] This cooperative energy transfer process produces laser emission at 470 nm and was pumped at either 653 or 969 nm. The excitation dynamics indicate that two or three separate energy transfer steps are involved in populating the upper laser level, depending on whether the pump wavelength is 653 nm or 969 nm pumping, respectively. This upconversion process is illustrated in Fig. 43 for 969 nm pumping. The first step in the cooperative upconversion process involves cooperative energy transfer between two ions in the $^4I_{11/2}$ state to produce an ion in the $^4S_{3/2}$ state. This is the energy transfer process that produces 551 nm emission. (For 653 nm pumping the $^4I_{11/2}$ state is populated by photon absorption to the $^4F_{9/2}$ state followed by non-radiative decay.) The second step involves cooperative energy transfer between an ion in the $^4I_{11/2}$ state and an ion in the $^4I_{13/2}$ state. Energy transfer results in an ion in the $^4F_{9/2}$ state. This process is also well-known and is the primary mechanism for populating the red-emitting $^4F_{9/2}$ state. Decay from the $^4S_{3/2}$ state is not effective[63] in populating the $^4F_{9/2}$ state. (For 653 nm pumping the $^4F_{9/2}$ state is populated directly by photon absorption.) The third energy transfer step is cooperative upconversion between an ion in the $^4S_{3/2}$ state and one in the $^4F_{9/2}$ state, producing an ion in the $^2K_{13/2}$ level. Rapid relaxation produces the $^2P_{3/2}$ upper laser level.

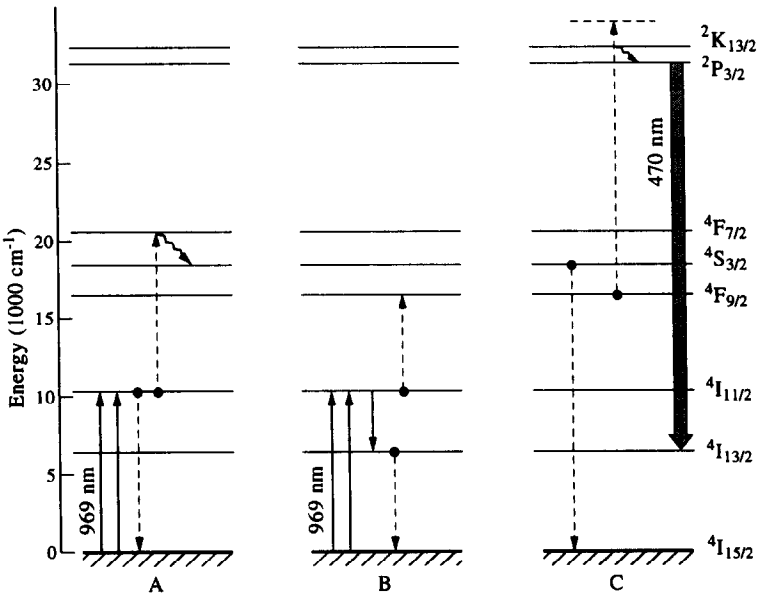

Fig. 43. Illustration of the "three-transfer" upconversion process in Er:YLF. Upconversion is shown for a pump wavelength of 969 nm. (A) 969 nm pump flux promotes ground state ions to the $^4I_{11/2}$ state. The first cooperative energy transfer interaction occurs between two ions in the $^4I_{11/2}$ state, promoting an ion to the $^4F_{7/2}$ state. The $^4S_{3/2}$ state is populated by relaxation from the $^4F_{7/2}$ state. (B) A fraction of the ions promoted to the $^4I_{11/2}$ state decay to the $^4I_{13/2}$ state. The second cooperative energy transfer interaction occurs between an ion in the $^4I_{13/2}$ state and one in the $^4I_{11/2}$ state, promoting an ion to the $^4F_{9/2}$ state. (C) An ion in the $^4S_{3/2}$ state participates in cooperative energy transfer with an ion in the $^4F_{9/2}$ state, producing an ion in the $^2K_{13/2}$ state. Relaxation populates the $^2P_{3/2}$ state and radiation to the $^4I_{11/2}$ state produces emission at 470 nm.

This upconversion process is more efficient for 653 nm pumping than for 969 nm pumping. Only 2 mW of output power was produced with 700 mW of pump power at 969 nm, while using 130 mW of pump power at 653 nm 6 mW of output power was obtained. For both wavelengths the output power depends linearly on the pump power. Due to thermal effects the 969 nm pump beam was chopped with a 5% duty cycle.

This "three-transfer" upconversion pump mechanism represents a loss mechanism for the 551 nm emission. For cooperative upconversion pumped in the 800 nm band the $^4S_{3/2}$, $^4I_{11/2}$ and $^4I_{13/2}$ states are occupied. However, energy transfer processes that populate the $^2P_{3/2}$ state deplete the population in the upper laser level of the 551 nm transition. In addition, the $^4I_{11/2}$ metastable level is required to produce the $^4S_{3/2}$ state through cooperative energy transfer. Upconversion to the $^4F_{9/2}$ state depletes the source of $^4I_{11/2}$ population, further lowering the efficiency of the green upconversion laser process. No 470 nm radiation was observed for any of the three upconversion pump mechanisms in Er:YALO, accounting to some extent for the high laser efficiency measured for 550 nm emission in that crystal.

Two other Er-doped fluoride hosts that have produced upconversion laser emission are CaF_2 and KYF_4. Er:CaF_2 was pumped[64] at 1.5 μm and produced upconversion emission at 855 nm. The operating temperature was 77°K. The maximum output power was 64 mW, produced with 235 mW of absorbed pump power. Based on the absorbed pump power the efficiency is 27%. As in trio upconversion in Er:YLF, no evidence of spiking was observed.

An interesting report of room temperature upconversion laser operation for Er:YLF, Er:KYF_4 and Er:YAG has been published.[48] The doping levels in YLF were 1% and 5%, in KYF_4 the doping was 1% and in YAG the doping level was 0.5%. In Er:YLF simultaneous lasing was observed at 551 nm and 850 nm, the latter wavelength being a result of the $^4S_{3/2} \rightarrow {}^4I_{13/2}$ transition. For the two fluorides, the upconversion pump mechanism was two-photon absorption using a Kr-ion laser and a pulsed Ti:sapphire laser. The upconversion laser output in each case was 0.95 mJ. The Er:YAG laser performance was found to be much less efficient than the fluorides and the output energy was not reported.

The Er:YALO results can be briefly reviewed to obtain a sense of perspective. The most efficient results were obtained through cooperative energy transfer upconversion. While the 166 mW output power reported[56] is not as high as McFarlane's[20] report of 467 mW obtained for Er:YLF, the optical conversion efficiency of 17% is somewhat higher than that reported in Ref. 20. More important, there are very few reports of upconversion laser emission at power levels over 100 mW and it is significant that this type of performance has been achieved in a perovskite material.

We conclude this section by noting the great range of pump mechanisms and operating conditions that have produced efficient upconversion laser emission in Er-doped materials. A review of the upconversion laser dynamics and description of additional upconversion wavelengths in the 600–700 nm range for Er:YLF has been published[65] by McFarlane *et al.*

3.4.2.4. *Tm^{+3}-doped upconversion lasers*

Tm-doped upconversion lasers produce emission in the blue. The earliest demonstration[66] of upconversion emission in a Tm-doped crystal was performed with Tm:YLF. The doping level was 1% and both 77°K and room temperature operation were demonstrated. At 77°K, pulsed dye lasers producing 649 nm and 781 nm emission were combined to produce upconversion by sequential two-photon absorption. Approximately 180 μJ of 450 nm laser output was obtained using 3.5 mJ of pump power at 649 nm and 9.9 mJ at 781 mm. Laser threshold operation at room temperature was achieved with approximately 30 mJ of pump power from each of the two lasers but no output power was reported. The upconversion energy levels and pump mechanism are illustrated in Fig. 44.

To produce cw operation in Tm:YLF, a monolithic crystal was pumped[40,50] with cw dye lasers. Both two-photon absorption and photon avalanche upconversion were demonstrated.

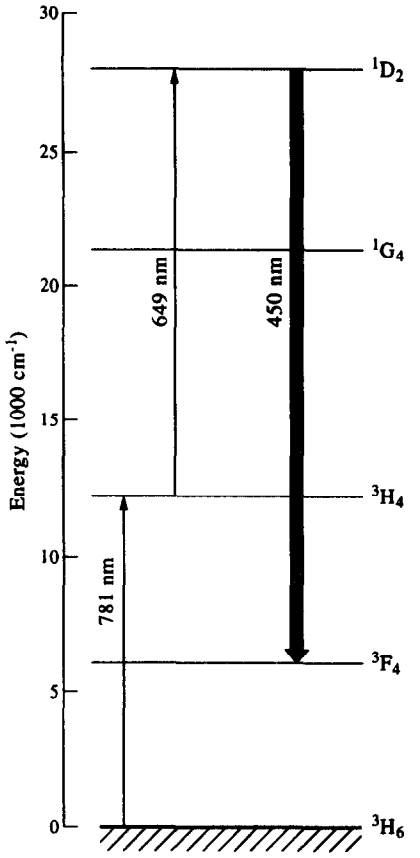

Fig. 44. Partial energy level diagram and excitation pump mechanism for Tm:YLF. Sequential two-photon absorption is illustrated.

The two-photon pump mechanism is similar to that used by Nguyen *et al.*[66] illustrated in Fig. 44. The best performance was obtained at 15°K, where 9 mW of output power was produced using 400 mW of pump power at 648 nm and 140 mW at 784 nm. The doping level was 1.8%. Lasing at 483 nm was also observed along the $^1G_4 \rightarrow {}^3H_6$ transition. The terminal Stark level lies 270 cm^{-1} above the lowest Stark component of the ground state. In this case a single pump wavelength at 629 nm was used and upconversion pumping is by photon avalanche. The pump transition is $^3F_4 \rightarrow {}^1G_4$. The $^3F_4$ state is metastable, with a lifetime of 12 ms. Photon avalanche pumping involves cross relaxation energy transfer from the $^1G_4$ upper laser level. The result of this process is that a ground state ion is promoted to the metastable state while the donor ion decays to the $^3H_4$ state. Although the donor ion in the $^3H_4$ can relax to the metastable $^3F_4$ state, a second cross relaxation process with another ground state ion also is possible. In this event three ions in the metastable state are produced by a sequence of two cross relaxation energy transfer interactions between an ion in the $^1G_4$ upper laser level and two ground state ions.

As with Er:YALO, photon avalanche pumping proved substantially more efficient than sequential two-photon absorption. At 26°K, 30 mW of 483 nm output power was obtained with an incident pump power of about 500 mW at 629 nm. The output for both two-photon absorption and photon avalanche pumping was not purely cw but contained self-pulsing oscillations.

Upconversion laser emission has also been reported[67] for Tm:YAG. The pump mechanism is primarily sequential two-photon absorption but upconversion also requires cross relaxation

energy transfer. The pump mechanism is illustrated in Fig. 45. The initial step involves absorption of a 785 nm photon to produce the $^3H_6 \rightarrow {}^3H_4$ transition. Cross relaxation energy transfer occurs with a ground state ion as in photon avalanche upconversion, producing two ions in the $^3F_4$ state. Absorption of a pump photon at 638 nm produces the $^3F_4 \rightarrow {}^1G_4$ transition and the $^1G_4 \rightarrow {}^3H_6$ radiative transition produces 486 nm emission. Blue fluorescence was observed when pumping with only 638 nm photons, suggesting photon avalanche upconversion under single wavelength excitation. The Tm:YAG monolithic resonator crystal was doped with 3% Tm. Pumping with 340 mW at 785 nm and 195 mW at 638 nm produced 70 μW of output power. The output consisted of 14 ns wide self-pulsed emission.

3.4.2.5. *Summary and tables*

The results presented for upconversion lasers doped with Pr, Nd and Tm are summarized in Table 3, while the Er-doped lasers are summarized in Table 4. Note that Er:YALO, Er:YAG and Tm:YAG are the only oxide-based upconversion laser hosts listed.

For both Tables 3 and 4, TP indicates two-photon sequential upconversion, CET indicates cooperative energy transfer upconversion, PA indicates photon avalanche upconversion, RT indicates room temperature, SP indicates self-pulsing, CH indicates chopped and QS/ML indicates Q-switched/mode locked operation.

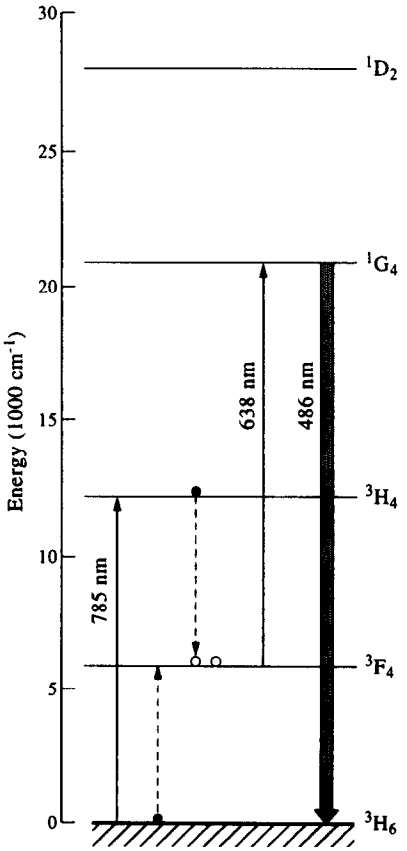

Fig. 45. Partial energy level diagram of Tm:YAG showing the upconversion processes involved in sequential two-photon absorption. Solid vertical lines represent radiative transitions. The dashed lines represent cross relaxation energy transfer between two ions, one in the $^3H_6$ ground state and the other in the $^3H_4$ state. Cross relaxation produces two ions in the $^3F_4$ state.

Table 3. Summary of upconversion laser results for Pr^{3+}-, Nd^{3+}- and Tm^{3+}-doped crystals

Crystal	Output wavelength (nm)	Pump mechanism	Pump wavelength (nm)	Temperature (°K)	Output power, mode of operation	Reference
Pr:$LaCl_3$	644	PA	677	80–210	240 mW, cw	38
Nd:LaF_3	380	TP	590 + 800	20–90	12 mW, cw	39
Nd:YLF	413	PA	604	30	< 10 μW, cw	39
Tm:YLF	450, 453	TP	649 + 781	77–RT	0.2 mJ, pulsed	66
Tm:YLF	483	PA	629	< 160	30 mW, SP	40, 50
	450	TP	648 + 784		9 mW, SP	
Tm:YAG	486	TP	638 + 785	10–30	0.07 mW, SP	67

3.4.3. *Crystals co-doped with sensitizer ions*. The earliest work on upconversion materials utilized co-doped crystals. One ion, termed the "sensitizer" or donor ion absorbs pump light and subsequently transfers its energy to the co-doped acceptor ion. Upconversion results from two or more successive transfers from donor ions to an acceptor ion. Co-doped systems were the focus of extensive upconversion research in previous decades and two sensitized upconversion lasers will be briefly described in this section.

The most extensive work on co-doped upconversion was performed with the Yb^{3+} ion as the sensitizer and various trivalent rare earth ions as activators. Through cooperative upconversion energy transfer, two Yb ions transfer their energy successively to an acceptor ion in the ground state, promoting it to an excited state. Radiation from this state is produced at an energy higher than the energy of the excited Yb ion. Sensitized energy transfer is shown in Fig. 46 for the Yb–Er system. Yb ions are promoted to the $^2F_{5/2}$ state by absorption of pump photons. Two successive transfers from the Yb ion are required to produce green emission from the Er ion. The first transfer from an Yb ion in the $^2F_{5/2}$ state promotes the ground state Er ion to the $^4I_{11/2}$ state. This state is metastable. Cooperative energy transfer between a second Yb ion in the $^2F_{5/2}$ state and the Er ion in the metastable state promotes the Er to the $^4F_{7/2}$ state. Rapid relaxation populates the visible-emitting $^4S_{3/2}$ state. Note that the Yb ion has only one excited state, the $^2F_{5/2}$ level.

In the early work on upconversion, sensitized systems were preferred because the donor ion excitation processes are direct. For singly doped systems the donor levels are often populated by multiphonon relaxation, while for the Yb ion the excited state is populated directly by the pump radiation. Sensitized materials distinguish the donor and acceptor ions

Table 4. Summary of upconversion laser results for Er^{3+}-doped crystals

Crystal	Laser wavelength (nm)	Pump mechanism	Pump wavelength (nm)	Temperature (°K)	Output power, mode of operation	Reference
Er:YLF	551	CET	802	50–90	5 mW, SP	57, 58
Er:YLF	544, 551, 561	CET	797	49	467 mW, SP	20
Er:YLF	551	CET/TP	791 diode	40–90	0.1 mW, SP	59
Er:YLF	551	CET/TP	802 diode	50	2.3 mW, SP	60
Er:YLF	551	CET	797 diode	48	100 mW, SP	17
Er:YLF	544, 551	CET	1550	9–77	34 mW, cw	61
Er:YLF	544, 551	CET	1500	9–95	2 mW, QS/ML	35
Er:YLF	470	CET	653	< 35	6 mW, CH	62
			969		2 mW, cw	
Er:CaF_2	855	CET	1510	77	64 mW, cw	64
Er:YLF	551, 850	TP	647 + 810	RT	0.95 mJ, pulsed	48
Er:KYF_4	562	TP	647 + 810	RT	0.95 mJ, pulsed	48
Er:YAG	561	TP	647 + 810	RT	low, pulsed	48
Er:YALO	550	TP	792 + 840	30	0.8 mW, cw	18
Er:YALO	550	TP	785 + 840	34	8 mW, cw	37
Er:YALO	550	CET	807	34	166 mW, cw	37
Er:YALO	550	PA	791	7	33 mW, cw	56

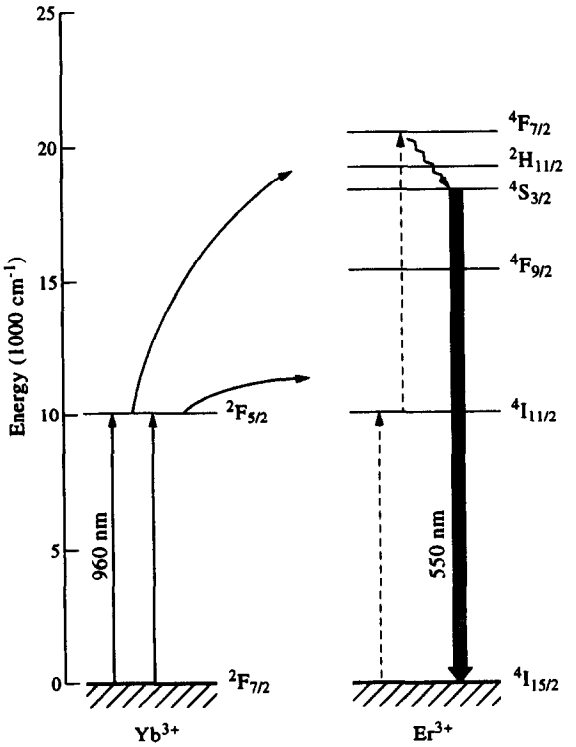

Fig. 46. Sensitized upconversion in Yb^{3+},Er^{3+}-doped BaY_2F_8. Two successive transfers from Yb ions in the $^2F_{5/2}$ state to the Er ion produce green emission from the $^4S_{3/2}$ state. The first transfer promotes the ground state Er ion to the $^4I_{11/2}$ metastable state, while the second transfer promotes the Er ion from the metastable state to the $^4F_{7/2}$ state. Relaxation populates the $^4S_{3/2}$ state.

by species rather than by excitation level, providing clarity to the energy transfer process. Compared to the Yb ion, the complex level structure of the rare earth activator ions makes ion pair interaction processes more difficult to model. These interactions include concentration quenching and prevent high activator doping densities.

On the other hand, one of the most serious problems with co-doped systems is the high back transfer rate from the acceptor ion to the donor. This manifests[2] itself in systems such as Yb–Er by producing a linear rather than quadratic dependence of the upconversion fluorescence on the Yb ion density. Nonetheless, laser action in sensitized systems is possible and in fact the first demonstration[5] of upconversion laser emission was produced in two co-doped materials. These sensitized crystals are Yb, Er:BaY_2F_8 and Yb, Ho:BaY_2F_8 and the results of laser operation will be described briefly below.

In the Yb–Er system, laser emission at 671 nm was obtained on the $^4F_{9/2} \rightarrow {}^4I_{15/2}$ Er transition. The Yb ion is excited at 960 nm and two successive cooperative energy transfer interactions populate the $^4S_{3/2}$ state. Relaxation then populates the $^4F_{9/2}$ upper laser level. Cooperative energy transfer between Er ions in the $^4I_{11/2}$ and $^4I_{13/2}$ metastable states also populates the $^4F_{9/2}$ upper state. Population in the $^4I_{13/2}$ state is produced by decay from the $^4I_{11/2}$ state and the cooperative energy transfer interaction between two metastable state Er ions is efficient in the 6% Er-doped crystal used by Johnson and Guggenheim.[5] Figure 47 illustrates upconversion in the Yb–Ho system. Laser emission is produced at 552 nm on the $^5S_2$, $^5F_4 \rightarrow {}^5I_8$ transition. The first Yb $\rightarrow$ Ho energy transfer promotes the activator ion from the ground state to the $^5I_6$ state, while a second successive transfer from an excited Yb ion promotes the Ho ion from the $^5I_6$ state to the $^5S_2$, $^5F_4$ states.

Both crystals produced stimulated emission at 77°K. As noted in Section 3.2.4 the crystals were pumped with a flashlamp and the flashlamp emission was filtered to prevent direct excitation into the upper laser level of the activator ion. The filter for the Yb–Er system absorbed lamp emission at wavelengths shorter than 670 nm. Threshold was achieved with 195 J into the lamp. Johnson and Guggenheim[5] believed it unlikely that direct flashlamp excitation of the Er activator ions into the $^4I_{9/2}$, $^4I_{11/2}$, and $^4I_{13/2}$ states, followed by cooperative upconversion, would populate the upper laser level. Relative to successive Yb → Er energy transfer, this Er ion pair interaction was considered substantially less efficient. Laser threshold for 552 nm emission in the Yb–Ho crystal was achieved with 635 J into the filtered flashlamp. The filter that was used for pumping Ho transmitted wavelengths longer than 610 nm. When this filter was replaced with one that transmitted wavelengths longer than 400 nm, the laser threshold was reduced to 355 J. This observation indicates that direct pumping of the upper laser level is comparable in efficiency to upconversion pumping of Ho. Demonstration[68] of a conventional flashlamp pumped Ho:CaF_2 laser emitting at 551 nm had been reported previously.

3.5. *Upconversion fiber lasers*

The upconversion lasers listed in Tables 3 and 4 indicate a remarkable range of wavelengths, output powers and operating modes. In addition, for many of the lasers the pump wavelengths can be produced by commercially-available semiconductor laser diodes. However, most of these lasers operate at temperatures below 100°K. Although room temperature upconversion laser emission was first reported[69] in 1987 for the Er doped $BaYb_2F_8$ crystal, few other upconversion lasers have operated near 298°K. As can be seen by reference to Tables 3 and 4, these crystals produce low energy, pulsed output at room temperature. Operation at cryogenic temperature is generally inconsistent with the production of practical, all solid-state visible emission and pulsed emission is unsuitable for applications of upconversion lasers such as optical data storage. As one of the compelling advantages of

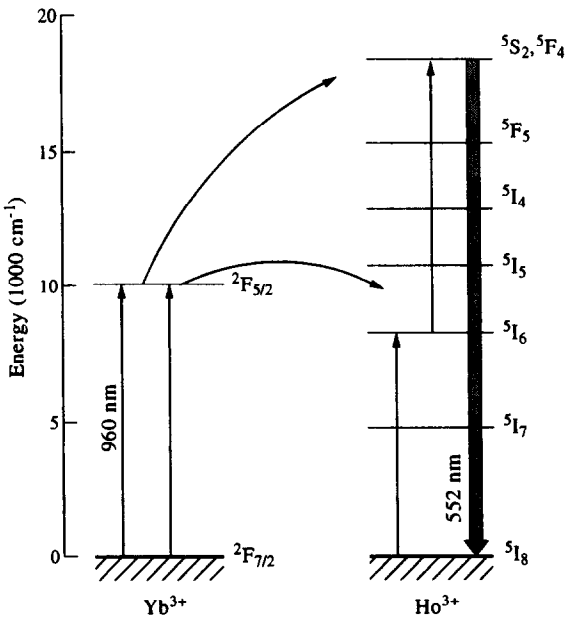

Fig. 47. Upconversion pumping and laser emission in the Yb^{3+},Ho^{3+}-doped BaY_2F_8. Two successive energy transfer interactions with excited Yb ions populate the $^5S_2$, $^5F_4$ upper laser level. Radiation to the $^5I_8$ ground state produces laser emission at 551.5 nm.

upconversion lasers is their potential to provide efficient visible emission, the demonstration of cw room temperature operation is an important milestone in achieving this goal.

In general the peak output efficiency for cw upconversion crystalline lasers occurs at temperatures below 50°K. At temperatures above the peak the output power and efficiency degrade. One of the reasons for this is the increase in the terminal laser level population with increased temperatures. The Boltzmann population increases rapidly with temperature. For laser transitions that terminate on a high lying Stark level of the ground state or a long-lived metastable state, the increased population reduces the net gain and increases the threshold pump power. These effects were described in Section 3.3.4 in relation to the Er:YALO temperature dependence illustrated in Fig. 25.

An additional phenomenon related to thermal degradation of the laser output arises from the temperature-induced increase in the multiphonon relaxation rates[28,36] as discussed in Section 3.3.4. Increased relaxation rates can be helpful when the excited state population involved in upconversion is produced through non-radiative decay. However, increased relaxation produces shorter excited state lifetimes as well and can have a negative impact on the upconversion efficiency. Similarly, ion pair transfer processes that require additional energy from the crystal lattice become more efficient at increased temperatures. For example, in Er:YALO the production[49] of the $^4I_{9/2}$ state by cross relaxation from the $^4S_{3/2}$ state requires 589 cm^{-1} from the lattice. This process, which was described in Section 3.3.5, does not occur at cryogenic temperatures but has been observed at 298°K. While not necessarily detrimental to upconversion, additional channels for energy transfer have the effect of reducing the branching ratio for the desired energy flow pathway.

An associated effect is the thermally-induced population of electronic states that lie several hundred wavenumbers above an electronic state involved in upconversion. An example of this is the $^2H_{11/2}$ state in Er:YALO, which lies 632 cm^{-1} above the $^4S_{3/2}$ state. Excitation into different states opens up new channels for energy transfer. This is true not only because of energy conservation but also reflects the overlap of the ion interaction matrix. From the Fermi Golden Rule, the transition rate W for a specific ion pair interaction is given[2] by

$$W = \frac{2\pi}{\hbar} |\langle \Psi | H_{ij} | \Psi' \rangle|^2 \rho \tag{36}$$

where Ψ' and Ψ are the wavefunctions for the system before and after the energy transfer interaction, respectively, and H_{ij} is the part of the Hamiltonian for the entire crystal that describes the ion pair coupling. Thermal population of additional electronic states expands the wavefunctions in the ion interaction matrix expression given by Eqn (36) and has the effect of increasing the energy transfer rates. Since the increase is not necessarily restricted to the rates that produce population in the upper laser level, this effect may prove detrimental to the upconversion pump efficiency.

Line broadening, introduced by increasing the crystal temperature, is a further obstacle to efficient room temperature upconversion. As mentioned in Section 3.3.5, the absorption and emission linewidths increase[44] with increasing temperature. This reduces the absorption and stimulated emission cross sections. As a result, pumping is less efficient, the gain is lower and the threshold pump power is higher. In addition, the higher temperature distributes the electronic state population over more Stark levels (and occasionally pushes part of the population into higher lying electronic states as mentioned above). Consequently, there is a diminished population of absorbers in a given Stark level for both the ground state as well as the initial excited states involved in two-photon absorption or photon avalanche upconversion. This serves to further reduce the pump efficiency.

The most promising approach to room temperature upconversion laser operation is the fiber laser. Using a core composed of heavy metal fluoride-doped glass, optical fibers containing trivalent Pr, Nd, Ho, Er and Tm ions have produced efficient room temperature

upconversion laser emission. The fiber material is fluorozirconate (ZBLAN) glass and is single mode. Fluorozirconate is preferred to silica glasses due to the narrower phonon spectrum. Wavelengths throughout the visible and down to 381 nm have been demonstrated in fiber lasers at room temperature. In this section we will review some of the concepts and results of upconversion fiber research. A table at the end of this section summarizes the information presented. There has been a great deal of activity in the development of upconversion fiber lasers and this review is designed to provide only a sample of the work reported.

The fiber geometry provides an extended waveguide, confining both the pump radiation and the extracting optical flux to a small cross section over an extended length. Due to the tight confinement and long interaction length, high excitation densities and pump efficiencies are achieved. Fiber lengths are typically 1 m. The problem of terminal level absorption at room temperature is alleviated by ground state depletion. The pump flux removes a significant fraction of the ground state population through promotion to excited states, reducing the reabsorption losses. In general the activator densities are less than 0.1%. This low density effectively eliminates cooperative energy transfer upconversion pump processes. On the other hand, sequential two-photon absorption at room temperature often requires only one pump wavelength due to the number and width of the absorption lines. This upconversion process has proven to be a convenient excitation technique for upconversion fiber lasers.

The first upconversion fiber laser[70] was Tm-doped ZBLAN and operated at 77°K. Two output wavelengths were observed, one at 455 nm and the other at 480 nm. A 1.7 m long single mode fiber was used with a Tm doping density of 0.125%. The energy levels of Tm in ZBLAN are similar to those shown in Fig. 44 for Tm:YLF. A krypton ion laser was used as a pump source, operating simultaneously at 647.1 nm and 676.4 nm. Two-photon absorption leads to population of both the $^1D_2$ state and the $^1G_4$ states. The 676 nm photon promotes a Tm ion from the ground state to the $^3H_4$ state. This state is metastable with a lifetime of 1.4 ms. Relaxation from the $^3H_4$ state populates the $^3F_4$ state, which has a lifetime of 6.0 ms. Absorption of the shorter wavelength pump photon at 647 nm populates the $^1D_2$ state or $^1G_4$ state depending on whether the initial state is the $^3H_4$ state or the $^3F_4$ state, respectively.

Self-terminating emission at 455 nm was observed, corresponding to the $^1D_2 \rightarrow {}^3F_4$ transition. After termination of the 455 nm output, self-pulsed emission due to the $^1G_4 \rightarrow {}^3H_6$ transition was observed at 480 nm. The krypton pump laser was chopped and the fiber was maintained at 77°K. The output power depended linearly on the dual wavelength input power and with 90 mW of pump power 400 μW of output power at 480 nm was obtained.

The general pumping processes and upconversion resonator design for a cw, visible laser diode pumped Tm-doped ZBLAN laser are described[71] in a U.S. patent assigned to Phillips Corp. A room temperature single mode fiber produced 0.5 mW cw at 450 nm when pumped with a 10 mW visible laser diode. The fiber core diameter was 5 μm and the fiber length was approximately 1 m. The 450 nm laser emission in this work was not self-terminating but operated cw. Population build-up in the metastable $^3F_4$ normally prevents continuous 450 nm emission. However, the laser diode emission bandwidth used in the patented design is broader than that of the krypton ion laser used in Ref. 70. In addition, the absorption bandwidth is greater at 298°K than 77°K. The pump flux in this case promotes ions from the $^3F_4$ terminal laser level back up to the $^1G_4$ state. Transitions from the $^1G_4$ state to the ground state produce 470 nm fluorescence. This mechanism maintains[71] the population inversion in the $^1D_2$ state relative to the $^3F_4$ state under cw operation. It had been shown[72] that continuous laser emission is possible under certain conditions even when the lifetime of the terminal level is greater than the lifetime of the upper laser level. One of these conditions requires relaxation from the upper laser level to the ground state.

The first cw room temperature upconversion laser was demonstrated[73] in a Ho-doped ZBLAN fiber. The Ho energy levels in ZBLAN are illustrated in Fig. 48. The fiber length

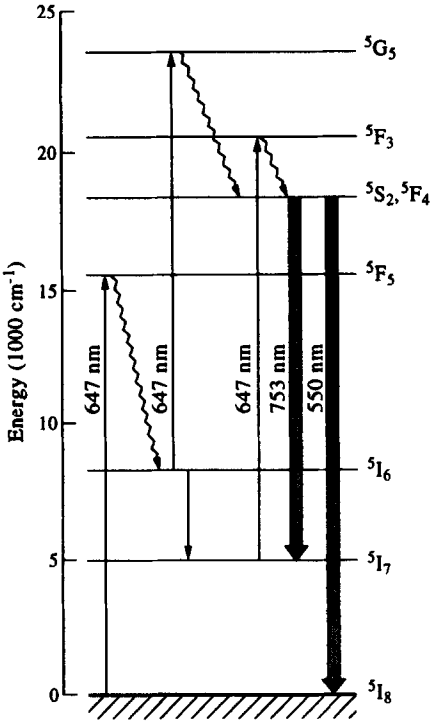

Fig. 48. Partial energy level diagram illustrating upconversion in a Ho-doped ZBLAN fiber. The vertical arrows labeled 647 nm show the pathway for sequential two-photon absorption pumping to produce population in the $^5S_2$, $^5F_4$ upper laser level. Wavy lines indicate non-radiative decay. Absorption of the first 647 nm photon promotes an ion in the ground state to the $^5F_5$ level. Rapid relaxation populates the metastable $^5I_6$ level. (The intermediate $^5I_4$ and $^5I_5$ states participate in relaxation but are not illustrated.) The $^5I_6$ level can decay to the $^5I_7$ level, or can absorb a 647 nm photon to populate the $^5G_5$ state. Relaxation from the $^5G_5$ state produces the $^5S_2$, $^5F_4$ upper laser level. Alternatively, the $^5I_7$ state can absorb a 647 nm photon to populate the $^5F_3$ state, which then relaxes to the upper laser level. The laser transition at 550 nm is indicated and is due to the $^5S_2$, $^5F_4 \rightarrow {}^5I_8$ transition, while the 753 nm laser emission is due to the $^5S_2$, $^5F_4 \rightarrow {}^5I_7$ transition.

was approximately 1 m and the doping density was 0.12%. Laser operation produced over 10 mW cw when pumped with a krypton ion laser at 647 nm. The pump power was about 300 mW. The laser output power depended linearly on the pump power and the reported slope efficiency was 20%. The output wavelength was centered at 550 nm and is due to the $^5S_2$, $^5F_4 \rightarrow {}^5I_8$ transition. Tunability between 540 nm and 553 nm was demonstrated with an intracavity dispersive prism. The tuning range and center wavelength for a specific fiber was found to depend on its length but over this range tuning was continuous. Laser emission at 753 nm was also observed, due to the $^5S_2$, $^5F_4 \rightarrow {}^5I_7$ transition.

Room temperature cw laser emission at 491 nm, 520 nm, 605 nm and 635 nm was produced[74] in a Pr-doped ZBLAN fiber. The energy level diagram for Pr in ZBLAN is similar to that for Pr in $LaCl_3$ shown in Fig. 41. A relatively large 4.6 μm core diameter, 10 m long fiber was used to demonstrate efficient upconversion emission at 635 nm. The Pr doping level was 560 parts per million (ppm). Upconversion by sequential two-photon absorption was produced by two Ti:sapphire lasers emitting pump flux at 835 nm and 1.01 μm, respectively and is illustrated in Fig. 41. The longer wavelength photon promotes a Pr ion in the $^3H_4$ ground state to the $^1G_4$ intermediate state. This level has a lifetime of 100 μs. The shorter wavelength photon excites the intermediate state to the thermally-coupled $^3P_1$, $^1I_6$, $^3P_0$ multiplet. The lifetime of the multiplet is 40 μs. With a total of 2.7 W of dual wavelength pump power, 185 mW was obtained at 635 nm on the $^3P_0 \rightarrow {}^3F_2$ transition. The optical

conversion efficiency is 7%. With either the long or short pump wavelength power fixed, the red laser output power was linearly dependent on the pump power at the other wavelength. Fixing the longer wavelength power at 1 W, the slope efficiency with respect to the 835 nm power was 14%.

A 1.2 m long fiber was used to produce laser emission on the orange, green and blue wavelengths. Using this fiber and an output mirror that was 0.40 R at 605 nm, emission at 605 nm produced 30 mW of output power. The laser transition is $^3P_0 \rightarrow {}^3H_6$. Laser emission at 635 nm was prevented by the low reflectivity of the output mirror (0.20 R) at the red wavelength. The slope efficiency with respect to the 835 nm pump power was 7%. Green emission at 520 nm on the $^3P_1$, $^1I_6 \rightarrow {}^3H_5$ transition was produced with a high reflectivity output mirror. The threshold power was 160 mW. The laser output power at 520 nm was approximately 1 mW due to the high reflectivity output coupler. At pump powers sufficiently above threshold simultaneous laser emission in the red and green were observed. Emission at 491 nm on the $^3P_0 \rightarrow {}^3H_4$ transition was obtained with a highly reflective output mirror and about 1 mW was produced at this wavelength. The threshold power was 200 mW and at higher power simultaneous laser emission at 635 nm was produced.

The first demonstration[75] of a room temperature Er-doped ZBLAN fiber laser produced 23 mW of cw power at 546 nm using an absorbed pump power of 800 mW. The energy level diagram for Er is shown in Fig. 15. A 2.4 m long ZBLAN fiber doped with 500 ppm Er ions was pumped with a cw Ti:sapphire laser emitting at 801 nm. The upconversion pump process is sequential two-photon absorption. The first transition promotes the Er ion to the $^4I_{9/2}$ state, and relaxation populates both the $^4I_{11/2}$ and $^4I_{13/2}$ states. A second photon absorbed by an ion in either of these metastable states is promoted to the $^4F_{5/2}$ or $^2H_{11/2}$ state, respectively. Relaxation populates the $^4S_{3/2}$ state and green emission results from the $^4S_{3/2} \rightarrow {}^4I_{15/2}$ transition.

The threshold pump power was 100 mW at 801 nm but it was found that pump wavelengths from 791 nm to 812 nm produced green emission. The pump bandwidth that keeps the threshold power below 120 mW is approximately 10 nm and is centered at 801 nm. This implies that the $\sim$2.4 nm bandwidth produced by standard high power laser diodes would be an effective pump source for this fiber. The dependence of the upconversion laser emission on pump power was linear only at low pump powers. Above approximately 250 mW the laser emission dependence begins to bend over. It was suggested[75] that this saturation-type behavior is due to simultaneous laser emission at 850 nm. The longer wavelength emission is due to the $^4S_{3/2} \rightarrow {}^4I_{13/2}$ transition and was observed under various conditions. It was also observed that variations in the pump power and pump wavelength produced changes in the output wavelength. Under certain conditions simultaneous green emission was observed on several lines ranging from 543 to 548 nm.

The work cited above for Pr, Ho, Er and Tm-doped ZBLAN fibers is representative of the earliest reports on upconversion fiber laser emission. Recent results have addressed higher power, higher efficiency and new wavelengths. A demonstration[76] of laser emission in a Ho-doped ZBLAN fiber produced 38 mW cw at room temperature. The 550 nm laser emission results from the $^5S_2$, $^5F_4 \rightarrow {}^5I_8$ transition (see Fig. 48). Fiber lengths used ranged from 0.20 to 0.86 m and the core diameter was 11 μm. The Ho doping density was 0.1%. Pumping with a cw dye laser at 643 nm, threshold powers were obtained ranging from 66 to 130 mW, depending on the output coupling. The maximum output power of 38 mW was achieved with a 0.70 R output mirror and an absorbed pump power of 270 mW. The laser output power dependence on the pump power was approximately linear and the slope efficiency obtained for the 0.70 R output mirror was 24%. No indication of output power saturation was observed. Tunability of the green output wavelength was observed, as had been noted in Ref. 73. In this case, tuning was obtained by varying the pump power. Increasing the pump power from 150 mW to 240 mW, the center wavelength of the green emission blue-shifted by approximately 4 nm. The blue shift was attributed to the reduced population in the ground

state population at higher pump power. The ground state is the terminal laser level for the 550 nm transition.

Recently reported[77] results for a multi-wavelength Pr-doped ZBLAN fiber laser show significantly improved performance relative to Ref. 74. A Ti:sapphire laser operating at 860 nm was used to pump a ZBLAN fiber co-doped with Pr and Yb ions. The doping densities were 0.3% and 2% for Pr and Yb, respectively. The fiber core diameter was 3 μm and fiber lengths between 0.2 m and 10 m were used. Laser emission at 635 nm, 615 nm, 520 nm and 491 nm was produced, with maximum cw output powers of 300 mW, 44 mW, 20 mW and 4 mW, respectively. Threshold power for the four wavelengths ranged between 21 mW and 60 mW. The highest slope efficiency was reported for the 635 nm output wavelength. Based on launched power, which was estimated to be 40% of the power incident on the focusing objective, the slope efficiency was 52%.

By tuning the output wavelength of the Ti:sapphire pump laser, the pump bandwidth range for upconversion laser operation was determined to be 785–885 nm. The four upconversion fiber laser output wavelengths could be tuned by inserting a dispersing prism between the fiber end and the output coupler. The four tuning ranges were 635–637 nm, 605–622 nm, 517–540 nm and 491–493 nm. The large tuning range for the 520 nm output is due in part to the overlap of two transitions. The 520 nm emission is due to the $^3P_1$, $^1I_6 \rightarrow {}^3H_5$ transition, while the $^3P_0$ state, which is part of the thermally coupled $^3P_1$, $^1I_6$, $^3P_0$ multiplet, produces emissions at 535 nm on the $^3P_0 \rightarrow {}^3H_5$ transition.

The shortest wavelength reported[78] to date for a room temperature upconversion fiber laser is 381 nm. A 2.2 μm core ZBLAN fiber was doped with 0.1% Nd. Fiber lengths of 0.39–0.45 m were used. Pumping was provided by a 590 nm cw dye laser and the fiber was maintained at room temperature. Emission at 412 nm results from the $^2P_{3/2} \rightarrow {}^4I_{9/2}$ transition, while 381 nm emission results from the $^4D_{3/2} \rightarrow {}^4I_{9/2}$ transition. The energy levels for the Nd ion are illustrated in Fig. 42. At 412 nm about 500 μW of output power was obtained with 320 mW of incident power. The power launched into the fiber was estimated at less than 30% of the incident power. The output power dependence on the pump power was approximately linear and the output power slope efficiency was 0.5%. The maximum 381 nm output power was about 80 μW. The slope efficiency was 0.2% but was linear only for the shortest fiber length. The 381 nm output displayed self-pulsing but the 412 nm output was cw.

Progress in the development of room temperature upconversion fiber lasers since 1990 suggests that additional improvements in both the fiber laser and semiconductor pump sources will lead to practical and efficient moderate power visible lasers in the near future. We conclude this section with a tabular review of the upconversion fiber lasers discussed in this section. The abbreviations used for Table 5 are identical to those listed above Table 3 in Section 3.4.2.5. All fiber hosts are ZBLAN and the table is organized by activator ion.

4. THE EFFECT OF UPCONVERSION PROCESSES ON CONVENTIONAL LASER OPERATION

4.1. *Introduction*

The energy transfer processes that are involved in upconversion pumping can affect the operation of conventional lasers. Conventional lasers are those in which the upper laser level is populated by the absorption of a single photon. The absorption promotes an ion from the ground state and emission is produced at a wavelength longer than the pump wavelength. Conventional, optically pumped rare earth ion-doped lasers can generate a substantial population in the metastable states that participate in upconversion. In this section we will discuss two aspects of upconversion related to the efficiency of conventional lasers. The first issue addresses the reduced optical conversion efficiency that results from ion pair interactions involving the upper laser level. The second addresses the role of upconversion processes

in removing bottlenecks from, or "unblocking", transitions that terminate on a metastable level.

4.2. *Reduced optical conversion efficiency due to upconversion processes*

Optically pumped lasers utilize well-defined energy flow pathways to populate the upper laser level. Production of the laser level by the pump flux is characterized by the pump efficiency, which is determined by the fraction of absorbed pump photons that populate the upper level. (The fraction of incident pump photons that are absorbed is generally included in the optical transfer efficiency.) For monochromatic pumping the pump efficiency can be high, while for pumping with broadband, black body sources the efficiency is generally lower. The laser quantum efficiency[15] is the product of the pump efficiency and the radiative efficiency of the upper laser level. The latter term measures the fraction of population in the upper laser level that produces laser emission.

Ion pair processes of the type involved in cooperative upconversion can be efficient in reducing the upper laser level population. Upconversion is particularly effective when involving ions in long-lived or metastable levels. As a consequence, ion pair energy transfer involving the upper laser level can increase the laser threshold power and lower the optical conversion efficiency. This can be shown quantitatively by reference to the conventional four-level laser illustrated in Fig. 49. Optical emission is produced by the $3 \rightarrow 2$ transition. Pumping proceeds with a rate constant W_{14} and relaxation populates upper laser level 3 with a rate constant W_{43}. Decay from level 3 to level 2 occurs with a rate constant W_{32}. Below threshold relaxation to level 2 is produced by non-radiative decay and spontaneous emission. The level 2 population decays to the ground state with a rate constant W_{21}. The rate equations for the model shown in Fig. 49 are

$$\frac{dn_4}{dt} = W_{14}n_1 - W_{43}n_4$$

$$\frac{dn_3}{dt} = W_{43}n_4 - W_{32}n_3$$

$$\frac{dn_2}{dt} = W_{32}n_3 - W_{21}n_2 \tag{37}$$

Table 5. Summary of upconversion fiber lasers

Activator ion	Laser wavelength (nm)	Pump mechanism	Pump wavelength (nm)	Temperature (°K)	Output power, mode of operation	Reference
Pr	635	TP	835 + 1010	RT	185 mW, cw	74
	605				30 mW, cw	
	520				~ 1 mW, cw	
	491				~ 1 mW, cw	
Pr, Yb	635	TP	860	RT	300 mW, cw	77
	615				44 mW, cw	
	520				20 mW, cw	
	491				4 mW, cw	
Nd	381	TP	590	RT	0.08 mW, SP	78
	412				0.50 mW, cw	
Ho	550	TP	647	RT	10 mW, SP	73
Ho	550	TP	643	RT	38 mW, cw	76
Er	546	TP	801	RT	23 mW, cw	75
Tm	455	TP	647 + 676	77	N/A, pulsed	70
	480				0.40 mW, SP	
Tm	450	TP	650-diode	RT	0.50 mW, cw	71

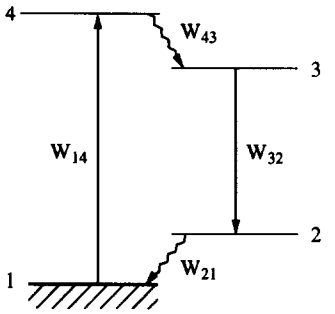

Fig. 49. Schematic representation of an optically pumped four-level laser. The laser transition is $3 \rightarrow 2$. Optical pumping proceeds with a rate constant W_{14} and relaxation produces upper laser level 3 with a rate constant W_{43}. Decay to level 2 is produced with a rate constant W_{32}, and relaxation brings the population in level 2 back to the ground state. The relaxation rate constant from level 2 is W_{21}.

where the n_j designate the number densities in level j. The model does not include spontaneous emission from level 4 to the ground state, which is a reasonable approximation if the relaxation rate is rapid ($W_{43} \gg 1/\tau_{41}$). The steady state density in the upper laser level is then

$$n_3 = \frac{W_{14}}{W_{32}} n_1 \tag{38}$$

Above threshold n_3 is clamped but below threshold the upper laser level population density depends directly on the optical pump rate coefficient W_{14}.

Consider the case now where cooperative upconversion between two ions in level 3 produce an ion in level 5 and an ion in level 1, as illustrated in Fig. 50. If all of the population in level 5 decays to level 1, two upper state ions are removed for each energy transfer interaction. The rate equation for population in level 3 is then

$$\frac{dn_3}{dt} = W_{43} n_4 - W_{32} n_3 - 2\gamma n_3^2 \tag{39}$$

where the cooperative energy transfer rate coefficient γ has the same meaning as in Eqn (8). The steady state solution to Eqn (39) can be written as

$$n_3 = \frac{W_{14} n_1}{(W_{32} + 2\gamma n_3)} . \tag{40}$$

Equation (40) is quadratic and can be solved explicitly for n_3. However, simply comparing Eqns (38) and (40) for pump rates below threshold it is clear that cooperative energy transfer upconversion reduces the steady state population in the upper laser level for a given W_{14}. Note that the optical pump rate W_{14} is a constant times the pump intensity.

Laser threshold is reached when the round trip gain is equal to the round trip passive loss L. Near threshold the gain coefficient is equal to the small signal gain coefficient g_0. As noted in Section 3.3.4 the round trip small signal gain is $2\sigma n_3 \ell$, where the inversion density in the four-level laser is approximated by n_3. Then the threshold condition for the population in level 3, n_3^{th}, can be expressed as

$$n_3^{th} = \frac{L}{2\sigma\ell} . \tag{41}$$

The value of n_3^{th} is fixed by the resonator parameters and σ. From Eqn (40) it can be seen that when upconversion is effective in removing upper laser level population the pump intensity, or W_{14}, must increase to produce the required n_3^{th}. Upconversion reduces the laser optical conversion efficiency by increasing the pump threshold power.

A consequence of the level 3 population being clamped at its threshold value is that under laser operation the cooperative upconversion rate (as well as other rates that depend on the level 3 population density) is clamped as well. Increasing the optical pump flux above threshold increases the laser intensity but has no effect on the cooperative energy transfer rate. Efficient laser operation may therefore be obtained in a system where upconversion rates involving the upper laser level are high.

As the pump power increases the spontaneous emission and non-radiative rates remain constant, fixed by the threshold value of n_3. However, the stimulated emission rate, which depends on the intracavity intensity I, increases. The fraction of level 3 population that produces stimulated emission increases as this rate becomes more competitive with other processes that deplete the level 3 population. Because of this difference in pump power scaling, laser materials that exhibit low fluorescence quantum efficiencies can still produce high laser quantum efficiencies. To see this, note that the fluorescence quantum efficiency is $(1/\tau_r)/(1/\tau_r + 1/\tau_{nr})$ and reflects the relative magnitudes of the non-radiative and spontaneous emission rates. A low fluorescence quantum efficiency indicates that the non-radiative rates are large relative to the fluorescence rate. On the other hand, under laser operation the stimulated emission rate can be quite high relative to the non-radiative rates, even if the fluorescence rate is low. This is particularly true at high pump power.

As a consequence, the radiative part of the laser quantum efficiency, which is determined by the fraction of upper laser level population that produces laser emission, can be large even if the ion pair energy transfer rates are high. Therefore, the principal effect of cooperative energy transfer upconversion involving the upper laser level will be to lower the optical conversion efficiency as a result of the increase in the laser threshold power.

4.3. *Upconversion-assisted laser operation*

Ion pair interactions of the type that produce upconversion pumping can be detrimental to conventional laser operation when these processes involve ions in the upper laser level, as described in Section 4.2. On the other hand, upconversion pumping processes can involve population in the terminal laser level as well. In this case the effects of upconversion can be beneficial to the operation of the conventional laser. When a transition terminates on a metastable level, population build-up due to stimulated emission can reduce the laser efficiency. A related complication arises when the lifetime of the terminal laser level is longer than the lifetime of the upper level. Such transitions are required by classical laser theory to be self-terminating, preventing cw operation. As had been noted in Section 3.5 however, the possibility of relaxation from the upper laser level to the ground state can in certain cases permit[72] cw laser emission on a self-terminating transition. The effect of terminal level lifetime on cw laser operation will be described in more detail below.

For conventional lasers where the optical transition terminates on a metastable state it is possible for cooperative energy transfer to remove population from the lower laser level. As had been noted previously, ion pair energy transfer is most effective when it involves ions in the metastable state. Ideally, one result of this energy transfer interaction is the promotion of an ion from the metastable state to the upper laser level. We begin this section by describing the conditions for population inversion in a three-level laser. The inversion conditions are then related to those cited in Ref. 72 for cw lasing on self-terminating transitions. The role of upconversion pumping in shortening the lifetime of the terminal level is described and an example using the 2.7 μm self-terminating laser transition in Er is presented. The 2.7 μm laser can operate cw because cooperative energy transfer reduces the lifetime of the metastable level.

The generalized pumping scheme for a three-level laser is illustrated in Fig. 51. Figure 51 follows the notation commonly used in basic textbooks on laser physics. Level 2 is the upper laser level, level 1 is the terminal laser level, level 0 is the ground state, R_2 and R_1 are the

pump rates into the upper and lower laser levels, respectively, and $1/\tau_{21}$ is the rate for the $2 \rightarrow 1$ transition. The population inversion $\Delta n = n_2 - n_1$ is given[7] by

$$\Delta n = \frac{R_2\tau_2(1 - \tau_1/\tau_{21}) - R_1\tau_1}{1 + (\tau_1 + \tau_2 - \tau_1\tau_2/\tau_{21})[\sigma I/h\nu]} \tag{42}$$

where τ_1 and τ_2 are the lifetimes of the lower and upper laser levels, respectively and σ is the stimulated emission cross section for the laser transition. The condition for population inversion ($\Delta n > 1$) is that $\tau_2 > \tau_1\tau_2/\tau_{21}$. When $\tau_2 = \tau_{21}$, that is when no decay path from level 2 is available other than decay to the terminal laser level, the condition for inversion using Eqn (42) is the same as the condition for cw laser operation obtained from classical laser theory. As noted above, the classical condition is that $\tau_2 > \tau_1$.

The condition for cw laser emission in the general case where $\tau_2 < \tau_{21}$ had been shown in Ref. 72 to be identical to the condition for $\Delta n > 1$. This condition can be re-written as

$$\tau_2 > \xi\tau_1 \tag{43}$$

where $\xi = \tau_2/\tau_{21}$ is a branching ratio with a value between 0 and 1. It can be seen that an inversion will result if either ξ or τ_1 is small. However the inversion condition provides no indication as to whether small ξ or small τ_1 is preferable for laser emission. Furthermore, cw operation of a laser where $\tau_1 > \tau_2$ cannot result from only satisfying the condition for population inversion ($\tau_2 > \xi\tau_1$) since this does not allow for consideration of other factors that have a substantial impact on laser performance. These factors include the laser gain and efficiency. For example, it would be extremely difficult to operate a laser in the cw mode when ξ is very small and $\tau_1 \gg \tau_2$, even though this would satisfy the inversion condition. Put another way, maintaining a population inversion is a necessary but not sufficient condition for laser operation.

Pollack and Chang[79] have analyzed the range of values for the level lifetimes and ξ that satisfy the inversion condition and have concluded that in order to maximize the gain it is necessary that $\tau_1 < \tau_2$. This is identical to the condition for cw laser operation from classical laser theory. The observation of cw emission in a laser where the magnitudes of the ion lifetimes are $\tau_1 > \tau_2$ suggests that under laser operation upconversion pump processes

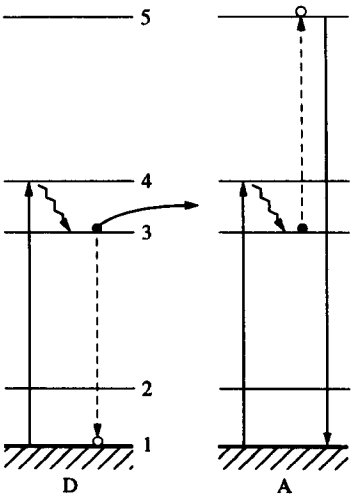

Fig. 50. Cooperative energy transfer in a four-level laser. Solid vertical lines represent absorption and emission, and dashed lines show the energy flow pathway involved in cooperative upconversion. Solid circles represent population prior to the ion pair interaction, while open circles represent the level occupancy after the interaction. "D" and "A" designate the donor and acceptor ion, respectively.

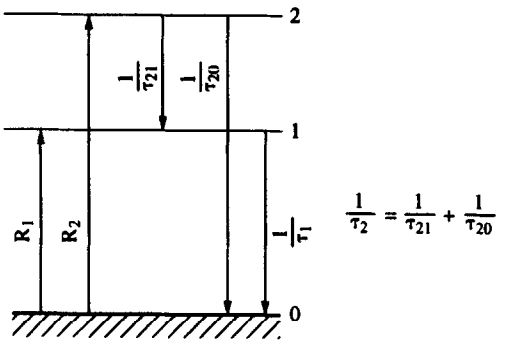

Fig. 51. Energy flow in a three-level laser. R_2 and R_1 are the pump rates into the upper and lower laser levels, respectively, $1/\tau_{21}$ is the rate for the $2 \rightarrow 1$ transition and $1/\tau_1$ is the decay rate for population in level 1.

are active in reducing the effective lifetime of the terminal laser level below that of the upper level.

This was verified by experimental measurements and modelling reported in Ref. 79 for five Er-doped crystals. The model is based on the 2.7 μm Er-doped laser. The 2.7 μm laser operates cw in various crystal hosts even though the lifetime of the $^4I_{13/2}$ terminal laser level is two to 50 times as large as the lifetime of the $^4I_{11/2}$ upper laser level. In YALO the lifetimes are 1.2 ms and 7.2 ms for the $^4I_{11/2}$ and $^4I_{13/2}$ states, respectively. The transition that produces 2.7 μm emission is $^4I_{11/2} \rightarrow {}^4I_{13/2}$ and the laser output should be self-terminating.

It is well-known that cooperative energy transfer involving ion pairs in the $^4I_{13/2}$ state is highly effective in Er-doped crystals. For example, the upper laser level for the 2.7 μm transition can be populated by cooperative energy transfer pumping as shown in Fig. 52. Pump flux at 1.5 μm promotes the $^4I_{15/2}$ ground state to the $^4I_{13/2}$ state and subsequent cooperative upconversion between two ions in the $^4I_{13/2}$ state promotes an ion to the $^4I_{9/2}$ state. Subsequent relaxation populates the $^4I_{11/2}$ upper laser level. Upconversion pumping at 1.5 μm produces laser emission at 2.7 μm on the $^4I_{11/2} \rightarrow {}^4I_{13/2}$ transition in crystal hosts such as YAG, YALO and YLF.

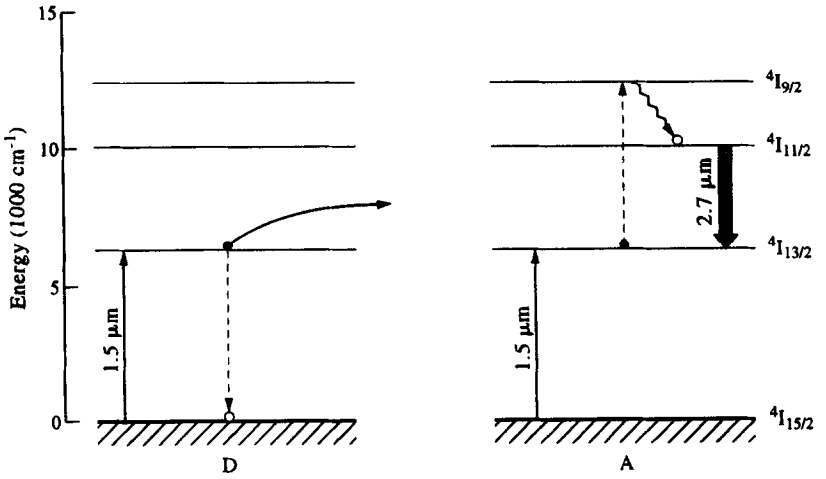

Fig. 52. Upconversion pumping of the 2.7 μm laser transition in trivalent Er. Pump flux at 1.5 μm promotes ions from the ground state to the $^4I_{13/2}$ metastable state. Cooperative upconversion produces an ion in the $^4I_{9/2}$ state, which then relaxes to the $^4I_{11/2}$ upper laser level. Laser emission is due to the $^4I_{11/2} \rightarrow {}^4I_{13/2}$ transition. The lifetime of the $^4I_{13/2}$ state is longer than that of the $^4I_{11/2}$ state.

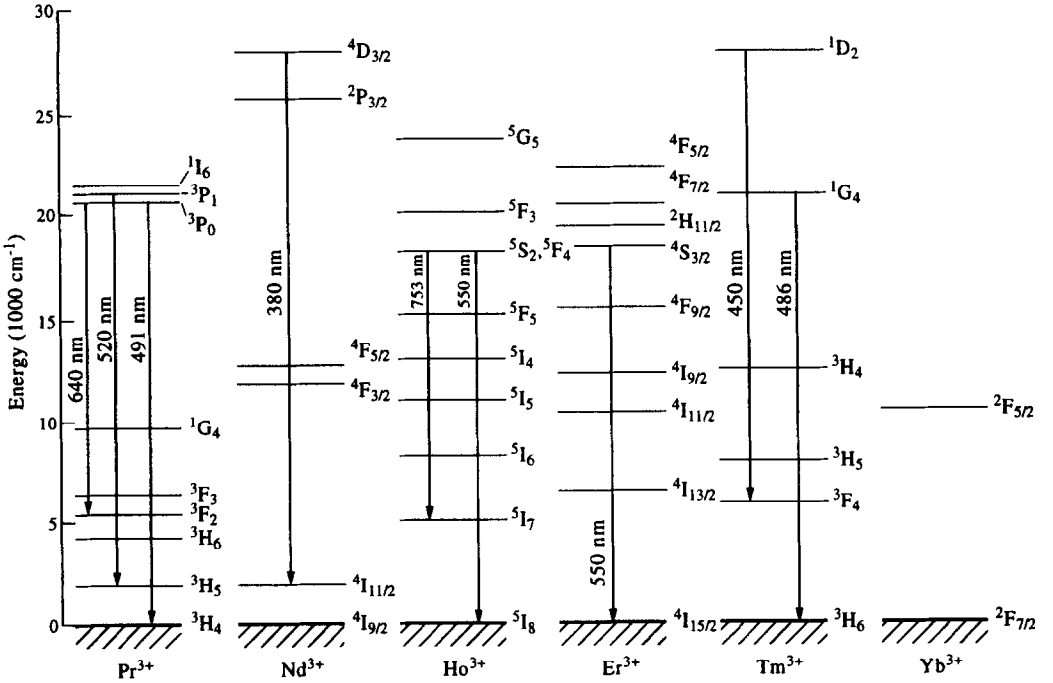

Fig. 53. Partial energy level diagrams for rare earth ions involved in upconversion. Energy levels for trivalent Pr, Nd, Ho, Er, Tm and Yb ions are shown and several of the upconversion laser transitions and wavelengths that are described in the text are noted.

Cooperative energy transfer upconversion involving the $^4I_{13/2}$ terminal level of the 2.7 μm transition is beneficial to laser operation in two ways. For one, population in the terminal level is removed, reducing the reabsorption loss. Each ion pair interaction removes two ions from the terminal laser level. The other benefit is that an ion is promoted to the upper laser level, increasing the pump efficiency. The net impact of upconversion pumping on the level lifetimes is to reduce the lifetime of the terminal level and increase the lifetime of the upper laser level.

Cooperative upconversion also affects ions in the upper laser level as discussed in Section 4.2. Two ions in the $^4I_{11/2}$ state can participate in cooperative energy transfer upconversion, populating the $^4F_{7/2}$ state. The $^4F_{7/2}$ state relaxes to the $^4S_{3/2}$ state. Some of the population from the $^4S_{3/2}$ level decays back to the $^4I_{11/2}$ state as had been described in Section 3.3.5 and some radiates directly to the ground state. In addition, some of the $^4S_{3/2}$ population returns to the $^4I_{11/2}$ state through cross relaxation as had been noted in the description of photon avalanche pumping. The overall effect of upconversion processes is therefore expected to be much greater on the lifetime of the $^4I_{13/2}$ state than the $^4I_{11/2}$ state.

The extensive results of their experimental investigation led Pollack and Chang[79] to conclude that under laser operation cooperative energy transfer changes the lifetime ratios of the upper and lower states from $\tau_1 > \tau_2$ ("wrong") to $\tau_1 < \tau_2$ ("right"). Although these results are specific to the case where the Er-doped crystals are pumped at 1.5 μm, the conclusions can be applied to other optical pumping conditions where cooperative upconversion processes are efficient.

5. CONCLUSIONS

In this review we have summarized the development of lasers pumped by upconversion processes. Upconversion lasers differ from conventional lasers by the pump mechanisms that

are used to produce the upper laser level. Two reviews of conventional lasers have been published in previous issues of *Progress in Quantum Electronics* and provide an overview of the numerous types of lasers that are in use today. A paper[80] by Imasaka and Ishibashi presents a survey of commercially available cw and pulsed lasers including gas phase, dye, semiconductor and solid state devices. An earlier review[81] by Penzkofer offers a more detailed examination of the variety and operation of solid state lasers.

Three general types of upconversion pumping have been discussed. These are sequential two-photon absorption, cooperative energy transfer and photon avalanche. Using Er:YALO as an example, the specific energy flow pathways for each of these upconversion processes were described in detail. Er:YALO is unique among upconversion materials in that all three pump mechanisms produce 550 nm emission when the crystal is pumped in the 800 nm band. The pump mechanism depends on the specific pump wavelength.

Experimental details of upconversion in Er:YALO were presented. The effects on laser operation of varying the pump power and crystal temperature were described using three-level ion models for upconversion pumping. The fluorescence emission and fluorescence excitation spectra that result from upconversion as well as the temporal evolution of the 550 nm laser emission were described. In addition, evidence for photon avalanche upconversion in Er:YALO was presented. Using the variation of the upconversion fluorescence intensity on pump power as well as the temporal evolution of the fluorescence pulse, the steps required to verify that the pump mechanism is photon avalanche were illustrated.

Er:YALO does not produce the type of evidence for photon avalanche that is easily recognized. However, it was shown that support for the assignment of photon avalanche pumping can be obtained using the temporal increase of the absorption of pump flux in conjunction with experimental evidence that eliminates the possibility of pumping by non-resonant sequential two-photon absorption. In spite of numerous experimental and theoretical studies of Er:YALO, upconversion energy flow pathways in this complex system remain somewhat uncertain.

Laser oscillation conditions were described. Threshold, gain and loss were discussed in terms of their relevance to upconversion lasers. The Findlay–Clay model was analyzed for upconversion pumping and rate equations were presented that show the impact of various competing ion processes on the upconversion laser output. Q-switched operation of upconversion lasers was described and equations for optimum output coupling were discussed. The practical considerations for upconversion laser resonator design were also addressed, including a comparison of the advantages of discrete and monolithic resonators for laser operation at cryogenic temperatures. The optimum pump optics for upconversion pumping were considered in terms of an end-pumped configuration where the pump and resonator waists are matched.

Upconversion laser development of rare earth ion-doped crystals was summarized. A wide range of upconversion wavelengths, crystal hosts, pump techniques and resonator designs have been demonstrated over the past three decades. Upconversion laser emission in crystals doped with trivalent Pr, Nd, Er and Tm was reviewed. An overview was presented with the emphasis placed on the laser operating conditions (temperature, output wavelength, output power, pump wavelength and mode of operation) as well as the resonator design and the overall efficiency. Yb–Er and Yb–Ho sensitized upconversion lasers were also described. Sensitized materials are those that contain co-dopant ions, usually Yb. The Yb ion absorbs pump flux and transfers the energy to the activator ion. Each of the sensitized crystals was maintained at 77°K and pumped with flashlamps.

The development of fiber lasers was summarized. Upconversion fiber lasers represent an important advance towards the goal of producing practical, all solid state visible lasers. ZBLAN fibers doped with trivalent Pr, Nd, Ho, Er and Tm have demonstrated cw laser emission. These lasers can be diode-pumped and operate at room temperature. Fiber lasers

have produced hundreds of milliwatts of visible emission and several fiber lasers generate tunable radiation when operated with intracavity tuning elements. The shortest wavelength fiber laser operated in the ultraviolet at 381 nm. Advances in this field have come at a rapid pace, with current research centering on higher power, new wavelength ranges and greater efficiency.

Upconversion pump processes in lasers extend to conventional lasers as well. Conventional lasers are those that are pumped by a single photon and produce emissions at wavelengths longer than the pump wavelength. The effect of ion pair energy transfer on a long-lived upper laser level in a conventional laser was described. Upconversion pumping acts as a saturable loss mechanism, removing some of the upper laser level population. As a consequence, the laser threshold power is increased and the optical conversion efficiency is lowered. Analytical expressions based on a four-level laser were presented for cooperative energy transfer involving the upper laser level.

In some crystals upconversion pump mechanisms involve the terminal laser level. If this level has a lifetime longer than that of the upper laser level the laser transition is generally self-terminating. However, cooperative energy transfer upconversion pumping not only reduces the effective lifetime of the lower laser level, it can also promote ions from the terminal level to the upper laser level. This is the case for the 2.7 μm transition in Er-doped crystals. Experimental and theoretical evidence is reviewed that identifies the role of upconversion energy transfer in producing cw emission on this laser transition.

Numerous energy level diagrams were presented throughout this review to illustrate the energy flow pathways for ion pair interactions. These figures also show the various optical absorption and emission transitions. Figure 53 combines in a single figure the energy level schematics for the five trivalent rare-earth ions that have demonstrated upconversion laser emission. The figure shows the energy levels involved in upconversion as well as many of the upconversion laser transitions. Figure 53 provides the perspective that is missing in the energy level diagrams for the individual ions and serves as a visual summary of the upconversion laser emission reported in this review. The Yb ion energy levels are also shown.

We conclude by noting that upconversion laser emission has numerous advantages for generating coherent visible emission compared to approaches involving non-linear optics. Unlike non-linear optical process, upconversion does not involve considerations such as phase matching, Poynting vector walk-off or fundamental beam quality. In addition, cw operation in the visible is efficient and easily obtained. The advantages of upconversion lasers are most pronounced in fibers, which operate at room temperature and do not require a narrowband, tunable pump source. These devices can be pumped by semiconductor laser diodes. As new fiber materials and pump sources are developed, cw visible and ultraviolet upconversion lasers operating at room temperature are expected to become a commercially viable, practical technology. In this regard we note that all-solid-state, diode pumped visible upconversion fiber lasers are presently available from several commercial suppliers.

Acknowledgements—This work was supported by the Office of Naval Research.

REFERENCES

1. F. E. Auzel, *Proc. IEEE* **61**, 758–786 (1973).
2. J. C. Wright, In: *Radiationless Processes*, pp. 239–295, F. K. Fong (ed.), Springer-Verlag, Berlin (1976).
3. N. Bloembergen, *Phys. Rev. Lett.* **2**, 84–85 (1959).
4. M. F. Joubert, S. Guy and B. Jacquier, *Phys. Rev. B* **48**, 10031–10037 (1993).
5. L. F. Johnson and H. J. Guggenheim, *Appl. Phys. Lett.* **19**, 44–47 (1971).
6. A. E. Siegman, *Lasers*, University Science Books, Mill Valley (1986).
7. J. T. Verdeyen, *Laser Electronics*, Prentice-Hall, Englewood Cliffs (1981).
8. W. Koechner, *Solid-state Laser Engineering*, p. 86, Springer-Verlag, New York (1976).
9. D. Findlay and R. A. Clay, *Phys. Lett.* **20**, 277–278 (1966).
10. R. Scheps, J. F. Myers and S. A. Payne, *IEEE Photonics Tech. Lett.* **5**, 1285–1287 (1993).

11. K. Kubodera, K. Otsuka and S. Miyazawa, *Appl. Opt.* **18,** 884–890 (1979).
12. R. B. Chesler, M. A. Karr and J. E. Geusic, *Proc. IEEE* **58,** 1899–1914 (1970).
13. W. G. Wagner and B. A. Lengyel, *J. Appl. Phys.* **34,** 2040–2046 (1963).
14. J. J. Degnan, *IEEE J. Quantum Electron.* **25,** 214–220 (1989).
15. R. Scheps, *Appl. Opt.* **28,** 89–91 (1989).
16. R. Scheps, P. Poirier, J. Myers and D. Heller, *LEOS '88 Conference Proceedings* IEEE Lasers and Electro-optics Society, 318–320, IEEE catalog number 88CH2683-1 (1988).
17. R. R. Stephens and R. A. McFarlane, *Opt. Lett.* **18,** 34–36 (1993).
18. A. J. Silversmith, W. Lenth and R. M. Macfarlane, *Appl. Phys. Lett.* **51,** 1977–1979 (1987).
19. M. J. Weber, M. Bass, K. Andringa, R. R. Monchamp and E. Comperchio, *Appl. Phys. Lett.* **15,** 342–345 (1969).
20. R. A. McFarlane, *Opt. Lett.* **16,** 1397–1399 (1991).
21. V. L. Donlan and A. A. Santiago, Jr., *J. Chem. Phys.* **57,** 4717–4723 (1972).
22. P. Gay, *The Crystalline State*, pp. 263–269, Hafner, New York (1972).
23. W. L. Bond, *Crystal Technology*, pp. 99–100, J. Wiley, New York (1976).
24. R. Scheps and J. F. Myers, *IEEE Photonics Tech. Lett.* **4,** 1–3 (1992).
25. P. A. Schulz, *IEEE J. Quantum Electron.* **24,** 1039–1044 (1988).
26. C. D. Hodgman (ed.), *Handbook of Chemistry and Physics*, 35*th Edition*, p. 2662, Chemical Rubber, Cleveland (1953).
27. R. Scheps and J. F. Myers, *Appl. Opt.* **33,** 969–978 (1994).
28. M. J. Weber, *Phys. Rev. B* **8,** 54–64 (1973).
29. R. Scheps and J. F. Myers, *IEEE J. Quantum Electron.* **30,** 1050–1057 (1994).
30. S. A. Payne, L. L. Chase, L. K. Smith, W. L Kway and W. F. Krupke, *IEEE J. Quantum Electron.* **28,** 2619–2630 (1992).
31. A. A. Kaminskii, *Laser Crystals*, pp. 346–360, Springer-Verlag, Berlin (1990).
32. A. A. Kaminskii, S. E. Sarkisov, I. V. Mochalov, L. K. Aminov and A. O. Ivanov, *Phys. Status Solidi (a)* **51,** 509–520 (1978).
33. J. S. Chivian, W. E. Case and D. D. Eden, *Appl. Phys. Lett.* **35,** 124–125 (1979).
34. M. J. Weber, M. Bass, T. E. Varitimos and D. P. Bua, *IEEE J. Quantum Electron.* **QE-9,** 1079–1086 (1973).
35. P. Xie and S. C. Rand, *Opt. Lett* **17,** 1116–1118 (1992); and P. Xie and S C. Rand, Erratum, *Opt. Lett.* **17,** 1822 (1992).
36. M. J. Weber, M. Bass and G. A. DeMars, *J Appl. Phys.* **42,** 301–305 (1971).
37. R. Scheps, *IEEE J. Quantum Electron.* **30,** 2914–2924 (1994).
38. M. E. Koch, A. W. Kueny and W. E. Case, *Appl. Phys. Lett.* **56,** 1083–1085 (1990).
39. W. Lenth and R. M. Macfarlane, *J. Lumin.* **45,** 346–350 (1990).
40. R. M. Macfarlane, R. Wannemacher, T. Hebert and W. Lenth, *Technical Digest of Conference on Lasers and Electro-Optics (CLEO '90)*, p. 250, Optical Society of America (1990).
41. See for example G. H. Dieke and H. M. Crosswhite, *Appl. Opt.* **2,** 675–686 (1963).
42. U. Oetliker, M. J. Riley, P. S. May and H. U. Güdel, *J. Lumin.* **53,** 553–556 (1992).
43. M. Pollnau, E. Heumann and G. Huber, *Appl. Phys.* **A54,** 414–410 (1992).
44. G. H. Dieke, *Spectra and Energy Levels of Rare Earth Ions in Crystals*, pp. 32–37 and pp. 347–349, Interscience, New York (1968).
45. R. A. McFarlane, *LEOS Conference Proceedings*, pp. 706–707, IEEE, Piscataway (1993).
46. F. Auzel, V. Chen and D. Meichenin, *J. Lumin.* **60/61,** 692–694 (1994).
47. H. Ni and S. C. Rand, *Opt. Lett.* **16,** 1424–1426 (1991).
48. R. Brede, E. Heumann, J. Koetke, G. Huber and B. Chai, *Appl. Phys. Lett.* **63,** 2030–2031 (1993).
49. J. Breguet, A. F. Umyskov, S. G. Semenkov, W. Lüthy, H. P. Weber and I. A. Shcherbakov, *IEEE J. Quantum Electron.* **28,** 2563–2566 (1992).
50. T. Hebert, R. Wannemacher, R. M. Macfarlane and W. Lenth, *Appl. Phys. Lett.* **60,** 2592–2594 (1992).
51. B. C. Collings and A. J. Silversmith, *J. Lumin.* **62,** 271–279 (1994).
52. F. Auzel and Y. Chen, *J. Lumin.* **65,** 45–56 (1995).
53. V. A. Antonov, P. A. Arsenev, K. E. Bienert and A. V. Potemkin, *Phys. Status Solidi (a)* **19,** 289–299 (1973).
54. A. A. Kaminskii, T. I. Butaeva, A. O. Ivanov, I. V. Mochalov, A. G. Petrosyan, G. I. Rogov and V. A. Fedorov, *Sov. Tech. Phys. Lett.* **2,** 308–310 (1976).
55. W. E. Case, M. E. Koch and A. W. Kueny, *J. Lumin.* **45,** 351–353 (1990).
56. R. Scheps, *IEEE J. Quantum Electron.* **31,** 309–316 (1995).
57. W. Lenth, A. J. Silversmith and R. M. Macfarlane, In: *Advances in Laser Sciences III*, pp. 8–12, A. C. Tam, J. L. Gole and W. C. Stwalley (eds.) American Institute of Physics, New York (1988).
58. W. Lenth, J. C. Baumert, G. C. Bjorklund, R. M. Macfarlane, W. P. Risk, F. M. Schellenberg and A. J. Silversmith, *Proc. SPIE* **898,** 61–67 (1988).
59. F Tong, W. P. Risk, R. M. Macfarlane and W. Lenth, *Electronics Lett.* **25,** 1389–1391 (1989).
60. T. Hebert, W. P. Risk, R. M. Macfarlane and W. Lenth, In: *Proc. Adv. Solid state Lasers*, pp. 379–383, H. J. Jenssen and G. Dube (eds.) Optical Society of America, Washington (1990).
61. P. Xie and S. C. Rand, *Opt. Lett.* **17,** 1196–1198 (1992); and P. Xie and S. C. Rand, Erratum, *Opt. Lett.* **17,** 1822 (1992).
62. T. Hebert, R. Wannemacher, W. Lenth and R. M. Macfarlane, *Appl. Phys. Lett.* **57,** 1727–1729 (1990).
63. J. P. van der Ziel, F. W. Ostermayer and L. G. van Uitert, *Phys. Rev. B* **2,** 4432–4441 (1970).
64. P. Xie and S. C. Rand, *Appl. Phys. Lett.* **57,** 1182–1184 (1990).
65. R. A. McFarlane, M. Robinson and S. A. Pollack, *Proc. SPIE* **1223,** 294–302 (1990).

66. D. C. Nguyen, G. E. Faulkner, M. E. Weber and M. Dulick, *Proc. SPIE* **1223,** 54–63 (1990).
67. B. P. Scott, F. Zhao, R. S. F. Chang and N. Djeu, *Opt. Lett.* **18,** 113–115 (1993).
68. Y. K. Voronko, A. A. Kaminskii, V. L. Osiko and A. M. Prokhorov, *Sov. Phys. JETP Lett.* **1,** 3–5 (1965).
69. B. M. Antipenko, S. P. Voronin and T. A. Privalova, *Sov. Phys. Techn. Phys.* **32,** 208–209 (1987).
70. J. Y. Allain, M. Monerie and H. Poignant, *Electron. Lett.* **26,** 166–168 (1990).
71. U. S. Patent 5,067,134, Device for generating blue laser light, E. W. J. L. Oomen, November 19 (1991).
72. R. S. Quimby and W. J. Miniscalco, *Appl. Opt.* **28,** 14–16 (1989).
73. J. Y. Allain, M. Monerie and H. Poignant, *Electron. Lett.* **26,** 261–263 (1990).
74. R. G. Smart, D. C. Hanna, A. C. Tropper, S. T. Davey, S. F. Carter and D. Szebesta, *Electron. Lett.* **27,** 1307–1309 (1991).
75. T. J. Whitley, C. A. Millar, R. Wyatt, M. C. Brierley and D. Szebesta, *Electron. Lett.* **27,** 1785–1786 (1991).
76. D. S. Funk, S. B. Stevens, S. S. Wu and J. G. Eden, In *Visible and UV Lasers, Proceedings Volume* 2115, pp. 40–44, R. Scheps (ed.) SPIE, Bellingham (1994).
77. P. Xie and T. R. Gosnell, In: *Laser Tech Briefs* (Insert in *NASA Tech Briefs*), pp. 14a–17a, American Business Publications, New York, June (1995).
78. D. S. Funk, J. W. Carlson and J. G. Eden, In: *UV and Visible Lasers and Laser Crystal Growth, Proceedings Volume* 2380, pp. 108–114, R. Scheps and M. L. Kokta (eds.), SPIE, Bellingham (1995).
79. S. A. Pollack and D. B. Chang, *Optical and Quantum Electron.* **22,** S75–S93 (1990).
80. T Imasaka and N. Ishibashi, *Prog. in Quantum Electron.* **14,** 131–249 (1990).
81. A. Penzkofer, *Prog. in Quantum Electron.* **12,** 291–427 (1988).